The Forelimb and Pectoral Girdle of *Pachyrhinosaurus lakustai* (Ceratopsia, Centrosaurinae)

by

Rebekah Marion Vice

A thesis submitted in partial fulfillment of the requirements for the degree of

Master of Science

in

Systematics and Evolution

Department of Biological Sciences
University of Alberta

Abstract

Ceratopsidae is a group of non-avian dinosaurs known for their distinctive cranial ornamentation and horns. This ornamentation has become the focal point of ceratopsid research and therefore has led to a state of affairs in ceratopsid palaeontology in which taxa are diagnosed on the basis of cranial morphology and the postcranial skeleton is generally neglected and assumed to be unimportant. However, recent studies have begun to alter this situation by introducing descriptions of articulated or associated ceratopsid skeletons. This thesis sets out to build on previous understandings of ceratopsid postcranial elements in order to detect, and distinguish between, intraspecific and interspecific variation within Ceratopsidae. This sample was drawn from the upper Campanian Pipestone Creek Bonebed in the Wapiti Formation near Grande Prairie, Alberta, where hundreds of *Pachyrhinosaurus lakustai* elements have been collected over the past few decades, making this species an ideal focal point for the present study. Morphological and allometric analyses of the forelimb and pectoral girdle of *P. lakustai* revealed multiple characters potentially unique to the species, as well as variation within the genus *Pachyrhinosaurus*. Other characteristics of the scapula and humerus that differentiate Centrosaurinae from Chasmosaurinae, including the ratio of the anterior and posterior widths of the scapula to the midshaft width, were identified. Such characters are key to identifying ceratopsid skeletons as accurately as possible when cranial material is not available.

Furthermore, histological sampling was used in this study to determine the growth trajectory and age range of specimens from the Pipestone Creek Bonebed. This revealed an that juveniles were more abundant in the sample than subadults or adults. The youngest individual was determined to be under a year old, and the oldest at least 21 years old. The overall growth

curve of *P. lakustai* is typical for non-avian dinosaurs in being sigmoidal, the rate of body mass increase greatest in subadults.

Lastly, *P. lakustai* manual pathologies apparently resulting from stresses produced during normal locomotion were discovered and described. This is the first description of this pathology in a centrosaurine ceratopsid, but similar pathologies have been documented in Chasmosaurinae. CT analyses and morphological comparisons suggested that these pathologies were consistent with the unique step cycle described by Thompson and Holmes (2007) for *Chasmosaurus irvinensis*, therefore expanding the potential scope of this kinematic hypothesis to centrosaurines. Overall, this comparative study of the forelimb and pectoral girdle of ceratopsids revealed taxonomically significant characteristics that may be used in the identification of ceratopsid material in the absence of the cranium. These analyses have implications for understanding the behaviour and ecology of these animals, underlining the importance of studying the postcrania of ceratopsids and paving the way for future studies on this topic.

Preface

This thesis is an original work by Rebekah Vice. No part of this thesis has been previously published. C. Sullivan was the supervisor for this thesis and was involved with concept formation and manuscript edits for all chapters.

Acknowledgements

First and foremost I would sincerely like to thank my supervisor, Dr. Corwin Sullivan. Thank you for your constant help and support over the last few years and of course for making this entire thesis possible. Prior to graduate school I was fortunate enough to have a few amazing mentors over the years. Mrs. Beverley Jealous, who taught me the benefit of hard work and dedication, not to mention how to play the instrument that got me through some of the hardest days. Ms. Redmond and Mrs. Schneider, who pushed me to always do my best. And of course, Dr. Hillary Maddin and Dr. Michael Ryan; you both are the reason I have gotten where I am today. Your mentorship and guidance gave me the confidence and knowledge to pursue this dream.

I would also like to thank Dr. Philip Currie for his feedback and assistance throughout my degree. A huge thanks to Darren Tanke, Brandon Strilisky and all the collections staff at the Royal Tyrrell Museum of Palaeontology for allowing me to visit their collections and thin section material for this project. Thanks as well to Derek Larson, Calla Scott, Jackson Sweder and Cam Reed at the Philip J. Currie Dinosaur Museum for allowing me to visit the collections and to join the field crew at the Pipestone Creek Bonebed. Margaret Currie and Kieran Shepard from the Canadian Museum of Nature, and Dr. Kevin Seymour at the Royal Ontario Museum, thank you all for your assistance during collections visits to your respective institutions. Thank you to Dr. Michael Doschak in the Faculty of Pharmacy and Pharmaceutical Sciences at the University of Alberta, for devoting your time and resources to CT scanning a specimen for me. Thank you to Dr. David Evans and the palaeontology graduate students at the University of Toronto and Royal Ontario Museum for hosting the palaeohistology workshop and allowing me to use your equipment, and to Clive Coy, Howard Gibbins, Robin Sissons, and all the volunteers

in the University of Alberta Laboratory for Vertebrate Palaeontology for your constant hard work and help in preparing my material. And a huge thank you to the entire palaeontological community at the University of Alberta; graduate students and professors, and everyone in between. Thanks especially to Dr. Aaron LeBlanc for teaching me how to make histological sections and answering my many questions along the way.

Of course, none of this would have been possible without the endless support from my family and friends. To all my friends, both old and new, who have kept a smile on my face through the insanity of school. To my partner, Sam, who has been my biggest cheerleader these past few years, and who has been by my side every step of the way. To my family; Mum, Dad, Moriah and Lianna; thank you for always believing in me, for listening to every rant, every problem, sharing in all the good times and the bad times too. Thank you to everyone who has supported me through it all. Here is to you all.

Table of Contents

List of Tables

List of Figures

List of Institutional Abbreviations

AMNH, American Museum of Natural History, New York City, New York, USA.

CMN, Canadian Museum of Nature, Ottawa, Ontario, Canada.

PJCDM, Philip J. Currie Dinosaur Museum, Wembley, Alberta, Canada.

NHMUK, Natural History Museum, London, UK.

NSM, National Museum of Nature and Science, Tokyo, Japan.

ROM, Royal Ontario Museum, Toronto, Ontario, Canada.

TMM, Texas Memorial Museum, Austin, Texas, USA.

TMP, Royal Tyrrell Museum of Palaeontology, Drumheller, Alberta, Canada.

UALVP, University of Alberta Laboratory for Vertebrate Palaeontology, Edmonton, Alberta, Canada.

UAMES, University of Alaska Museum, Earth Science Collection, Fairbanks, USA.

UMNH, Natural History Museum of Utah, Salt Lake City, Utah, USA.

USNM, Smithsonian National Museum of Natural History, Washington, D.C., USA.

YPM, Yale Peabody Museum of Natural History, New Haven, Connecticut, USA.

Chapter 1 – Introduction

A History of Pachyrhinosaurus

Ceratopsids, or horned dinosaurs, are an iconic group of non-avian dinosaurs within Ceratopsia (Dodson et al., 2004). Ceratopsids can be divided into the two major clades; Centrosaurinae and Chasmosaurinae. While chasmosaurines are known for their triangular squamosals, elongate frills and well-developed brow horns, centrosaurines possess a much shorter, rectangular frill with elaborate ornamentation on the posterior margin. *Pachyrhinosaurus* is a particularly unusual and well-sampled genus of centrosaurine ceratopsid dinosaur, known from the species *Pachyrhinosaurus canadensis* (Sternberg, 1950) and *Pachyrhinosaurus lakustai* (Currie et al., 2008) from the Upper Cretaceous of Alberta, and *Pachyrhinosaurus perotorum* (Fiorillo and Tykoski, 2012) from the Upper Cretaceous of Alaska. *Pachyrhinosaurus* and *Achelousaurus* form the clade Pachyrostra, which was the last major centrosaurine clade to appear in the Cretaceous (Chiba et al., 2017).

The first *Pachyrhinosaurus* specimen to be discovered and described was a partial skull found near Nobleford, Alberta on the north side of the Little Bow River (Fig. 1.1, locality 1). This skull was reportedly discovered by J. S. Stewart, although the precise date is unknown (Sternberg, 1950). In 1945 a local resident and geologist, Oscar A. Erdman, discovered another skull around 30 km south of the original locality in exposures known as Scabby Butte (Fig. 1.1, locality 2). Shortly after this discovery a student located a third skull only about 275 m from the original site. These specimens were all assigned to the new genus and species *Pachyrhinosaurus canadensis* by Charles Sternberg (1950). At the time *P. canadensis* was the only known ceratopsid with a nasal boss rather than a horn core, making it a unique ceratopsian that Sternberg (1950) placed in his new family Pachyrhinosauridae. Following Sternberg's publication, staff from the Canadian Museum of Nature (then known as the National Museum of

Natural Sciences) returned to Scabby Butte in May, 1957 to conduct the "first systematic scientific excavation of an Alberta ceratopsian bonebed" (Tanke, 2006, p. 49). In late 1960 a better-preserved *P. canadensis* skull was discovered near Drumheller, Alberta, in the valley of the Red Deer River (Fig. 1.1, locality 3), by the Drumheller and District Museum Society (Langston, 1967). This discovery not only provided fresh information regarding the species and its overall morphology, but also expanded its known geographic range.

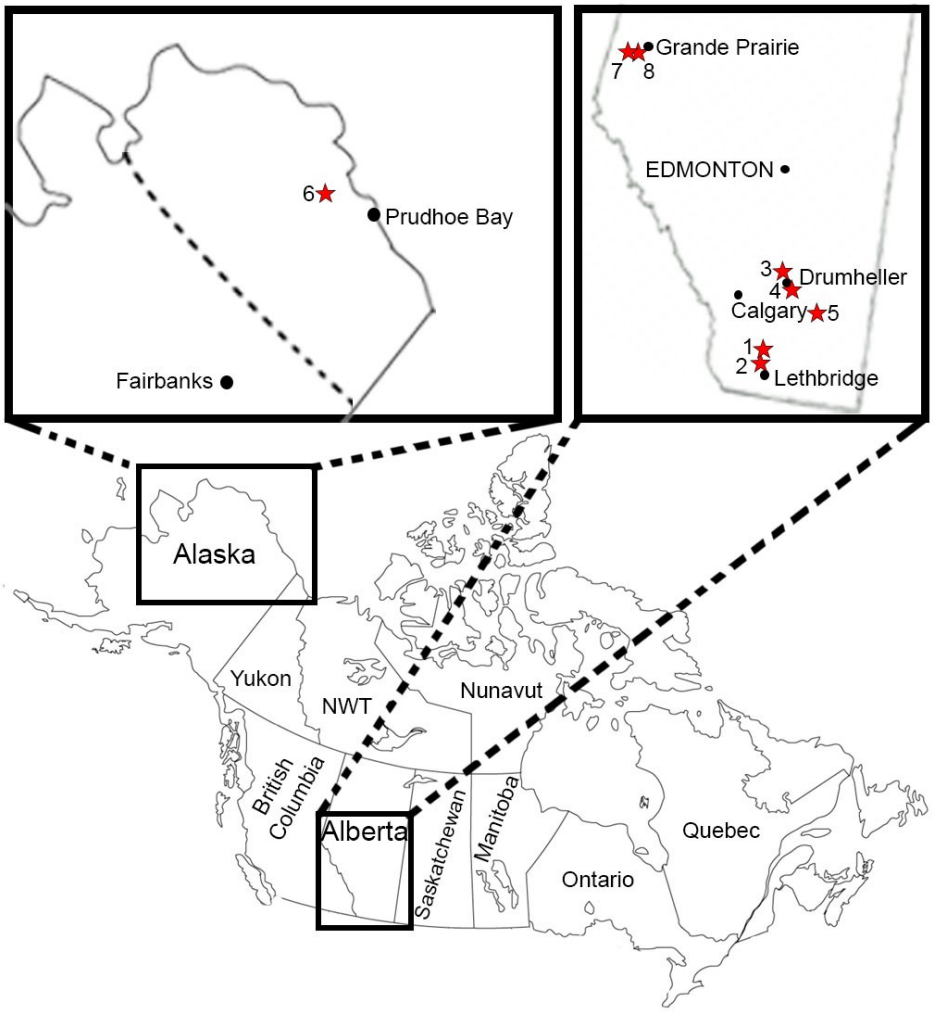

Figure 1.1. Localities where *Pachyrhinosaurus* specimens have been found.
Map showing known *Pachyrhinosaurus* localities as numbered red stars, and nearby cities/towns as black circles. 1) *Pachyrhinosaurus canadensis*, Little Bow River, Alberta, 2) *Pachyrhinosaurus canadensis,* Scabby Butte, Lethbridge, Alberta, 3) *Pachyrhinosaurus canadensis*, Red Deer River Valley, Alberta, 4) Isolated *Pachyrhinosaurus canadensis* specimens, Rosedale and Cambria, Alberta, 5) *Pachyrhinosaurus*-like ceratopsid, Dinosaur Provincial Park, Iddesleigh, Alberta, 6) *Pachyrhinosaurus perotorum*, Kikak-Tegoseak Quarry, Alaska, 7) *Pachyrhinosaurus lakustai*, Pipestone Creek Bonebed, Wembley, Alberta, 8) Unidentified *Pachyrhinosaurus,* Wapiti River Bonebed. Abbreviations; NWT, Northwest Territories.

Since the species was first described, numerous *P. canadensis* specimens have been found in southern Alberta. In the 1990s a number of partial *Pachyrhinosaurus canadensis* specimens were discovered south of Drumheller near Rosedale and Cambria, Alberta (Fig. 1.1, locality 4) (Tanke, 2006). Field crews from the Royal Tyrell Museum of Palaeontology investigated both localities and collected a few elements from Cambria, none of which have been described in any detail. No specimens were collected from the Rosedale locality.

In 2001 the TMP began to excavate a nearly complete, disarticulated adult ceratopsid skeleton near Iddlesleigh, Alberta in Dinosaur Provincial Park (Fig. 1.1, locality 5) (Ryan et al., 2010). Although this skeleton bears a pachyostotic nasal boss and postorbital bosses, it cannot be definitively identified as *Pachyrhinosaurus* as it lacks the diagnostic posterior parietal. Therefore, it is often referred to as a *Pachyrhinosaurus*-like ceratopsid, or as the Iddesleigh ceratopsid. In the interim, the known diversity of the genus has continued to increase; three species of *Pachyrhinosaurus* have been named to date. Fiorillo and Tykoski (2012) described *Pachyrhinosaurus perotorum* from the Colville River on the North Slope of Alaska (Fig. 1.1, locality 6). Prior to this discovery, *Pachyrhinosaurus lakustai* was erected by Currie et al. (2008)

based on specimens from near Grande Prairie, Alberta (Fig. 1.1, locality 7) in the small town of Wembley, Alberta.

The first *P. lakustai* elements were discovered by a high school teacher, Al Lakusta, in the fall of 1972. These specimens were from what would come to be known as the Pipestone Creek Bonebed. Pipestone Creek is a monodominant bonebed, with approximately 99% of the material collected belonging to *Pachyrhinosaurus lakustai* (Fanti and Currie 2007). The site is the only one known to produce *P. lakustai*, and is also among the densest dinosaur bonebeds in the world, yielding over 200 bones per square metre in some areas. Over the next few years Al Lakusta collected a multitude of small specimens from the bonebed, but it wasn't until 1983, when Darren Tanke, of the Royal Tyrrell Museum of Palaeontology (TMP), heard of Pipestone Creek, that the TMP took an interest in the site (Tanke, 2006). Tanke identified a number of frill fragments belonging to a centrosaurine ceratopsian, but could not narrow down the identification further. In 1985 Tanke revisited the collection, which was then housed at the Grande Prairie Pioneer Museum (GPPM) and included the personal fossil collection of the GPPM curator Bert Tieman. Tieman's collection included what Tanke identified as the first nasal boss discovered at Pipestone. This discovery led to the beginning of the formal excavation of the site by the RTMP, beginning in 1986 (Tanke, 2006). Excavations by the TMP continued annually until 1989, and yielded 15 skulls of varying completeness as well as hundreds of *P. lakustai* elements representing a wide range of ontogenetic stages. In subsequent years the site was sporadically excavated by the TMP, as well as by the University of Alberta (2008-2016), and from 2017 onwards it has been excavated annually by the Philip J. Currie Dinosaur Museum in Wembley.

Geology and Taphonomy of the Pipestone Creek Bonebed

Pachyrhinosaurus lakustai is known solely from the Pipestone Creek Bonebed in Wembley, Alberta. Even with hundreds of elements having already been collected from this site, decades' of work potentially remain to be completed here. Exploratory borehole cores show that the bonebed extends at least another 70 metres away from Pipestone Creek (Fanti and Currie, 2007). This monodominant bonebed occurs in Upper Cretaceous rocks of the Wapiti Formation, a volcanic ash layer dated to 73.25 ± 0.25 million years, being situated 28 metres above the bonebed (Currie et al., 2008). This places the bonebed in the Campanian. The bones reside in a 4 m thick soft dark carbonaceous siltstone and exhibit high amounts of plastic deformation, as is typical for mudstone deposits (Currie and Fanti, 2007). Levee, overbank deposits, and low-angle ripples indicate various syndepositional hydraulic reworking events at the site. Furthermore, Ralrick and Tanke (2008) studied the overall direction of flow and the probable transportability of the different skeletal elements, and determined there was an abundance of fluvial influence in the deposition of the bonebed. Although no clear flow direction was determined, Ralrick and Tanke (2008) did note an abundance of easily transportable elements, supporting their hypothesis that the bonebed does not represent the original deposition site, but that the elements have since been transported. Overall, the Pipestone Creek Bonebed has a complex taphonomic history, and exhibits evidence of scavenging, deformation, crushing and transportation that has yet to be fully analysed. For a full geological description of the site see Currie et al. (2008).

A Problem in Ceratopsid Palaeontology

Researchers have taken advantage of the abundance and wide ontogenetic range of the Pipestone material to study the skull of *P. lakustai* in great detail. The initial description of *P.*

lakustai (Currie et al., 2008) included a thorough account of the cranial elements, and was published alongside a CT analysis of the inner ear and brain cavity (Witmer and Ridgely, 2008). Additionally, Kruk's (2015) unpublished Master's thesis included *P. lakustai* specimens in an ontogenetic study of the boss of *Pachyrhinosaurus.* Other studies of the Pipestone Creek Bonebed (Fanti and Currie, 2007; Ralrick and Tanke, 2008) have focused on the overall taphonomy of the site, and have not described the postcranial anatomy of *P. lakustai*.

The emphasis on cranial osteology reflects common practice in ceratopsid palaeontology, as virtually all documented features that are diagnostic within Ceratopsidae pertain to the skull (Dodson et al., 2004). Therefore, the postcranium is often neglected and assumed to lack diagnostic features (Chinnery, 2004). Casual observation of ceratopsid collections and literature suggests that ceratopsid postcrania that are collected rarely are prepared; those that are prepared rarely are described; and those that are described are typically associated with a skull and are rarely figured or given detailed attention. This is the basis of a problem in ceratopsid palaeontology. One cannot describe what is not collected. One cannot associate potentially diagnostic features with a particular taxon if they occur on a bone that cannot be identified taxonomically. However, one cannot refer a ceratopsid postcranial bone to a smaller clade unless it happens to be preserved together with a skull. Therefore, we are left with a surplus of unidentified isolated ceratopsian postcrania in collections and out in the field that will remain useless for many purposes until we are able to identify ceratopsid taxa based on postcrania alone.

This problem dates back to the very first ceratopsian ever named, *Agathaumas sylvestris* Cope, 1872. This specimen consists entirely of postcranial bones, including sixteen vertebrae, a sacrum, ribs, pelvic elements, and unidentified limb elements. Because there is no associated skull, however, this specimen cannot be confidently diagnosed, and *Agathaumas sylvestris* is

accordingly considered a nomen dubium. A more recent analysis of the specimen tentatively identified it as a *Triceratops* based on overall size, morphology and location (Breithaupt, 1999). A similar fate befell the second ceratopsian to be named, *Polyonax mortuarius* Cope, 1874. The holotype of this species includes vertebrae, fragmentary limb bones, and what are now known to be horn cores (Glut, 1997). Again, however, lack of diagnostic cranial material has resulted in *P. mortuarius* being regarded as a nomen dubium (Weishampel et al., 1990).

Cope's (1876) discovery and description of the holotype of the nominal species *Monoclonius crassus* (now AMNH 3998) marked the first time that diagnostic cranial elements could be associated with any ceratopsian specimen (Creisler, 1992). However, this description is not without its faults, mainly as *Monoclonius* is now considered a nomen dubium, with the majority of specimens identified as immature individuals of *Centrosaurus* (Ryan et al., 2001). Cope (1876) even misidentified the parietal portion of the frill as an episternal bone, and included a description of teeth, supposedly from the same specimen, which were later identified as belonging to a hadrosaur (Hatcher, 1907). These teeth have since been lost and are assumed to have been associated with the other material by mistake (Creisler, 1992).

Marsh's (1888) description of *Ceratops montanus* (USNM 2411) (now also a nomen dubium (Dodson and Currie, 1990)) was the first study of any ceratopsian to included correctly identified adult cranial material. As discoveries continued, however, the literature came to be dominated by studies that focused mainly (or in some cases solely) on cranial material. This began with a description of *Triceratops flabellatus* that only considered the skull (Marsh, 1889a) even though a considerable amount of the skeleton had also been recovered (Marsh, 1889b).

A number of subsequent papers on ceratopsids would include descriptive information on both cranial and postcranial elements. With known diagnostic features limited to the cranium,

however, postcrania continued to be relatively neglected in most cases. Hatcher's (1907) description of *Triceratops prorsus*, Gilmore's (1917) description of *Brachyceratops* and Brown's (1917) description of *Centrosaurus* (then *Monoclonius*) *apertus* were quite thorough, providing brief descriptions of most postcranial elements, but illustrated most of the bones in only one view. These studies were fairly thorough by the standards of the time, but still provided only limited information with which to begin assessing the distributions of postcranial features. Lull (1933) was the first to draw comparisons involving postcranial morphology across ceratopsid taxa. While his description of '*Monoclonius'* was relatively comprehensive, with most elements figured in posterior and anterior views, he extensively compared this putative taxon only to *Triceratops* and *Centrosaurus*, rather than to the full range of ceratopsids known at the time (e.g., *Anchiceratops* and *Chasmosaurus*). Lull (1933) also made brief comparisons between two *Chasmosaurus* specimens, but presented limited descriptive information and did not provide figures of the individual elements. In the following decades, although students of many other fossil vertebrate groups routinely published detailed descriptions of postcranial anatomy (e.g., Stokely, 1947; Andrews and Westoll, 1970; Galton, 1981) ceratopsid workers focused almost exclusively on documenting cranial features. In recent years, however, ceratopsid researchers have worked to fix this problem. Their work has resulted in a few notably comprehensive studies of ceratopsid postcrania, including descriptions of articulated and associated ceratopsid specimens (e.g., Mallon and Holmes, 2010; Maidment and Barrett, 2011; Holmes and Ryan, 2013; Holmes, 2014). Mallon and Holmes (2006) even compared the postcrania of two *Chasmosaurus* specimens in an effort to identify sexually dimorphic traits. These studies have affirmed the importance of the postcranium, including its value as a source of palaeobiological inferences.

The Pipestone Creek Bonebed provides an excellent sample with which to pursue this type of research. Given the large sample size and the wide range of ontogenetic stages represented in the material, it should be possible to build an understanding of the postcranial anatomy of *P. lakustai* as it varies amongst individuals as well as age and size classes.

Current Study

The focus of this thesis is on the potential importance of the postcrania of ceratopsids. Are any diagnostic features present in the postcranium, and what can be learned about the growth and behaviour of ceratopsids based on the postcranium alone? These questions will be explored by analyzing a large sample of *P. lakustai* forelimb and pectoral girdle elements. Using morphological comparisons to other ceratopsids, as well as allometric analyses, I can identify interspecific variation in the postcrania of ceratopsids and document variation within *P. lakustai* due to individual variation as well as ontogeny. Histological analyses will make it possible to determine the range of ontogenetic ages represented in the Pipestone Creek Bonebed sample and plot a growth trajectory. This will allow me to compare the growth of *P. lakustai* to that of other ceratopsids and other groups of non-avian dinosaurs. Lastly, I will analyse and report the first known instance of manual pathologies apparently caused by habitual locomotion in a centrosaurine ceratopsid. Similar pathologies have been previously described in two *Chasmosaurus* specimens (Rega et al., 2010), and are hypothesized to result from the unique step cycle of ceratopsids outlined by Thompson and Holmes (2007). These pathologies in *Pachyrhinosaurus* will be explored by using morphological descriptions and micro-CT analyses to illuminate the nature of the pathology as well as its connection to locomotion.

Chapter 2 - Osteology of the Forelimb and Pectoral Girdle of Pachyrhinosaurus (Ceratopsia: Centrosaurinae)

Introduction

The Pipestone Creek Bonebed is a monodominant bonebed near the town of Wembley, Alberta and the only known locality to yield *Pachyrhinosaurus lakustai* remains. Pipestone is known as one of the densest dinosaur bonebeds in the world and has produced hundreds of specimens. Over 90% of these specimens belong to the centrosaurine ceratopsid dinosaur *P. lakustai.* They include nearly every element in the skeleton, and represent various stages in ontogeny. The locality has been sporadically excavated, since its discovery in 1972, by the Royal Tyrell Museum of Palaeontology (TMP), the University of Alberta Laboratory for Vertebrate Palaeontology (UALVP), and the Philip J. Currie Dinosaur Museum (PJCDM).

With the multitude of specimens collected from the Pipestone Creek Bonebed belonging to one species, the bonebed has been the subject of numerous publications including a monograph published in 2008 (Currie et al., 2008; Ralrick and Tanke, 2008; Witmer and Ridgely, 2008). However, none of these publications sought to analyse the multitude of postcranial elements at the site, and instead solely focused on the skull and the overall taphonomy of the bonebed. This is a widespread limitation in the ceratopsid literature. Due to the importance of the cranium for distinguishing among ceratopsid taxa, the postcranium is often neglected and assumed to lack diagnostic features.

In recent years this cranial bias has been increasingly counterbalanced by numerous studies, beginning with the work of Chinnery (2004), that have examined ceratopsid postcrania in some detail. Chinnery performed morphometric analyses on ceratopsian elements identifiable to the genus level and often the species level, some belonging to isolated skeletons and others from bonebeds. In the course of this research she compiled an extensive database of linear measurements of appendicular elements of a wide range of ceratopsian taxa (including basal

ceratopsians, centrosaurines and chasmosaurines). This allowed Chinnery to investigate patterns of variation in the shapes of these elements. She did identify proportional differences between centrosaurine and chasmosaurine postcrania, but could not detect any meaningful patterns of variation at lower taxonomic levels.

Chinnery's (2004) study established the existence of morphological diversity among ceratopsid postcrania, which led to a series of studies on ceratopsid postcranial material. These studies included a detailed atlas (Holmes et al., 2006) and description (Holmes and Ryan, 2013) of the postcranium of *Styracosaurus albertensis*, as well as descriptions of *Anchiceratops* (Mallon and Holmes, 2010), *Chasmosaurus* (='*Vagaceratops*') *irvinensis* (Holmes, 2014) and *Chasmosaurus belli* (Maidment and Barrett, 2011), and a reevaluation of the postcrania of two *Chasmosaurus* specimens (Mallon and Holmes, 2006). Even following this spate of ceratopsid postcranial descriptions, however, ceratopsid researchers continue to debate the taxonomic relevance of ceratopsid postcrania. Mallon and Holmes (2006) and Maidment and Barrett (2011) have put forward the best arguments in support of the importance of the postcranium.

Mallon and Holmes (2010) redescribed the chasmosaurine specimen CMN 8547, originally discovered and described by Charles Sternberg (1929). Sternberg assigned this specimen to *Anchiceratops*, without specifying the reasons for this decision. Although this specimen has a nearly complete and fully articulated postcranium, there are very few associated skull fragments, and none that are diagnostic of *Anchiceratops* (Mallon and Holmes, 2010). The authors concluded that this specimen does belong to Chasmosaurinae, and suggested that Sternberg likely assigned it to *Anchiceratops* by default rather than on the basis of diagnostic morphological evidence. This designation may have been because *Anchiceratops* was the only known ceratopsid from the lower Edmonton Group at the time of Sternberg's report. Mallon and

Holmes (2010) noted several unique features of this skeleton that could eventually prove to be taxonomically diagnostic, as well as some that seemed to possibly indicate a semi-aquatic lifestyle. In the absence of more informative skull material, however, the postcranial characters present in the specimen cannot be attributed to any particular chasmosaurine taxon.

Maidment and Barrett (2011) provided another detailed description of the skull and postcranium of a ceratopsid, in this case a specimen of *Chasmosaurus belli* (NHMUK R4948) collected in 1919-1920 by the Canadian fossil collector William E. Cutler. The skeleton includes a nearly complete skull and is largely disarticulated. This mode of preservation allowed the specimen to be confidently identified and the various skeletal elements to be described in detail and figured in multiple views. Maidment and Barrett (2011) also highlighted the potential taxonomic importance of the postcranial skeleton and even discussed differences in humeral and scapular morphology between centrosaurines and chasmosaurines.

These studies have brought us closer to the possibility of being able to identify postcranial specimens in the absence of skull material, which would allow researchers to carry out ontogenetic or behavioural analyses on a headless specimen and still have a good idea of what taxon they were working with. However, both Mallon and Holmes (2010) and Maidment and Barrett (2011) limited their focus to single skeletons, unlike Chinnery (2004), and therefore had no definitive basis for determining if any observed differences between their respective specimens and other ceratopsids were taxonomically significant as opposed to reflecting the anatomical idiosyncrasies of single individuals.

From this perspective, the Pipestone Creek Bonebed material is particularly useful in constituting a large sample of the single taxon *P. lakustai*, allowing for a detailed description of the postcranial features of this species that considers intraspecific variation. Pipestone is also

exceptional in that nearly every element is represented at various ontogenetic stages, from juvenile to adult. This makes it possible to document variation during the process of growth and aging. Furthermore, equivalents of some postcranial elements present in the Pipestone sample have been recovered from the Wapiti River Bonebed in Grande Prairie and/or the Scabby Butte locality near Nobleford, Alberta. The Wapiti River Bonebed produces what may be an otherwise unknown species of *Pachyrhinosaurus* (Kruk, 2015), but may also be *Pachyrhinosaurus canadensis* (Fanti et al, 2015). For the purpose of this study this material is referred to as the "WRB *Pachyrhinosaurus.*" The Scabby Butte locality represents another site in southern Alberta with *P. canadensis* remains. These remains allow for the facilitation of anatomical comparisons among different species of *Pachyrhinosaurus.*

The present study uses a combination of quantitative data, as employed by Chinnery (2004), and qualitative data, as employed by Mallon and Holmes (2010) and Maidment and Barrett (2011), to comprehensively evaluate variation within *Pachyrhinosaurus* and between *Pachyrhinosaurus* and other ceratopsids. For this study, a large number of *P. lakustai* forelimb and pectoral girdle elements were measured and compared to other ceratopsid material to identify points of taxonomic variation. Regression analysis was completed using a suite of measurements for each element in order to examine ontogenetic allometry in *Pachyrhinosaurus*. *Pachyrhinosaurus* material from the Wapiti River Bonebed near Grande Prairie, Alberta, and *P. canadensis* material from Scabby Butte near Nobleford, Alberta (Fig. 1.1) was used for comparison to *P. lakustai* from the Pipestone Creek Bonebed.

Materials and Methods

Specimen Selection and Linear Measurement Data Collection

Pachyrhinosaurus lakustai forelimb and pectoral girdle elements were selected from the collections at the PJCDM, TMP, and UALVP. In total 12 scapulae, 4 coracoids, 49 humeri, 12 radii, 14 ulnae, and 13 metacarpals were examined and measured. Highly incomplete or poorly preserved elements were ignored unless they exemplified an ontogenetic stage otherwise poorly represented in the sample, or were particularly informative for others reasons. The *P. lakustai* specimens represented a wide ontogenetic range, but most were either late juveniles (50-59% the total length of the largest specimen of a given bone in the sample) or adults (>90% the total length of the largest specimen), as outlined in Chapter 3 of this thesis.

Measurements for each element were selected to give the best possible estimates of changes in robustness and overall proportions throughout ontogeny. For the scapula the measurements included the blade length, the widths of the anterior and posterior ends, the maximum width (taken at the posterior end of the glenoid fossa), the midshaft width, and the mid-blade circumference (Fig. 2.1A). For the coracoid the measurements were limited to the dorsoventral height, and the width and length at the scapular attachment surface (Fig. 2.1B). For the humerus the measurements included the overall length, the widths of the proximal and distal ends, the length of the deltopectoral crest, and the mid-shaft circumference (Fig. 2.1C). For the radius the measurements included the overall length, the widths of the proximal and distal ends, the width at the ulnar facet, and the mid-shaft circumference (Fig. 2.1D). For the ulna the measurements included the overall length, the widths of the proximal and distal ends, the midshaft width, and the midshaft circumference (Fig. 2.1E). Small linear measurements were taken with calipers, while circumferential measurements and large linear measurements were taken with a cloth

measuring tape. All measurements were recorded to the nearest millimetre. The data were augmented by observing and measuring forelimb and pectoral girdle elements from a wide range of ceratopsids, including *Pachyrhinosaurus canadensis* and WRB *Pachyrhinosaurus* specimens, nine other centrosaurine species and nine chasmosaurine species. Information on some specimens was taken from the literature, but other specimens were observed and measured firsthand.

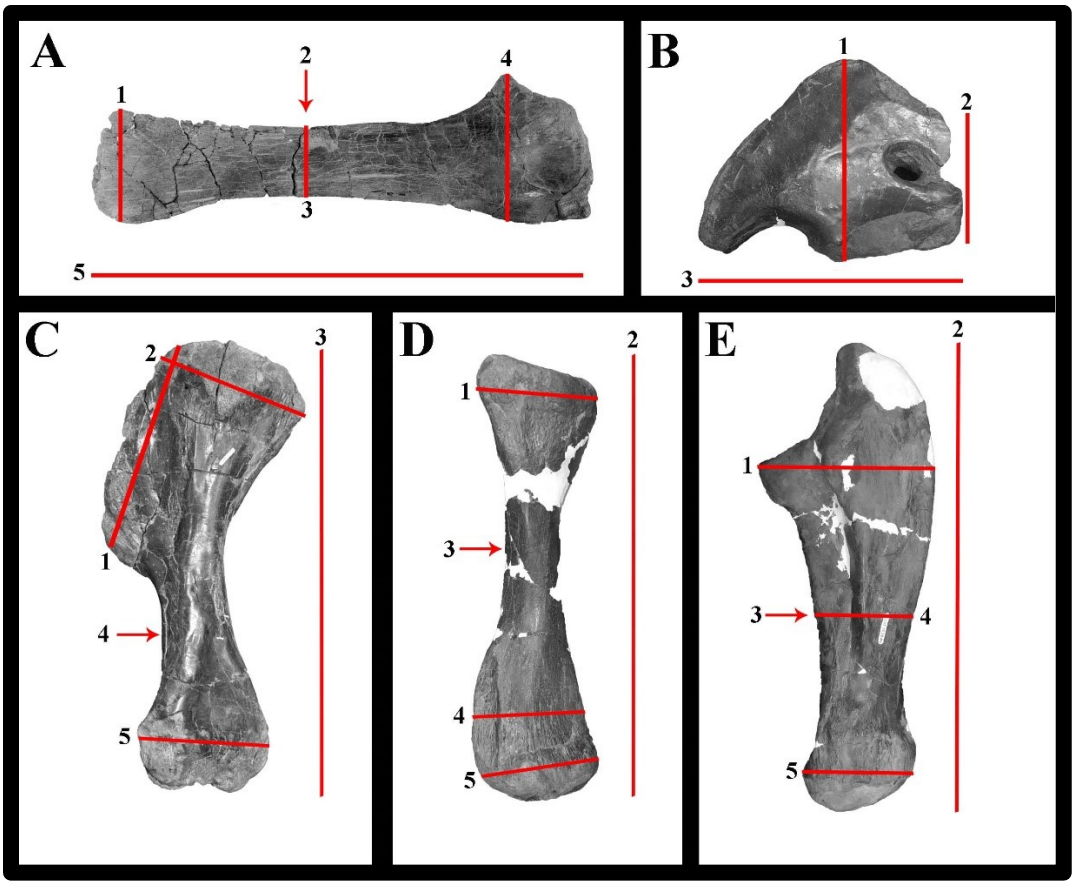

Figure 2.1. Linear measurements of ceratopsid shoulder girdle and forelimb bones. Red lines indicate where each measurement was taken. Red arrows indicate point at which circumference measurements were taken. A) Right scapula UALVP 60330 in medial view, 1. posterior width; 2. midshaft circumference; 3. shaft width; 4. maximum width; 5. length. B) Left coracoid TMP 1985.112.0029 in ventral view, 1. width; 2. scapular attachment length; 3. wdrsoventral height. C) Left humerus TMP 1989.055.1549 in lateral view, 1. deltopectoral crest

length; 2. proximal width; 3. length; 4. mid-shaft circumference; 5. distal width. D) Right radius TMP 1986.055.0264 in anterior view, 1. proximal width; 2. length; 3. mid-shaft circumference; 4. width at ulnar facet; 5. distal width. E) Left ulna TMP 1989.055.0227 in anterior view, 1. proximal width; 2. length; 3. mid-shaft circumference; 4. midshaft width; 5. distal width.

Anatomical Orientation

The general directional terminology for the descriptions is loosely based on the articulation described by Thompson and Holmes (2007). However, for simplicity's sake the scapula is assumed to lie parallel to the length of the body and the forelimb to extend straight ventrally from the shoulder with the joints fully extended and the manus fully pronated, sitting flush with the ground so that the ventral surface faces ventrally. The coracoid is considered to lie in a parasagittal plane, with the glenoid fossa oriented ventrally and the scapular attachment oriented posteriorly. The digits of the manus are all considered to be directed anteriorly and lie parallel to each other, with all metacarpals and phalanges all lying flush with the ground, and their distal ends pointed anteriorly. This is in no way to imply that the forelimb would have held this position in life, but is only intended to provide a frame of reference for the anatomical directions included in the given descriptions.

Testing Allometry Throughout Ontogeny

In order to test of allometric patterns throughout ontogeny in *P. lakustai*, the measurements were log-transformed and subjected to bivariate regression analyses. As this is a test of shape change throughout ontogeny, all other measurements were regressed separately on length, which was treated as the independent variable for each element and as a proxy for overall growth throughout ontogeny. The bivariate regressions were performed using Microsoft Excel's

Data Analysis Toolpak, and the calculated slopes were analysed as allometric coefficients relative to length for the measurements being tested. Values below 1.0, equal to 1.0 and above 1.0 are respectively interpreted as negative allometry, isometry and positive allometry. A 95% confidence interval was calculated for each slope value. Elements belonging to *Pachyrhinosaurus canadensis* and WRB *Pachyrhinosaurus* were not used in the regression computations, but were added to the regression plots to explore possible variation in allometry within the genus.

Description

Scapula

The scapula of *Pachyrhinosaurus* is long and mediolaterally thin in general form, as is typical in ceratopsids (Fig. 2.2). The blade remains dorsoventrally broad and lateromedially flattened throughout ontogeny, but the exact proportions of the scapula vary allometrically (Fig. 2.3). For this study 11 *P. lakustai* scapulae were measured, ranging from 197 mm long to 751 mm (Tab. 2.1). The two *P. canadensis* scapulae from Scabby Butte are considerably larger (with lengths of 782 mm and 743 mm for CMN 9721 and 9722, respectively). Furthermore, the distal end of the left scapula CMN 9722 is broken, and when intact this scapula was likely comparable in length to the right scapula CMN 9721. Similarity in original length between CMN 9721 and 9722 would also be expected based on Langston's (1975) observation that the two bones resemble each other so closely as to suggest they are from the same individual. The only complete WRB *Pachyrhinosaurus* scapula measured a mere 635 mm in length, suggesting it came from an immature individual. For *P. lakustai,* measurements of scapular robustness (mid-shaft width, proximal width, distal width, and mid-shaft circumference) all have allometric

coefficients of less than one with respect to scapular length (Fig. 2.3, Tab. 2.2). Of the robustness measures, mid-blade circumference remains the most isometric throughout ontogeny, with an allometric coefficient of 0.96. Maximum width, by contrast, decreases during ontogeny, with an allometric coefficient of 0.69. All measurements for *P. canadensis* and WRB *Pachyrhinosaurus* specimens fall close to the regression line for *P. lakustai*, suggesting similar allometry throughout the genus.

Table 2.1. Measurements of *Pachyrhinosaurus lakustai* scapula.

Specimen No.	Blade Length	Proximal Width	Distal Width	Shaft Width	Max Width	Circumference
PSB 2017.183	751	118	166		215	
TMP 1987.055.0055	390	56	81	69	124	148
TMP 1987.055.0087				62		
TMP 1987.055.0165	725	67		112	170	259
TMP 1987.055.0190	718	56	90	111	200	
TMP 1987.055.0230	197	48	90	36	75	81
TMP 1988.055.0024	532	53		107	201	238
TMP 1988.055.0093	565			82		
TMP 1989.055.0329	338	48	75	50	105	120

TMP 1989.055.1068	311	54		52	96	110
TMP 1987.055.0237	464	68	102	96	141	155
UALVP 53063	360					144

In most adult *Pachyrhinosaurus* scapulae the anterior end is badly broken or weathered, but juvenile (TMP 1987.055.0230) and subadult (TMP 1989.055.0329) scapulae are consistently rounded at the posterior end. The anterior surface, which contacts the coracoid (Fig. 2.2E), is typically flat and relatively polygonal in most ceratopsians. The flatness of the anterior surface is evident, for example, in the adult *P. lakustai* scapula TMP 1987.055.0190, despite considerable wear and breakage. The rounded anterior ends seen in smaller specimens are most likely due to erosion as some level of erosion tends to occur on all elements from Pipestone. However, this may also be due to limited ossification in smaller, less developed, individuals. The anterior end of the scapula is clearly mediolaterally expanded at all ontogenetic stages, but in the smallest specimens it is proportionately thinner towards the anterior edge (TMP 1987.055.0230). This thinning is typical in ceratopsids, as exemplified by *Chasmosaurus belli* (CMN 2245). In all cases the greatest expansion occurs just above the glenoid facet of the scapula, which faces anteroventrally and is slightly concave (Fig. 2.2D). This concavity is most evident in smaller specimens (TMP 1987.055.0230) but is also present to a lesser degree in adult specimens (TMP 1987.055.0087), including *P. canadensis* CMN 9722 but not CMN 9721. Concavity of the glenoid fossa, although not present in all ceratopsians, does occur in such centrosaurines as *Centrosaurus* CMN 506 and in such chasmosaurines, as *Chasmosaurus belli* CMN 2245. Opposite the glenoid fossa, on the dorsal side of the scapula, lies the acromion process (Fig.

2.2A-C). The appearance of this process varies quite drastically within ceratopsids. In most *P. lakustai* specimens of various ontogenetic stages, the acromion process appears as a slight anterodorsal projection, and is only separated from the proximal end of the bone by a distinct notch on the anterior side of the process. In juvenile (TMP 1987.055.0230) and subadult (TMP 1989.033.0329) specimens the process is poorly defined, and somewhat mediolaterally compressed. In adult specimens (TMP 1987.055.0190) the process is more robust, and in fact is mediolaterally thickened in comparison to the blade, but not to the same extent as the glenoid fossa. In larger specimens the acromion process appears incomplete on the lateral side, but not on the medial. This suggests that the acromion processes of these specimens broke off, but were originally deflected laterally as described by Maidment and Barrett (2011) in *Chasmosaurus belli* (NHMUK R4948) and as observed in *Styracosaurus* (CMN 344; see also Holmes et al., 2006), *Triceratops* (CMN 34824) and an indeterminate pachyrhinosaurin (TMP 2002.076.0001). However, this deflection seems to be absent in some ceratopsians, such as *Centrosaurus* (CMN 506) and the WRB *Pachyrhinosaurus* (UALVP 54724). In general, the acromion process of a centrosaurine differs from that of a chasmosaurine in being less robust and in being separated from the shaft by a notch in some specimens, but apparently not all. The medial side of the anterior portion of the scapula is slightly concave, due to mediolateral expansion of the dorsal and ventral margins. However, this concavity is less clear in some specimens (TMP 1987.055.0230) than others (TMP 1989.055.0329). As this concavity is common in ceratopsians, including *P. canadensis* and WRB *Pachyrhinosaurus*, it can be inferred that *P. lakustai* specimens lacking the concavity have undergone deformation.

The dorsoventral height of the scapula drastically decreases posterior to the glenoid fossa (Fig. 2.2A, B), as is common in ceratopsians. The portion of the bone posterior to the glenoid

fossa is the blade of the scapula. The narrowing is most pronounced in smaller specimens, the minimum shaft width being only 40% the width of the proximal end in TMP 1989.055.0093. Among larger specimens, the shaft width is 65% of the proximal width in TMP 1987.055.0165, and 71% in *P. canadensis* CMN 9722. This reduction is more extreme in centrosaurines included in this study, in which the blade averages 57% of the width of the distal end compared to 85% in the chasmosaurines. The mediolateral thickness of the scapula also decreases distally (Fig. 2.2C, D). The mediolateral expansion of the bone in the vicinity of the glenoid fossa extends distally on the lateral side of the element, forming a scapular ridge (Fig. 2.2B-D) as in all other ceratopsians. The ridge extends obliquely posterodorsally towards the distal end of the element, forming a line from the glenoid fossa to the posterodorsal corner of the blade. As the ridge continues posterodorsally it becomes less pronounced, eventually receding into the lateral surface of the shaft approximately halfway to the posterior end from the glenoid fossa. This ridge, although present in all *P. lakustai* scapulae, is most noticeable in adult specimens (particularly TMP 1987.055.0087) but is almost unidentifiable in smaller juvenile specimens (TMP 1987.055.0055). The scapular ridges are much more robust in *P. canadensis* and WRB *Pachyrhinosaurus* specimens than in *P. lakustai*, being both proportionally wider and more laterally prominent in the first two species. This robustness is also observed in other centrosaurines (e.g., *Centrosaurus* CMN 506; *Styracosaurus* CMN 344, and pachyrhinosaurin TMP 2002.76.0001). In chasmosaurines the scapular ridge is about as laterally pronounced as is typical in centrosaurines, but is more narrow and ridge-like, and extends farther distally along the shaft (e.g., *Anchiceratops* CMN 8547; *Chasmosaurus* CMN 2280).

Towards the posterior end of the element, the shaft expands slightly dorsoventrally in individuals of all ontogenetic stages. In all *Pachyrhinosaurus* specimens examined the posterior

end is broken or worn so that it appears relatively rounded, while in other centrosaurines the posterior end expands so that it appears relatively angular, as observed in *Centrosaurus* CMN 57053 and *Styracosaurus* CMN 344. This relatively angular appearance is common in chasmosaurines as well, implying that the rounded appearance seen in *Pachyrhinosaurus* is probably due to breakage and weathering. Dorsoventral flaring of the distal end of the scapular blade is seen in all ceratopsids but is particularly pronounced in chasmosaurines, in which the width of the midpoint of the blade averages 59% of that of the distal end compared to 84% in centrosaurines.

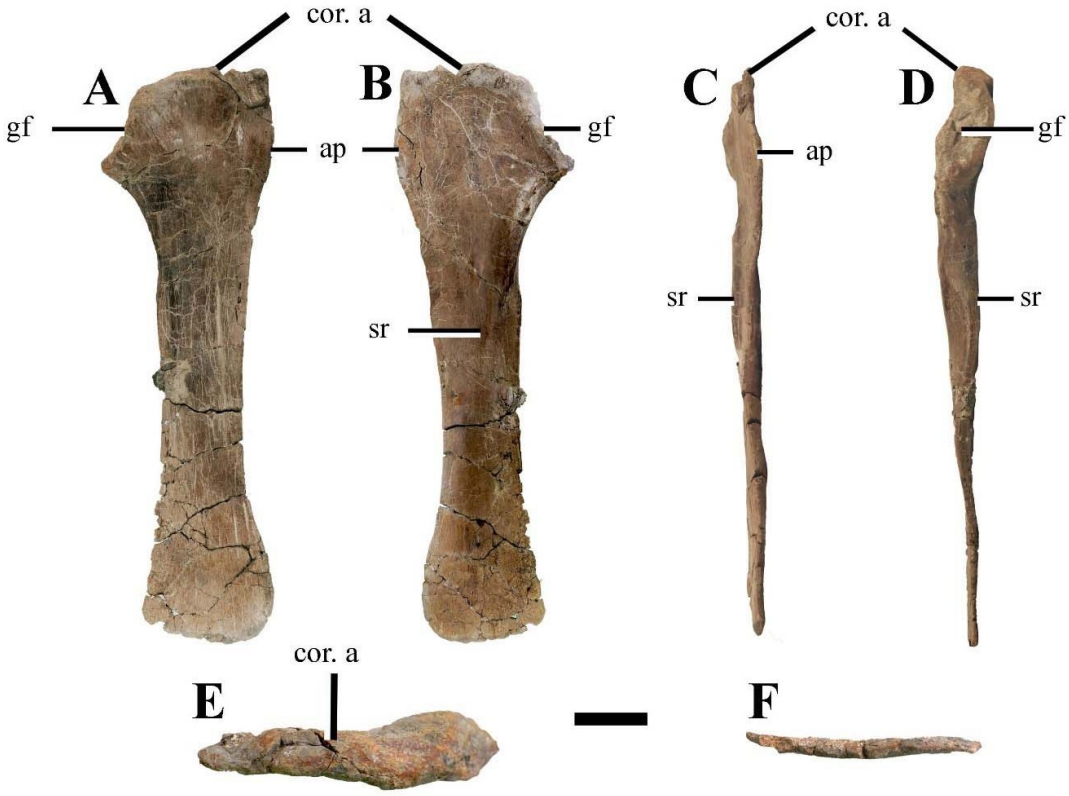

Figure 2.2. *Pachyrhinosaurus lakustai* scapula.
UALVP 60330, right scapula, in A) medial, B) lateral, C) dorsal, D) ventral, E) anterior, and F) posterior views. Scale is 10 cm for A-D and 5 cm for E-F. Abbreviations: ap, acromion process; cor. a, coracoid attachment; gf, glenoid fossa; sr, scapular ridge.

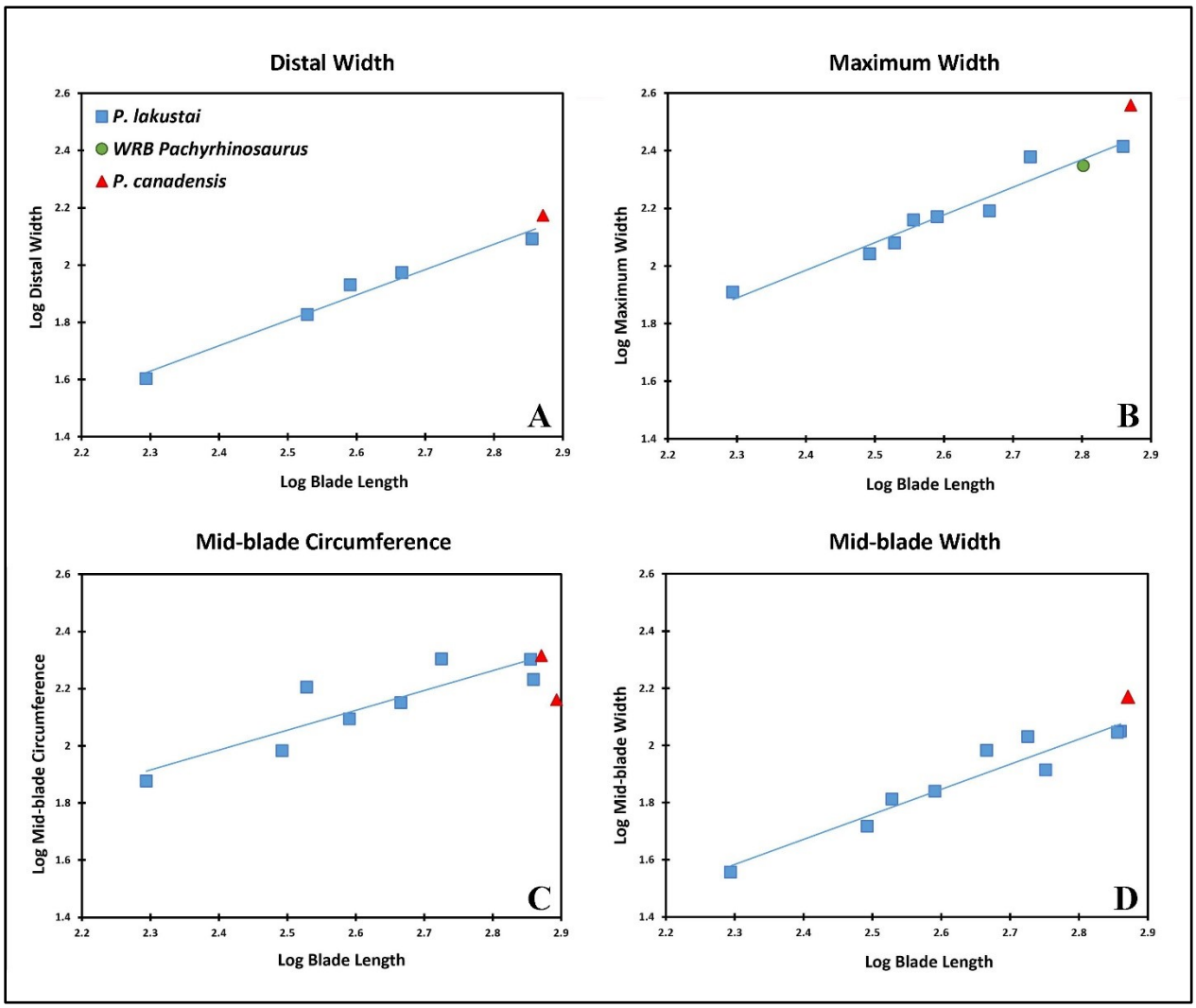

Figure 2.3. Allometry in the scapula of *Pachyrhinosaurus.*

Linear regressions of A) distal width, B) maximum width, C) mid-blade circumference, and D) mid-blade width on length for the scapula of *P. lakustai.* Measurements for the other *Pachyrhinosaurus* species are plotted on the graphs, but were not included in the data set used to compute the regression lines.

Table 2.2. Linear regression results for scapular allometry in *Pachyrhinosaurus lakustai.*

Scapular Measurement	Allometric Coefficient	Intercept	95% Confidence Interval Lower Bound	95% Confidence Interval Upper Bound	R^2
Blade Width	0.876	-0.4311	0.63	1.11	0.91
Max Width	0.6949	0.3166	0.31	1.08	0.77
Circumference	0.9600	-0.3190	0.71	1.21	0.94
Width of Distal End	0.8856	-0.4073	0.61	1.16	0.97

Coracoid

The coracoid of *Pachyrhinosaurus lakustai* is difficult to describe in general terms, as most specimens have undergone far more plastic deformation than is typical for other elements preserved at the Pipestone Creek Bonebed. This is most likely due to the element being thin mediolaterally, and to its overall plate-like morphology (Fig. 2.4). Most available *P. lakustai* coracoids were also fragmentary, so only four minimally deformed and relatively complete specimens (Tab. 2.3) were used for this study. One WRB *Pachyrhinosaurus* coracoid (UALVP 54450) was available for comparison. These coracoids are all from relatively mature individuals given their large size, with dorsoventral heights ranging from 174 mm to 247 mm. As the heights of the scapular attachments are greater than the widths of most *P. lakustai* scapulae, the coracoids are identified as adult specimens. All coracoids so far collected from the Pipestone Creek Bonebed are similarly large, so no identifiable juvenile coracoids are available for analysis. There is also evidence in each Pipestone specimen of fragmentation of the sutural surface due to separation from the scapula. Therefore, it is probable that the coracoid had begun to fuse to the scapula, as is known to occur in mature ceratopsians (Maidment and Barrett, 2011).

As no fused *P. lakustai* scapulocoracoids appear to have been collected, however, it is possible that the scapula and coracoid did not fuse even in adults, the condition described by Lehman (1989) for the scapula and coracoid of *Chasmosaurus mariscalensis*. However, the posterior surface of the coracoid is sub-rectangular and highly worn and broken in many specimens, in connection with the attachment of the scapula to the coracoid (Fig. 2.4). The surface is more severely broken in larger specimens (e.g., TMP 1985.112.0029), which may be indicative of firmer fusion with the scapula leading to more destructive separation between the two bones in high-energy depositional environments. In the smallest of the specimens (TMP 1987.055.0094), the posterior sutural surface remains more intact.

Table 2.3. Measurements of *Pachyrhinosaurus lakustai* coracoids.

Specimen No.	Width	Dorsoventral Height	Scapular Attachment Height
TMP 1985.112.0029	247	164	139
TMP 1986.055.0013	200	150	118
TMP 1987.055.0294	174	151	119
TMP 1988.055.0007	225	160	128

The coracoid of *P. lakustai* has the overall shape typically seen in ceratopsids, with a robust posterior portion and a thinner anterior one. The glenoid fossa forms a 120° angle with the sutural surface, as in many other ceratopsids (e.g., *Centrosaurus* CMN 506; *Chasmosaurus* CMN 2245; *Triceratops* CMN 34824). The glenoid fossa of the coracoid in *P. lakustai* is mediolaterally thick and forms a broad, flat, posteroventrally-facing surface that is proportionally larger than in many other ceratopsids (e.g., *Agujaceratops,* TMM 42303-1, *Centrosaurus,* ROM 767, *Chasmosaurus,* ROM 843, *Styracosaurus,* CMN 344, *Triceratops,* CMN 34824,). The

coracoid foramen is situated anterior to the contact surface for the scapula, and midway between the dorsal and ventral margins of the element. The foramen is elliptical, opens slightly more broadly on the lateral side than on the medial side, and pierces the bone surface obliquely, such that the opening is more dorsally positioned on the lateral side than on the medial side. This morphology is similar to that illustrated by Lehman in *Chasmosaurus mariscalensis* (1989: fig. 1.15) and observed in *Styracosaurus* (CMN 344). In *Centrosaurus* (ROM 767; Brown, 1917), in contrast, the foramen pierces the bone diagonally so that it is more dorsally positioned on the medial side, rather than the lateral side.

Anteroventral to the glenoid fossa, the ventral edge of the element is slightly embayed, so that the edge of the glenoid fossa forms a ventral projecting lip that is far more prominent in some specimens (TMP 1988.055.0007) than others (TMP 1987.055.0294). Still further anteroventrally, the coracoid projects ventrally to form the sharp hooked process seen across Ceratopsidae. The anterior margin of the element gradually curves into the ventral margin, giving the bone a semi-lunate outline. Some individuals (e.g., TMP 1987.055.0294) have gradually curving anterior and ventral coracoid edges, and others have distinct anterior corners between anterodorsally-facing and anteroventrally-facing edges (TMP 1985.112.029, TMP 1988.055.0007). Overall, the element is thinner anteriorly, but this attenuation appears to be subject to ontogenetic variation, with small specimens having proportionally thinner anterior and ventral edges (TMP 1987.055.0294) than large specimens (TMP 1988.055.0007).

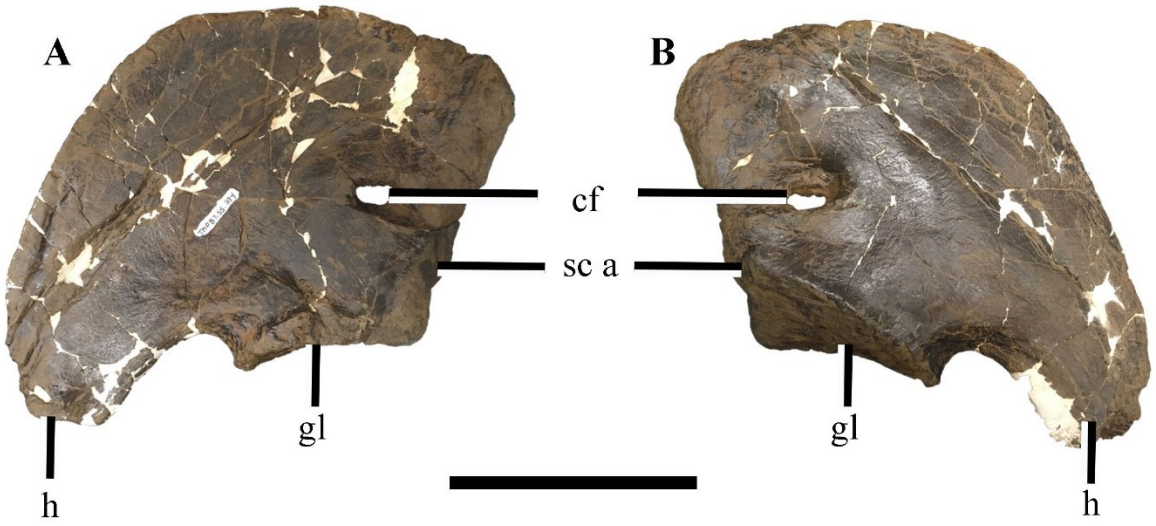

Figure 2.4. *Pachyrhinosaurus lakustai* coracoid.
TMP 1987.055.0294, right coracoid, in A) medial, and B) lateral views. Scale is 10 cm. Abbreviations: cf, coracoid foramen; h, hooked process; gl, glenoid fossa; sc a, scapular attachment.

Humerus

The humerus of *Pachyrhinosaurus* is robust, as is typical in ceratopsids. At early ontogenetic stages, the deltopectoral crest extends along nearly three quarters of the length of the bone, whereas the distal condyles and shaft are proportionally smaller than in adults (Fig. 2.5). The lengths of the 50 *P. lakustai* humeri studied ranged from 145 mm (juvenile) to 573 mm (adult), with the adult humeri falling within the typical range of lengths for other adult ceratopsids (Tab. 2.4). The largest humerus (635 mm long, 311 mm in circumference) was the only one definitely referable to *Pachyrhinosaurus canadensis* (CMN 10640) and was much larger than the largest *Pachyrhinosaurus lakustai* humerus that was complete enough for a length measurement to be taken (573 mm long, 218 mm circumference). TMP 1989.055.0317 had the greatest midshaft circumference of any *P. lakustai* humerus (242 mm) but was too incomplete

for its length to be measured. One incomplete WRB *Pachyrhinosaurus* humerus was available, but no measurements could be taken from it. Several humeral measurements, including distal width, midshaft circumference, and length of deltopectoral crest, are positively allometric. The largest allometric coefficients pertain to distal width, indicating that this parameter increases more rapidly throughout growth than others considered in the analysis. Proximal width, midshaft circumference and length of the deltopectoral crest are approximately isometric with coefficients close to one.

Table 2.4. Measurements of *Pachyrhinosaurus lakustai* Humerus.

Specimen No.	Length	Proximal Width	Shaft Width	Circumference	Distal Width	Deltopectoral Crest Length
PCB 2018.078	320	85	39	113	68	188
TMP 1983.055.0012		89				
TMP 1983.055.0043			36		89	
TMP 1983.055.0052						
TMP 1983.055.0054					96	
TMP 1983.055.0076			81.5			
TMP 1985.112.0016			100min		189	
TMP 1985.112.0088			36		78	

TMP 1986.055.0043	302	94	38	113	85	169
TMP 1986.055.0161	240	62		91	50	118
TMP 1986.055.0058	332	69.8	44.3		52min	
TMP 1986.055.0073	538	130min	78		159	
TMP 1986.055.0119	564	153	76.7		196	
TMP 1986.055.0186	296	88.3	46.4		82.3	
TMP 1986.055.0199	248.6	75	30.4		73.8	
TMP 1986.055.0226	314	101	40.6		76	
TMP 1986.055.0259	260min	104max	40		79.5	
TMP 1986.055.0278	420min		78			
TMP 1986.055.0282			46.7		83.5	
TMP 1987.055.0039a	194		28.8		65	
TMP 1987.055.0265	310					
TMP 1987.055.0301	326	71	43.2		75min	

TMP 1988.055.0061	537	182	83.8	221	173	
TMP 1988.055.0089			55			
TMP 1989.055.0226	320			118		
TMP 1989.055.1468	196	58.8		77.5	58	107
TMP 1989.055.1549	573	190	83.3	218	168	314
TMP 1989.055.1571	145min		28.3	81	54	
TMP 1989.055.0250	205	68	25.5		68	
TMP 1989.055.0400	288	85	39.9		86.1	
TMP 1989.055.0407	559	170	90		213	
TMP 1989.055.0426	413		57.5		127	
TMP 1989.055.0470	221	62min	33.6		63	
TMP 1989.055.0510	306	85	43.3		77	
TMP 1989.055.0639	350min	117max	44		109	
TMP 1989.055.0695	287	88	37.9		84	

TMP 1989.055.0940	499		77.4		153	
TMP 1989.055.1255	315est	111	42.8			
TMP 1989.055.1301	369	83	51.3		112max	
TMP 1989.055.1349	318	90	43		73	
TMP 1989.055.1468	194.5	58.8	25.9		53min	
TMP 1989.055.1497		57	30.7		60	
TMP 1986.055.0108	331est	112max	47.5	122	96	
TMP 1986.055.0230	534		80.5	230	140	300
TMP 1989.055.0317			78.9	242		
TMP 1989.055.0639	350min	116	44	125	109	205
UALVP 53517	210			83		
UALVP 57910	240	75		95	66	140

*Abbreviations: est, estimated; max, maximum; min, minimum.

The humeral head is not well-preserved in any of the *P. lakustai* adult humeri examined for this study, and appears to have broken off post-mortem in some of the larger specimens (e.g., TMP 1989.055.1549) (Fig. 2.5A). In the juvenile specimen TMP 1986.055.0043 the humeral

head protrudes posteriorly and gives rise to a slight ridge that extends down the midline of the proximal portion of the posterior side of the bone. The ridge is narrow at the proximal end of the bone, but rapidly expands to a mediolateral width approaching that of the shaft. This ridge is present in other juvenile specimens that lack the humeral head (TMP 1986.055.0161), as well as in adult specimens (TMP 1989.055.1549). In adults, however, the ridge seems to originate distal to the humeral head, rather than from the head itself as in juveniles. The humeral head protrudes posteriorly, giving the proximal end of the element a triangular outline. In *P. canadensis* CMN 10640, the head is anteroposteriorly thicker than the rest of the proximal end of the bone, but to a lesser degree than in TMP 1986.005.0043, so that CMN 10640 has a more rectangular proximal end. The humeral head is much more prominent in chasmosaurines than in centrosaurines, protruding farther posteriorly in the former group as well as forming a slight proximal peak (e.g., *Chasmosaurus* CMN 41357 and CMN 2280, *Arrhinoceratops* TMP 2014.016.0110). In some taxa (e.g., *Chasmosaurus* and *Styracosaurus*) the humeral head overhangs the posterior surface of the proximal part of the bone, forming a lip. The lip is especially prominent in CMN 2280 (*Chasmosaurus russelli*) and CMN 344 (*Styracosaurus albertensis*).

The medial tubercle is prominent in some juvenile specimens (TMP 1986.055.0161) as a sharp, obtuse protrusion that is most apparent in posterior view, but there is no evidence of a distinct medial tubercle in any adult specimen of *Pachyrhinosaurus* (Fig. 2.5A,B). Neither *P. lakustai* nor *P. canadensis* displays the notch described in *Chasmosaurus belli* by Maidment and Barrett (2011). The notch separates the medial tubercle from the dorsal surface of the humerus, and in both *Pachyrhinosaurus* species these structures are continuous with one another. The notch appears to be lacking in all centrosaurines with preserved tubercles, regardless of

ontogenetic stage (e.g., *Centrosaurus* TMP 2002.108.0083 and CMN 57053, and *Styracosaurus* CMN 344).

The deltopectoral crest is proportionally large, as in all ceratopsids (Fig. 2.5A, B, D). In the *P. lakustai* humeri measured for this study, the deltopectoral crest is 49.2% to 59.2% the length of the entire humerus, compared to a range of 46.4% to 64.3% for centrosaurines in general and 47.8% to 63.3% for chasmosaurines. In *P. lakustai* the deltopectoral crest appears to grow isometrically with an allometric coefficient of 1.03 (Fig. 2.6, Tab. 2.5). The crest protrudes laterally, appears sub-rectangular in medial or lateral view, and extends from the proximal end of the bone to the narrow midshaft region. The crest curves anteriorly as it extends laterally, creating the concave anterior surface described in *Centrosaurus* (ROM 767), *Styracosaurus* (CMN 344) and an indeterminate pachyrhinosaurin (TMP 2002.076.0001) by Maidment and Barrett (2011). This bend was not as evident in *P. canadensis* CMN 10640 as in *P. lakustai*, but this may be due to deformation and severe weathering of the crest in the former. A pronounced concavity was also observed in *Centrosaurus* (TMP 2002.108.0083) and *Styracosaurus* (CMN 344). A distinct groove lies medial to the base of the deltopectoral crest on the anterior side of the humerus throughout ontogeny, as in various other ceratopsids such as *Centrosaurus* (ROM 767), *Chasmosaurus* (e.g., CMN 2280, CMN 2245, ROM 843, CMN 41357), *Styracosaurus* (CMN 344), TMP 2002.076.0001, and *Triceratops* (Hatcher, 1907). This groove is more distinct in some specimens than others but is apparent through all ontogenetic stages. The groove is not visible in *P. canadensis* CMN 10640, but this is most likely due to heavy plaster restoration in the relevant area.

At the base of the deltopectoral crest the humerus abruptly contracts to a narrow shaft, whose circumference is only about a third of the full length of the bone (Fig. 2.5A-D). The shaft

appears circular to subcircular in cross section. The distal end of the humerus is greatly expanded mediolaterally, relative to the narrow shaft, to form the ulnar and radial condyles. In most specimens the distal end is slightly rotated relative to the proximal end of the bone, so that the posterior surface of the distal end faces somewhat medially. Such humeral torsion is typical for ceratopsids, but is most drastic in *Spiclypeus* (CMN 57081). The radial and ulnar condyles are not as well defined as in some other ceratopsids, including *Chasmosaurus* (CMN 2245, CMN 2280), *Styracosaurus* (CMN 344), and *Triceratops* (CMN 34824), but are separated by a notch (Fig. 2.5F) slightly deeper than that seen in such centrosaurines as *Centrosaurus* (TMP 2002.029.0058) and *Wendiceratops* (TMP 2014.029.0058). This notch deepens further throughout ontogeny. The ulnar condyle protrudes slightly farther distally than the radial condyle in some juvenile *P. lakustai* specimens (TMP 1986.055.0043, TMP 1989.055.1468), as in *P. canadensis* CMN 10640, but the radial condyle protrudes farther distally in others (TMP 1986.055.0161). The condyles of adult *P. lakustai* (TMP 1989.055.1549) are about equally prominent in the distal direction, as is common in large ceratopsids, although in *Wendiceratops* (TMP 2014.029.0100, TMP 2014.029.0101) the radial condyle does protrude farther distally. A laterally-facing epicondyle occurs proximal to the radial condyle, but continues only a short distance further proximally before receding into the shaft of the humerus. This epicondyle is present throughout ontogeny in *Pachyrhinosaurus*, but is absent in many other ceratopsid humeri (*Arrhinoceratops* TMP 2014.016.0110; *Centrosaurus* TMP 2002.108.0083; *Chasmosaurus* CMN 2245). In *Wendiceratops* an epicondyle is present, but is not nearly as prominent as in *Pachyrhinosaurus*.

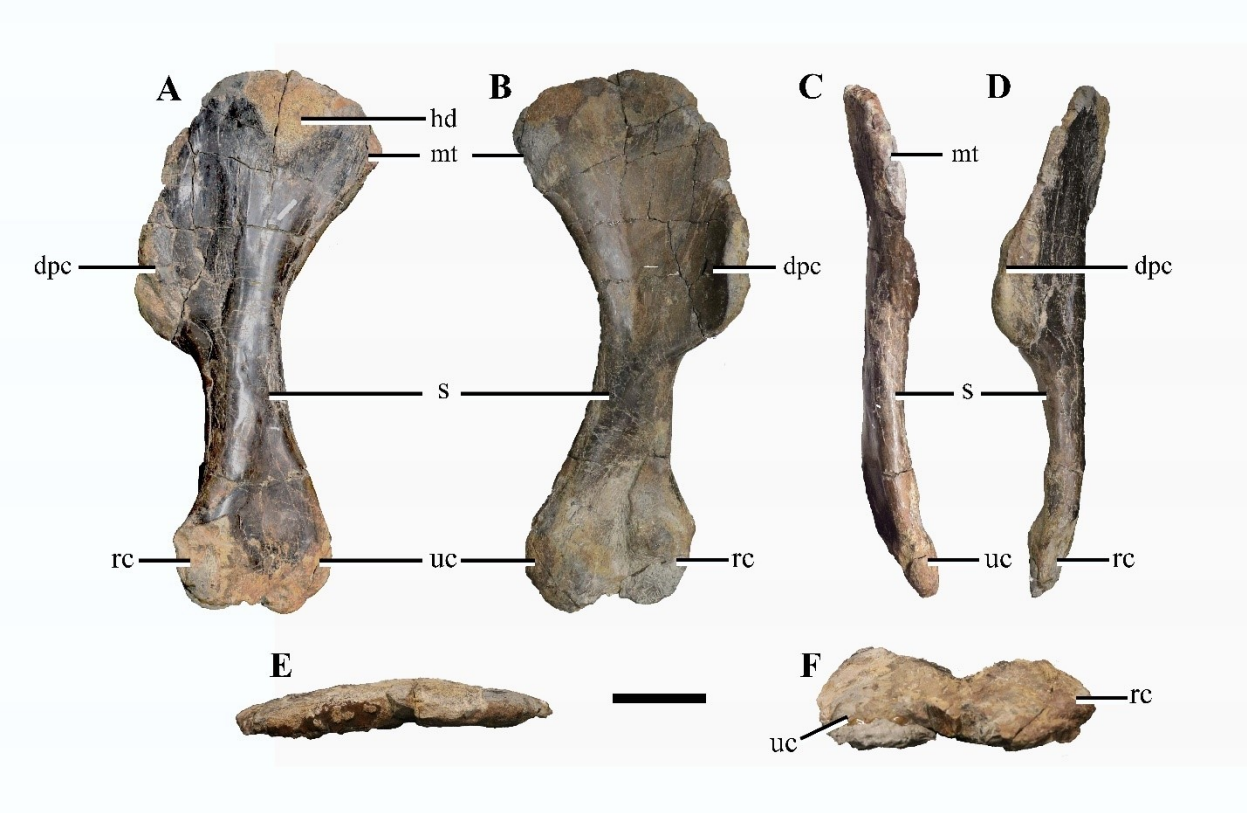

Figure 2.5. ***Pachyrhinosaurus lakustai*** **humerus.**

TMP 1989.055.1549, left humerus, in A) posterior, B) anterior, C) medial, D) lateral, E) proximal, and F) distal views. Scale is 10 cm for A-D and 5 cm for E-F. Abbreviations: dpc, deltopectoral crest; hd, broken base of humeral head; mt, broken base of medial tubercle; rc, radial condyle; s, shaft; uc, ulnar condyle.

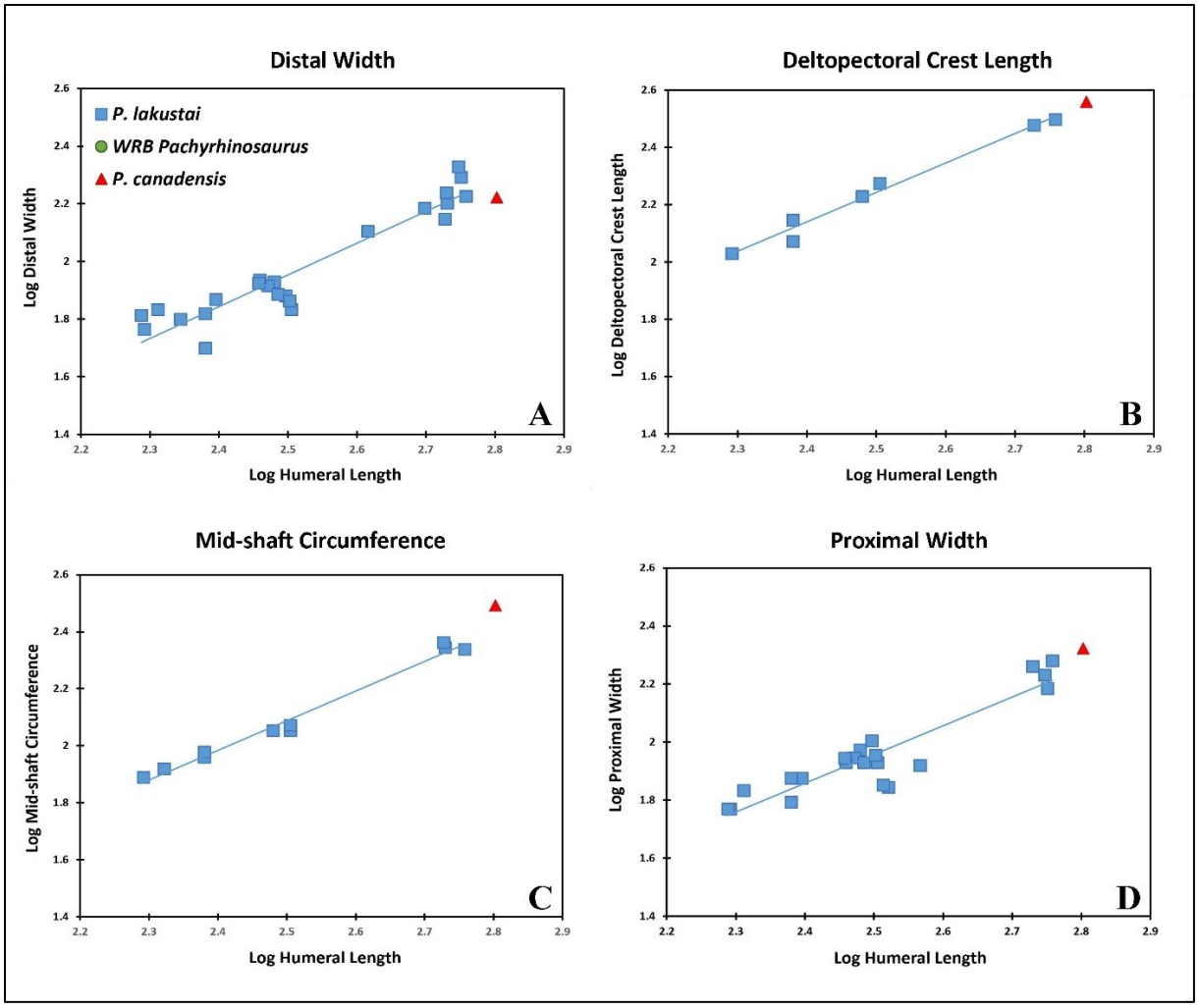

Figure 2.6. Allometry in the Humerus of *Pachyrhinosaurus.*

Linear regressions of A) distal width, B) deltopectoral crest length, C) mid-shaft circumference, and D) proximal width on length for the humerus of *P. lakustai*. Measurements for the other *Pachyrhinosaurus* species are plotted on the graphs, but were not included in the data set used to compute the regression lines.

Table 2.5. Linear regression of humeral allometry in *Pachyrhinosaurus lakustai.*

Humeral Measurement	Allometric Coefficient	Intercept	95% Confidence Interval Lower Bound	95% Confidence Interval Upper Bound	R^2
Deltopectoral Crest Length	1.031	-0.3318	0.88	1.18	0.98
Circumference	1.035	-0.5046	0.93	1.14	0.98
Width of Proximal End	0.9710	-0.4652	0.79	1.15	0.84
Width of Distal End	1.1025	-0.8037	0.94	1.26	0.89

Radius

The radius of *Pachyrhinosaurus* is long and narrow overall, with minor expansion of the proximal and distal ends (Fig. 2.7). For this study 12 *P. lakustai* radii were measured, ranging from 110 to 363 mm long (Tab. 2.6). As there are no known *P. canadensis* or WRB *Pachyrhinosaurus* radii, comparisons could not be made across species within the genus. The majority of the specimens studied are considered juveniles or adults, with only two specimens falling into the subadult size range. Most radial measurements taken are positively allometric, while some are isometric (i.e. midshaft circumference, distal width, and the width at the ulnar facet) (Fig. 2.8, Tab. 2.7). The width of the proximal end is positively allometric with a coefficient of 1.29, implying that the proximal end of the element widens rapidly compared to the length of the element. The *P. lakustai* radii tend to be a typical size range for adult ceratopsians, with other centrosaurine radii averaging 313 mm in length and chasmosaurine radii averaging 327 mm.

Table 2.6. Measurements of *Pachyrhinosaurus lakustai* radius.

Specimen No.	Length	Ulnar Facet Width	Proximal Width	Distal Width	Circumference
TMP 1909.055.1313	206	44	52	52	73.5
TMP 1986.055.0264	229	90	100	100	91
TMP 1987.055.0021	203				
TMP 1989.005.1496	301	73	59	100	135
TMP 1989.055.0683	110	31		34	50
TMP 1989.055.1247	362				132
TMP 1989.055.1339	341	115	103	129	145
TMP 1989.055.1462	190				71
TMP 1986.055.0096	196				78
UALVP 53077	340				146
UALVP 54446	350	102	106	106	176
UALVP 57317	363	98	100	103	131.5

In most specimens both ends are highly weathered and deformed. There is a great deal of morphological variability among the available radii, presumably reflecting some combination of deformation and genuine individual variation. In most specimens the proximal end of the radius tapers dorsally, rather than forming a substantial radial head as in TMP 1986.055.0264 (Fig. 2.7A, B). However, it is unlikely that a radius from a living individual would have exhibited this morphology, which is probably a product of weathering and deformation. The proximal end of the radius TMP 1986.055.0264 is flattened to form a distinct radial head (Fig. 2.7D), and this most likely represents the true morphology because a similar condition is seen in many other

ceratopsids (e.g., *Anchiceratops* CMN 8547; *Centrosaurus* ROM 1439 and CMN 2280; *Chasmosaurus* ROM 843; *Styracosaurus* CMN 344; *Triceratops* CMN 34824; and indeterminate pachyrhinosaurin TMP 2002.076.0001). This flat morphology would have permitted a mediolaterally broad articulation with the radial condyle of the humerus. The flat proximal end of TMP 1986.055.0264 slopes laterally, such that the posterior side of the proximal end extends farther dorsally than the anterior side. Similar oblique surfaces are present to lesser degrees in other *P. lakustai* specimens (UALVP 57327). As these elements are of different sizes, which undoubtedly reflects variation in age to some degree, the steepness of the slope may vary throughout ontogeny, being greater in younger individuals than in adults. The proximal end of the radius is oval in outline (Fig. 2.7E), the long axis of the oval being orientated anteroposteriorly. The lateral side of the oval is somewhat convex, while the medial side is more flattened. The flat posterior surface of the proximal part of the radius would have contacted the medial process of the ulna in life.

Beyond the expanded proximal end, the shaft of the radius narrows distally. However, the width of the shaft varies among individual specimens, ranging from 17% (TMP 1986.055.0264) to 93% (TMP 1989.005.1496) of the width of the proximal end. Similar variation was observed in all ceratopsids in this study and is probably partly due to preservational deformation. In all specimens the posterior surface of the shaft is less flattened than that of the proximal end, so that the shaft is relatively circular in cross-section. In some specimens (e.g., TMP 1989.005.1496), however, the shaft is still slightly compressed mediolaterally.

In most cases the distal end is expanded to a greater degree than the proximal end, with the distal width averaging 237% the width of the shaft. The distal end is mediolaterally compressed to a greater degree than the proximal end, being oval in cross-section and tapering

slightly towards the posterior side because of the ulnar facet. The ulnar facet is present on the posterior side of the distal end of the radius (Fig. 2.7A,C,D), and is one of the few identifiable features to occur on all *P. lakustai* radii. The facet originates at the base of the shaft, at the point where expansion of the distal end occurs and extends to the base of the distal articular surface. In well-preserved specimens the ulnar facet forms a slight lip on both the medial and lateral sides of the element (Fig. 2.7C,D), separating the facet from the shaft and from the distal articular surface. The facet projects farther medially than the distal articular surface, forming a separate, tapering process. The anterior surface of the facet is flat, while the posterior side is slightly concave to accommodate the surface of the ulna. This morphology is typical for centrosaurines (e.g., *Centrosaurus* ROM 767; indeterminate pachyrhinosaurin TMP 2002.076.0001; *Styracosaurus* CMN 344) but less easily identifiable in the chasmosaurine specimens examined in this study (*Anchiceratops* CMN 8547; *Arrhinoceratops* ROM 1439; *Chasmosaurus* CMN 2280). This difference may be due to distortion of at least some of the specimens studied, rather than a genuine difference between chasmosaurines and centrosaurines. However, absence of a clear concavity in the well-preserved radius of NHMUK R4948 described by Maidment and Barrett (2011) supports the hypothesis that this feature may indeed distinguish the two groups.

The radius of NHMUK R4948 is also unique in that a condyle is clearly present on the anterior side of the distal end, extending farther distally than the rest of the distal articular surface. This specimen also displays a clear depression between the condyle and the posterior side of the distal end, creating the appearance of two distinct condyles. No other ceratopsid examined, including *P. lakustai,* shows any clear evidence of distinct condyles on the distal end of the element. Instead, the distal end tends to appear somewhat rounded, with no part of the surface being especially prominent ventrally. The only possible exception is the smallest of the

available *P. lakustai* radii, in which the posterior side of the distal end extends slightly farther ventrally than the anterior side. However, this element is highly weathered and broken, and therefore not very reliable.

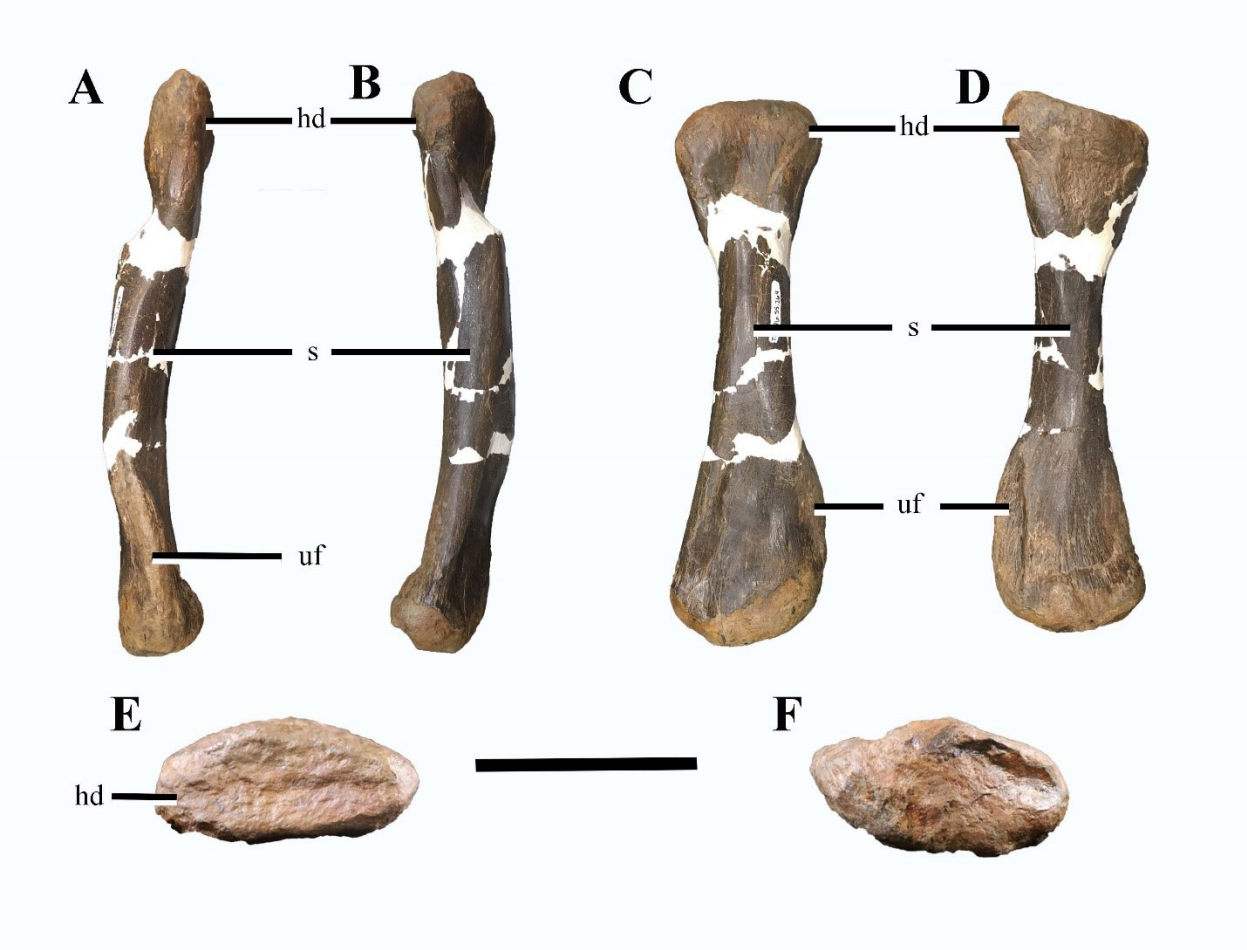

Figure 2.7. *Pachyrhinosaurus lakustai* radius.
TMP 1986.055.0264, left radius, in A) posterior, B) anterior, C) lateral, D) medial, E) proximal, and F) distal views. Scale is 10 cm for A-D and 5 cm for E-F. Abbreviations: hd, radial head; s, shaft; uf, ulnar facet.

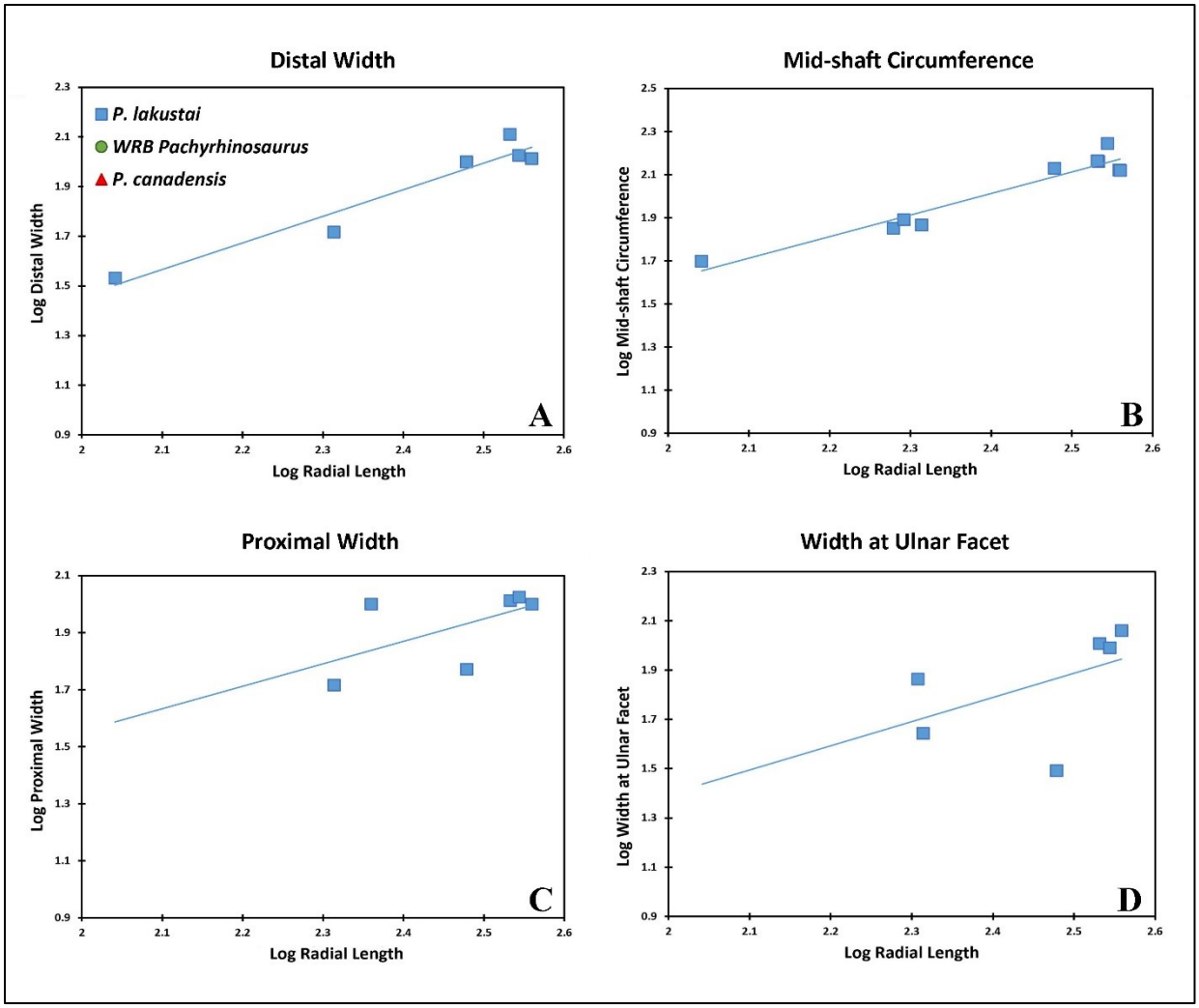

Figure 2.8. Allometry in the radius of *Pachyrhinosaurus.*

Linear regressions of A) distal width, B) mid-shaft circumference, C) proximal width, and D) width at ulnar facet on length for the radius of *P. lakustai*.

Table 2.7. Linear regression results for radial allometry in *Pachyrhinosaurus lakustai.*

Radial Measurement	Allometric Coefficient	Intercept	95% Confidence Interval Lower Bound	95% Confidence Interval Upper Bound	R^2
Circumference	0.9980	-0.3833	0.76	1.23	0.92
Distal Width	1.0713	-0.6844	0.67	1.47	0.93
Proximal Width	1.2917	-1.306	-0.03	2.61	0.76
Width at Ulnar Facet	1.0781	-0.7569	0.62	1.53	0.91

Ulna

The ulna of *Pachyrhinosaurus* is relatively robust, as is typical in ceratopsids (Fig. 2.9). For this study 14 *Pachyrhinosaurus lakustai* ulnae were measured, ranging from 206 mm to 465 mm long (Tab. 2.8). The two WRB *Pachyrhinosaurus* specimens fall within the same range UALVP 52044 and UALVP 52592, which are 406 mm and 390 mm long, respectively). Several ulnar measurements, including proximal width, midshaft circumference, width at midshaft, and distal width, are positively allometric with respect to the total length of the element (Fig. 2.10, Tab. 2.9). Distal width increases isometrically, with a coefficient of 1.06, while the remainder of the coefficients range from 1.22-1.29. It is important to note that no late-juvenile to sub-adult ulnae have been recovered from the bonebed. Sub-adult specimens are poorly represented in the available sample for all elements considered in this study, but for ulnae the ontogenetic gap is particularly wide, and indeed encompasses the large juvenile part of the size range. This gap is clear in the data with the seven smallest *P. lakustai* ulnae ranging from 200-249 mm in length,

and the larger ulnae range from 375-474 mm in length, and full documentation of ontogenetic changes in ulnar morphology.

Table 2.8. Measurements of *Pachyrhinosaurus lakustai* ulnae.

Specimen No.	Length	Proximal Width	Midshaft Width	Distal Width	Circumference
TMP 1986.055.0109	235	73	43	49	
TMP 1987.055.0176	211	72	38	44	92
TMP 1987.055.0263	227				75
TMP 1987.055.0089	393				
TMP 1987.055.0200	393				198
TMP 1988.055.0110	211				91
TMP 1989.055.0049	249	84	42	51	94
TMP 1989.055.0575	428				198
TMP 1989.055.0585	206				90
TMP 1989.055.1203	414				182
TMP 1989.055.0227	396	175	85	102	205
TMP 1987.055.0218	246				91
UALVP 53071					
UALVP 55736	465	165	100	90	205

The ulna of *Pachyrhinosaurus* is proximally broad and distally narrow. The olecranon process is well-defined in *P. lakustai* throughout ontogeny and is mediolaterally flattened in all specimens as a result of distortion (Fig. 2.9A-E), as is typical for material from the Pipestone Creek Bonebed. The olecranon process tapers dorsally as in most ceratopsids (*Anchiceratops*

CMN 8547; *Centrosaurus* ROM 1426; *Chasmosaurus* CMN 2245; *Wendiceratops* TMP 2013.020.0049). This dorsal tapering is more pronounced in some specimens; particularly the smallest (TMP 1987.055.0176) and largest (UALVP 55736) in the data set, than in others.

The proximal end of the ulna is generally quite rounded and anteriorly concave. The convexity of the posterior side varies among individuals. In some specimens (e.g., UALVP 55736, Fig. 2.9) the olecranon process rapidly tapers dorsally, whereas in others this structure tapers more gradually. Similar variation occurs across Ceratopsidae at the interspecific level, with some taxa displaying more abrupt tapering than others. In certain centrosaurine specimens (*Centrosaurus* ROM 1426; *Styracosaurus* CMN 344), the olecranon process bears a slight ridge on the posterior side, but this does not appear in every specimen and is therefore most likely an expression of individual variation.

Distal to the olecranon process, the medial process extends medially, forming a 110° angle with the olecranon process in medial or lateral view. The concave bone surface between the olecranon and the medial process is mediolaterally broad, forming the trochlear notch (Fig. 2.9B-D). The trochlear notch is characterized by a broad, flat, anterior-facing surface that is proportionally larger in large individuals (UALVP 55736) than in small ones (TMP 1989.055.0049), and is semi-lunar in medial and lateral views. In WRB *Pachyrhinosaurus* specimens the medial process is not as prominent as in *P. lakustai*, nor does the trochlear notch form a clear semi-lunar shape. This may be due to heavy erosion on the specimen examined (UALVP 52592), but it is notable that *P. lakustai* ulnae of the same size (TMP 1989.055.227) may show the semi-lunar shape despite being similarly eroded in this area. However, based on cranial measurements *P. lakustai* was smaller in adulthood than *P. canadensis* and WRB *Pachyrhinosaurus* (Fiorillo and Tykoski, 2012; Kruk, 2015). This implies that a WRB

Pachyrhinosaurus specimen of comparable size to a *P. lakustai* specimen may well represent a younger individual than the latter. Therefore, the apparent difference in medial process morphology between the two species may reflect ontogenetic rather than taxonomic variation, particularly given that no sub-adult *P. lakustai* ulnae are known for comparison. The anterior surface of the medial process is flattened (Fig. 2.9C), but not to the degree seen in *Chasmosaurus* (NHMUK R4948, ROM 843). As noted by Maidment and Barrett (2011) this is the site of articulation with the posterior surface of the radius, and the morphology of this area may affect the nature of the contact between the two bones.

The anterolateral process is well-defined in *Pachyrhinosaurus*, unlike in some other centrosaurines (e.g., *Wendiceratops* TMP 2013.020.0049), and this is particularly true of larger specimens (TMP 1989.055.227, UALVP 55736). The process lies on the anterolateral surface of the element and forms a right angle with the medial process in proximal view, as in all other ceratopsids. Throughout ontogeny, the anterolateral process is flanked by deep grooves. This morphology is especially well-developed in mature (UALVP 55736) and juvenile (TMP 1989.055.0049) specimens, and does not seem to be an artifact of deformation given that these specimens show no signs of crushing in the relevant areas. Similar grooves also appear in the indeterminate pachyrhinosaurin TMP 2002.076.0001, but not in any other group included in this study, and therefore may be a diagnostic feature of Pachyrhinosaurini. However, it is unclear if the same morphology occurs in the WRB *Pachyrhinosaurus*, owing to erosion of the anterolateral surfaces in UALVP 52044 and 52592. The anterolateral process extends anterolaterally, but is slightly smaller than the medial process. As described by Maidment and Barrett (2011), the presence of this large anterolateral process forces the radius to lie anteromedial to the ulna, rather than anterior to the ulna as in basal, bipedal ornithischians. This

keeps the manus of ceratopsids in a pronated position (Bonnan, 2003) and therefore makes possible the pattern of forelimb kinematics postulated by Thompson and Holmes (2007).

Beginning at the tip of the anterolateral process, a narrow spine extends distally along the length of the ulna, forming a ridge on the lateral surface of the element. This ridge is present in all stages of ontogeny, but appears better-defined and proportionally larger in mature individuals, extending from the anterolateral process to the midpoint of the ulna (Fig. 2.9C). This ridge is present in other centrosaurines (e.g., *Centrosaurus* ROM 1426), but is not well-developed in chasmosaurines (*Anchiceratops* CMN 8547; *Chasmosaurus* CMN 2280). In WRB *Pachyrhinosaurus* (UALVP 52592) a ridge is present, but more closely resembles the broad, poorly-defined ridges present in juvenile *P. lakustai* specimens than the narrower and sharper ones seen in adults. This lends weight to the interpretation that UALVP 52592 does not represent a fully mature specimen.

The ulna is widest at the level of the anterolateral process, and gradually tapers to a narrow shaft that reaches its minimum width just proximal to the expanded distal end of the ulna. The shaft of the ulna is oval in cross section, with the anteroposterior width exceeding the mediolateral depth. On the lateral side of the ulna, just proximal to the expanded distal end, lies a small, variably developed ridge. This ridge is present in some smaller individuals of *P. lakustai* (TMP 1989.055.0049), but is absent in others (TMP 1986.055.0109). In larger specimens the ridge is much better-developed and forms a small, round prominence (Fig. 2.9C,D). A similar pattern of variability is widespread in ceratopsids, as the ridge is clearly present in some *Centrosaurus* (ROM 767, ROM 1427) and *Chasmosaurus* (e.g., CMN 2245 and NHMUK R4948) specimens but less well-defined in others (*Centrosaurus* TMP 1987.036.0160; *Chasmosaurus* UTEP P.37.7.012; *Wendiceratops* TMP 2014.029.0058).

Beyond the ridge, the distal end of the ulna expands slightly anteroposteriorly, but is slightly compressed mediolaterally. In most cases the entire distal end is heavily rugose, as is typical for ceratopsids. In some *P. lakustai* specimens (including UALVP 55735) the posterior portion of the distal end of the ulna extends farther distally than the anterior portion. However, other specimens (TMP 1987.055.227) show the opposite condition, and in juvenile specimens (e.g., TMP 1989.055.0049) no part of the distal end is especially prominent. Therefore, this is most likely a case of individual variation.

The distinct differences seen in the WRB *Pachyrhinosaurus* specimen UALVP 52044 are most comparable to that of YPM 2015, as described by Lull (1933). These comparable features include a less-expanded anterolateral process and a less-defined ridge that runs from the anterolateral process. Lull (1933) reported the left ulna of YPM 2015 to measure 437 mm in length, and the right ulna to measure 457 mm in length. Therefore, YPM 2015 is larger than most ceratopsids included in the present study, with the exception of *Styracosaurus albertensis* CMN 344, *Chasmosaurus belli* ROM 843, *Pentaceratops sternbergii* PMU.R 268, and all the *Triceratops* specimens. These size comparisons suggest that YPM 2015 was an adult, and therefore that this morphology is not due to ontogenetic variation, but Lull et al. (1933) gave no indication of the age of the specimen. Tanke (2006) referred to this specimen as an adult, but gave no indication as to why.

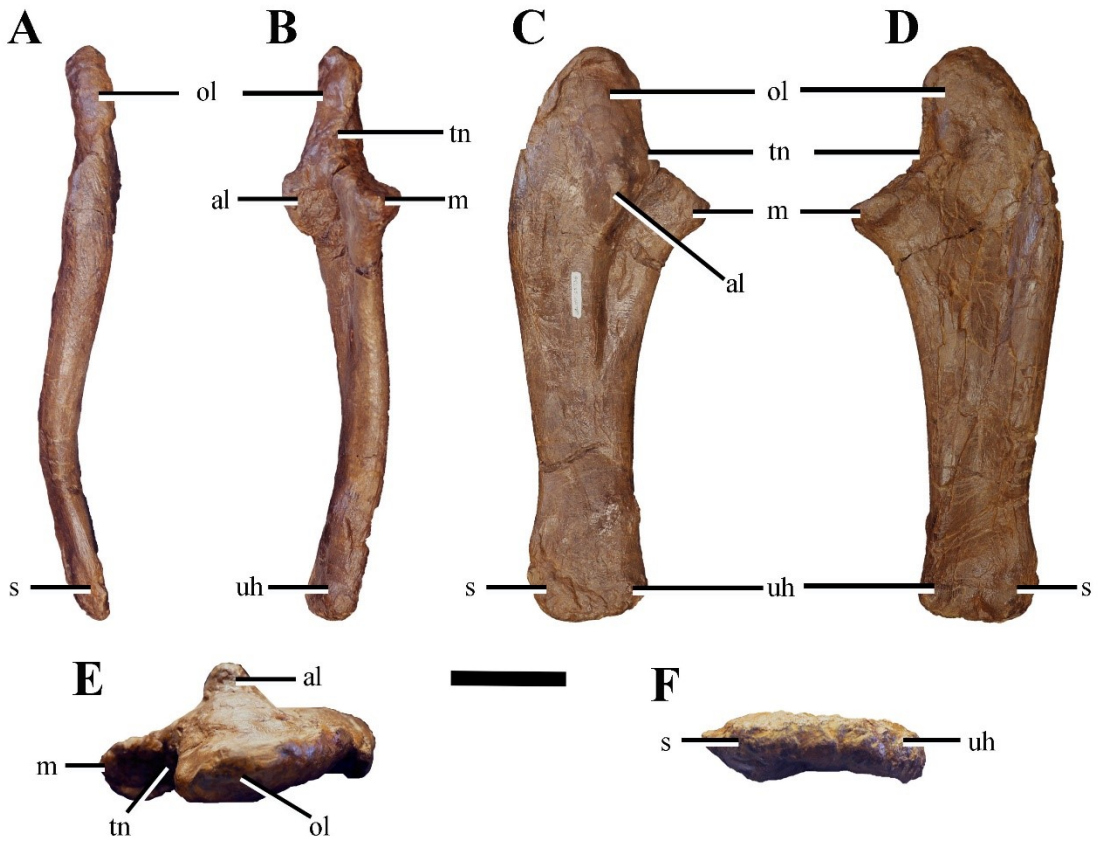

Figure 2.9. *Pachyrhinosaurus lakustai* ulna.

UALVP 55736, right ulna, in A) posterior, B) anterior, C) lateral, D) medial, E) proximal, and F) *distal* views. Scale is 10 cm for A-D and 5 cm for E-F. Abbreviations: al, anterolateral process; m, medial process; ol, olecranon process; pr, pronator ridge; sp, styloid process: tn, trochlear notch.

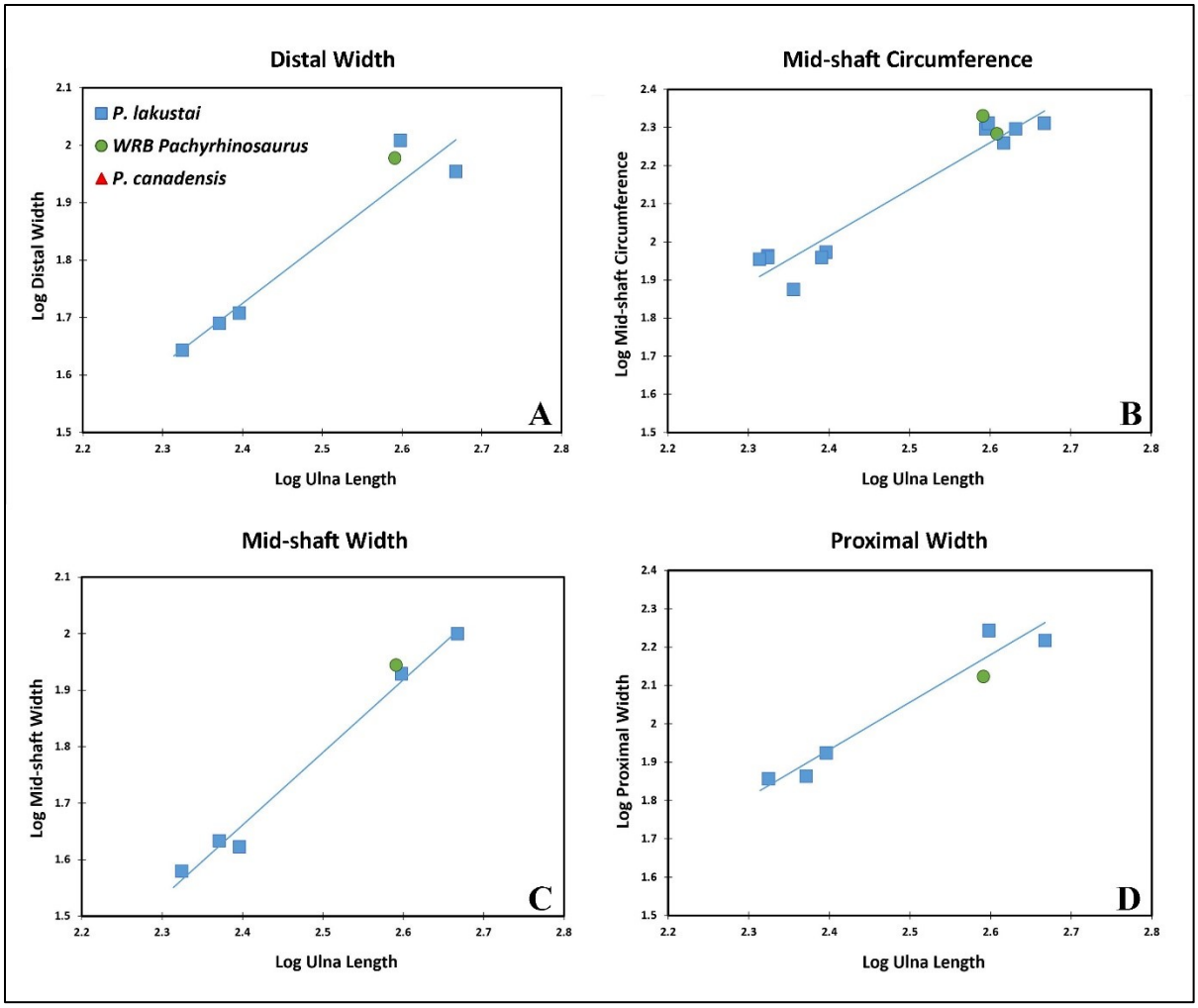

Figure 2.10. Allometry in the ulnae of *Pachyrhinosaurus*.

Linear regressions of A) distal width, B) mid-shaft circumference, C) mid-shaft width, and D) proximal width on length for the ulna of *P. lakustai*. Measurements for the other *Pachyrhinosaurus* species are plotted on the graphs, but were not included in the data set used to compute the regression lines.

Table 2.9. Linear regression results for ulnar allometry in *Pachyrhinosaurus lakustai.*

Ulnar Measurement	Allometric Coefficient	Intercept	95% Confidence Interval Lower Bound	95% Confidence Interval Upper Bound	R^2
Circumference	1.2280	-0.9326	0.98	1.47	0.93
Proximal Width	1.2396	-1.0424	0.70	1.78	0.95
Midshaft Width	1.2854	-1.4235	1.04	1.53	0.99
Distal Width	1.0636	-0.8276	0.50	1.63	0.92

Manus

Due to the taphonomic processes at work during the formation of the Pipestone Creek Bonebed, it is difficult to give a complete description of the manus of *P. lakustai*. Past descriptions of ceratopsian manus have been based on articulated or associated specimens (e.g., Thompson and Holmes, 2007; Fujiwara, 2009), and have relied heavily on the relative sizes of the various elements to ensure their correct identification, and often their position alone. However, this method cannot be used to identify manual elements from the Pipestone Creek Bonebed because the material from the site is almost entirely disarticulated and comes from individuals of sufficiently different sizes and ontogenetic stages that simple proportions cannot be relied on as a guide to identification. For purposes of this description, *P. lakustai* is hypothesized to have the same phalangeal formula, namely 2-3-4-3-2, reported previously for the articulated manus of *Centrosaurus apertus* (AMNH FR 5351) (Brown, 1917), and for those of *Chasmosaurus irvinensis* (CMN 41357) and *Chasmosaurus belli* (ROM 843) (Rega et al., 2010). No elements were identified in collections that resembled distal carpals, even though distal carpals 3 and 4 have been found in some articulated ceratopsid manus (Mallon and Holmes,

2010; Rega et al., 2010). Based on their sizes, all the metacarpals used in this study are hypothesized to be from mature individuals. Figure 2.11 and 2.12 are artistic representations of the full manus in a schematic, slightly exploded view (Fig. 2.11) and in reconstructed natural articulation (Fig. 2.12).

Table 2.10 Measurements of *Pachyrhinosaurus* metacarpals.

Specimen No.	Taxon	ID	Length	Proximal Width	Distal Width	Circumference
UALVP 57914	*P. lakustai*	MC I	90	57	46	124
UALVP 57434	WRB *Pachyrhinosaurus*	MC I	92	70	65	146
UALVP 55008	*P. lakustai*	MC II	121	45	40	81
UALVP 54961	*P. lakustai*	MC II	140	56	56	102
UALVP 57652	*P. lakustai*	MC II	100			75
UALVP 57687	*P. lakustai*	MC II	140			104
UALVP 54981	*P. lakustai*	MC III	66	35	29	55
UALVP 60360	*P. lakustai*	MC III	153	76	64	
UALVP 55416	*P. lakustai*	MC III	164	47	59	113
UALVP 57912	*P. lakustai*	MC IV	160			107
UALVP 55023	*P. lakustai*	MC IV	137	87	58	118
TMP 1989.055.1369	*P. lakustai*	MC V	80			106.5
UALVP 53621	*P. lakustai*	?	130	58	51	92

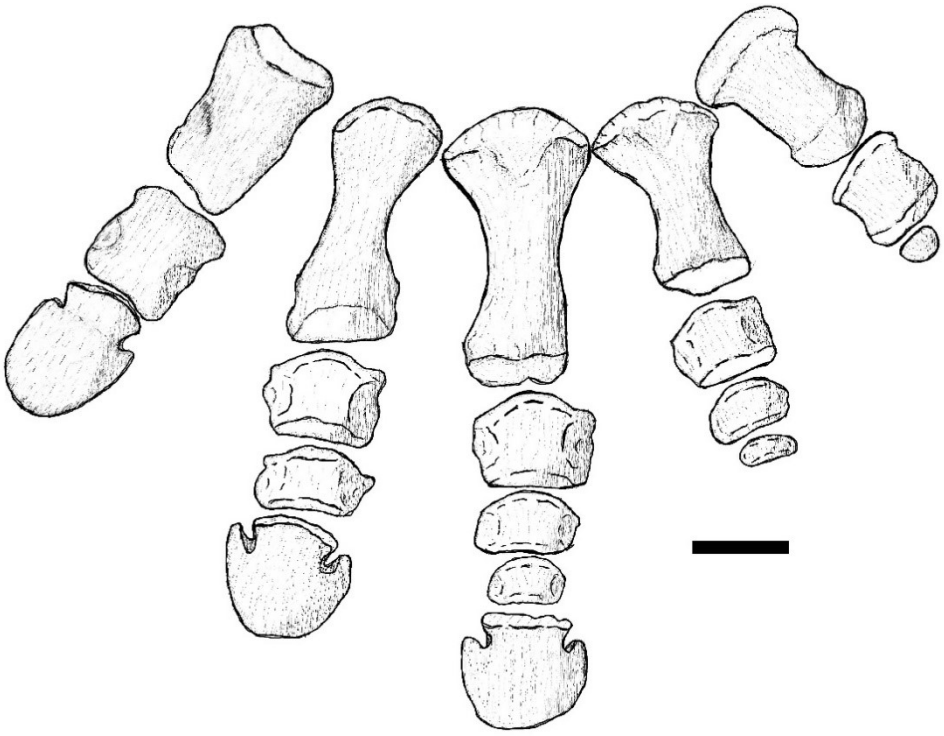

Figure 2.11. Reconstructed adult *Pachyrhinosaurus* manus in a schematic, slightly exploded layout.

Left manus in dorsal view. *P. lakustai* elements reconstructed using the following specimens: MC I, UALVP 57914; MC II, UALVP 54961; MC III, UALVP 55023; MC IV, UALVP 57912; MC V, TMP 1989.055.1369; Ph 1-I, UALVP 54282; Ph II-1, Ph III-1, Ph IV-1, UALVP 52948; Ph II-2, Ph III-2, Ph IV-2, Ph III-3, Ph IV-3, UALVP 54767. Elements not identifiable among the *P. lakustai* specimens examined for this study were reconstructed on the basis of *Centrosaurus* elements from AMNH FR 5351 and ROM 767. Scale is 5 cm.

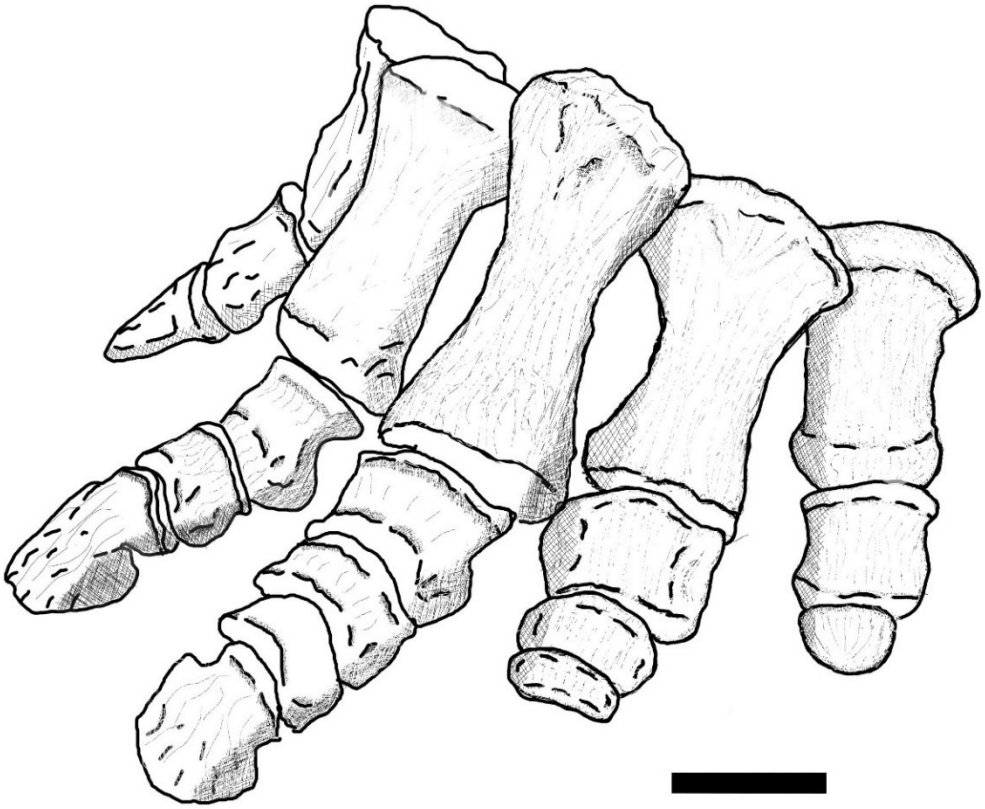

Figure 2.12. Reconstructed adult *Pachyrhinosaurus* manus in natural articulation. Articulated left manus in lateral view. *P. lakustai* elements reconstructed using the following specimens: MC I, UALVP 57914; MC II, UALVP 54961; MC III, UALVP 55023; MC IV, UALVP 57912; MC V, TMP 1989.055.1369; Ph 1-I, UALVP 54282; Ph II-1, Ph III-1, Ph IV-1, UALVP 52948; Ph II-2, Ph III-2, Ph IV-2, Ph III-3, Ph IV-3, UALVP 54767. Elements not identifiable among the *P. lakustai* specimens examined for this study were reconstructed on the basis of *Centrosaurus* elements from AMNH FR 5351 and ROM 767. Scale is 5 cm.

Metacarpal I

Metacarpal I is much shorter and stouter than metacarpals II-IV, with available examples of this element ranging from 90 to 123 mm in length and from 117 to 124 mm in midshaft circumference. The first metacarpal of WRB *Pachyrhinosaurus* (UALVP 57434) is even more

robust with a circumference of 146 mm and a length of 92 mm. This element has essentially the same overall shape as those in all other ceratopsids. The broad proximal end is elliptical in outline being wider mediolaterally than dorsoventrally, with a flat ventral side (Fig. 2.13). The proximal end is relatively flat, with no distinct grooves, as is the case for the proximal ends of all ceratopsid metacarpals. The proximal end tapers slightly into the main shaft of the bone. Distal to the proximal end, the ventral side of the element becomes slightly concave along its length, such that the proximal end forms a slight lip on the ventral side as it tapers to the shaft. The transverse expansion of the metacarpal is the same width as the shaft of the element, such is common across Ceratopsidae (e.g., *Centrosaurus,* ROM 767, and *Chasmosaurus,* ROM 843). Asymmetrical collateral ligament fossae are present on the radial and lateral sides of the distal end of the metacarpal. These shallow fossae are found on all well-preserved ceratopsid metacarpals, although they are not evident on more weathered specimens. A medially-projecting flange is situated ventral to the medial fossa in the WRB *Pachyrhinosaurus* specimen UALVP 57434. The distal end of the element is trapezoidal, the ventral margin being broader than the dorsal, and has distinct grooves for articulation with the phalanges.

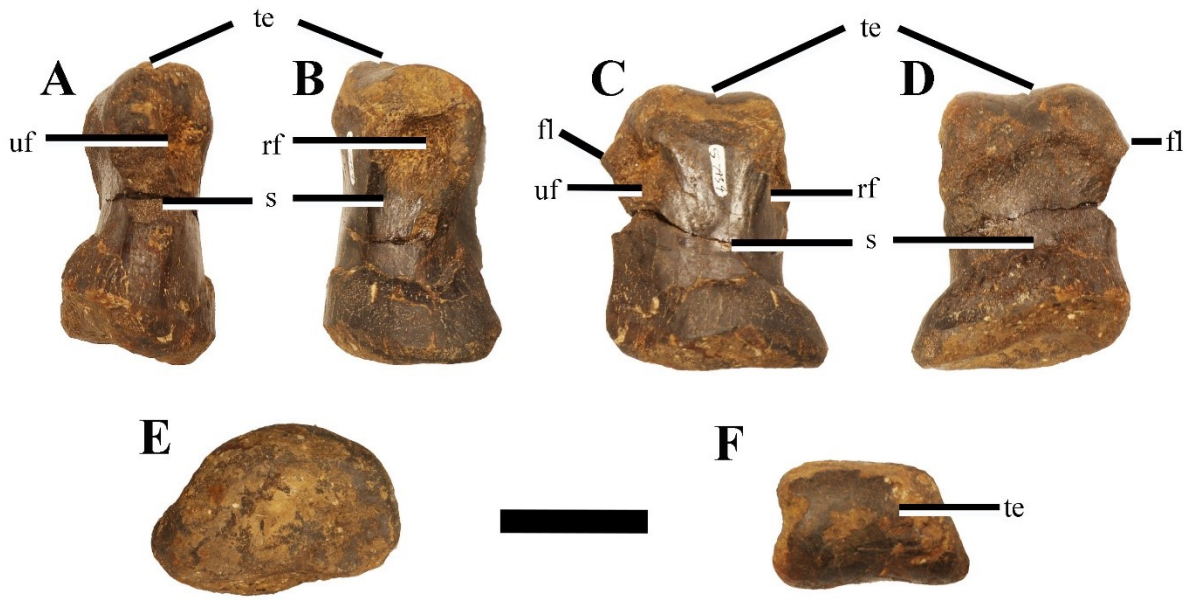

Figure 2.13. *Pachyrhinosaurus* metacarpal I.
UALVP 57434, left metacarpal I from WRB *Pachyrhinosaurus*, in A) lateral, B) medial, C) dorsal, D) ventral, E) proximal, and F) distal. *P. lakustai* first metacarpal was not used due to absence of non-pathological specimens. Scale is 5 cm. Abbreviations: te, transverse expansion; f, fossa; fl, flange; s, shaft.

Metacarpal II

The second metacarpal is much longer than the first (Fig. 2.14), the largest available specimen measuring 140 mm long. In most adult examples of this element (e.g., UALVP 57687, UALVP 54961) the medial side of the proximal end extends farther proximally than the lateral side, so that the proximal end is angled relative to the long axis of the shaft. This obliquity is not apparent in the second metacarpal of the *Centrosaurus* manus ROM 767, and may be a product of weathering. However, a similar morphology can be observed in metacarpal II of the left manus of *Chasmosaurus belli* (ROM 843). In smaller specimens (e.g., UALVP 55008) the proximal end is subcircular. At all ontogenetic stages the proximal end is sub-triangular in

outline with a depression on the lateral side. This depression is present in *Centrosaurus* (CMN 767) and *Chasmosaurus* (CMN 41358). Another depression lies on the dorsal side of the element, and is better-developed in larger, mature specimens than in smaller, younger ones. The lateral side of the proximal end is quite flat compared to the medial side to form a broad contact with the first metacarpal as seen in *Centrosaurus* (ROM 767), but not with the third metacarpal. The proximal end tapers into the shaft of the bone to a greater extent than occurs in the first metacarpal. The shaft accounts for just over half the length of the bone on average and expands again at the distal end of the metacarpal. The distal fossa described for metacarpal I is also present in metacarpal II and forms a distinct triangular projection on both the lateral and medial sides of the bone at the proximal edge of the fossa. These triangular processes are found in many ceratopsids, such as *Centrosaurus* (ROM 767) and *Chasmosaurus* (CMN 41357 and ROM 843), but are typically not pronounced on the lateral side. The distal transverse expansion is more distinct than in the first metacarpal; it is separated from the shaft by a precise boundary, and the distal surface becomes convex and distinctly grooved.

Figure 2.14. *Pachyrhinosaurus* metacarpal II.
UALVP 54961, *P. lakustai* left metacarpal II, in A) ulnar, B) medial, C) dorsal, D) ventral, E) proximal, and F) distal. Scale is 5 cm. Abbreviations: d, depression; te, transverse expansion; f, fossa; fl, flange; s, shaft.

Metacarpals III and IV

Metacarpal III and IV are very similar in shape and in ceratopsids are typically distinguished based on their proportions or position in the manus of articulated specimens. For this reason this description applies to both elements unless otherwise noted. The third metacarpal is typically longer relative to the width of the element than the fourth as seen in *Centrosaurus* (e.g., ROM 767 and AMNH FR 5351) and *Chasmosaurus* (e.g., ROM 843 and CMN 41357). (Fujiwara, 2009) noted a proximally located intermetacarpal contact on the medial side of

metacarpal III that is not present on metacarpal IV. This holds true in some chasmosaurine specimens (e.g., *Chasmosaurus,* CMN 41357), whereas others lack the intermetacarpal contact altogether (e.g., *Anchiceratops,* CMN 8457; *Chasmosaurus,* ROM 843). All centrosaurine specimens studied either show no evidence of this intermetacarpal contact (e.g., AMNH FR 5351) or lack the relevant portions of both metacarpals three and four due to breakage (ROM 767). Based on the ceratopsid material examined it can be inferred that UALVP 55023 (Fig. 2.15) is likely metacarpal III because it is slightly longer relative to its width in comparison to UALVP 57912 (Fig. 2.16), which is inferred to be metacarpal IV. However, there is no further evidence for this identification and both specimens may represent the same metacarpal.

The proximal ends of metacarpals III and IV are flared transversely, as is common in all ceratopsid manus (*Centrosaurus* ROM 767; *Chasmosaurus* CMN 41357 and ROM 843). The proximal end is sub-triangular in outline with a dorsal tip, and bears a distinct depression on the dorsolateral side. This depression is present in both small (UALVP 54981) and large (UALVP 55023, UALVP 57912) specimens, suggesting it occurs throughout all stages of ontogeny. No such depression is evident in the *Triceratops* manus (NSM PV 20397, Fujiwara, 2009: fig. 4). The medial side of the proximal end of metacarpal IV is relatively flat in *Triceratops,* but more ridge-like in *P. lakustai*. This triangular morphology with a dorsal tip appears to be limited to *Centrosaurinae*, as it was also observed in *Centrosaurus* (ROM 767) but not in Chasmosaurinae such as *Chasmosaurus* (CMN 41357, ROM 843) and *Triceratops* (Fujiwara, 2009).

Metacarpals III and IV rapidly taper distally into narrow shafts. In *Triceratops* (Fujiwara, 2009) the shaft tends to be more dorsoventrally compressed in metacarpal IV than in metacarpal III. In *P. lakustai,* however, there is no evidence of this type of variation that can be safely attributed to a distinction in shape between the two metacarpals rather than to ontogenetic

differences. The distal ends of these elements are subrectangular in outline in larger specimens (e.g., UALVP 57912 and UALVP 55023), and slightly more trapezoidal in younger ones (UALVP 54581). In all cases there appear to be indistinctly developed fossae on the medial and lateral sides of the distal end, with a small flange projecting laterally in a position ventral to the lateral fossa. In all specimens the distal end is quite flat, and bears distinct grooves as seen in all the other metacarpals.

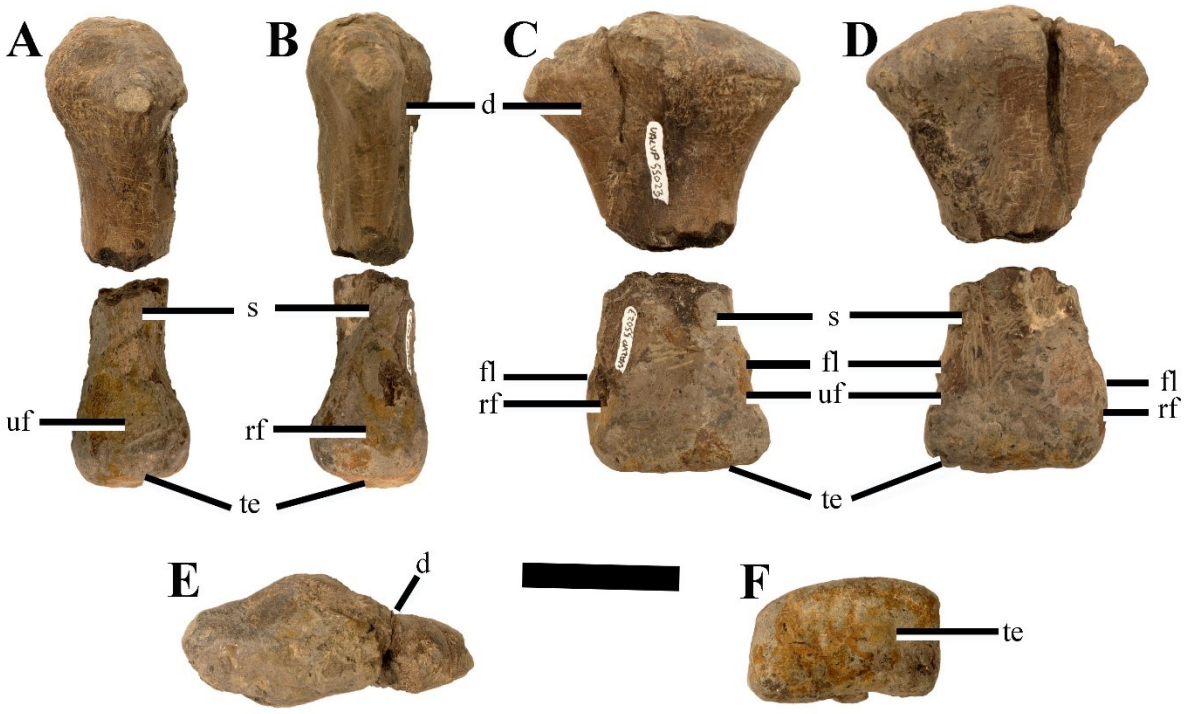

Figure 2.15. *Pachyrhinosaurus* metacarpal III or IV.
UALVP 55023, *P. lakustai* left metacarpal III or IV, in A) lateral, B) medial, C) dorsal, D) ventral, E) proximal, and F) distal. Scale is 5 cm. Hypothesized to be metacarpal III due to being more elongate than UALVP 57912, but may be metacarpal IV. Abbreviations: d, depression; te, transverse expansion; f, fossa; fl, flange; s, shaft.

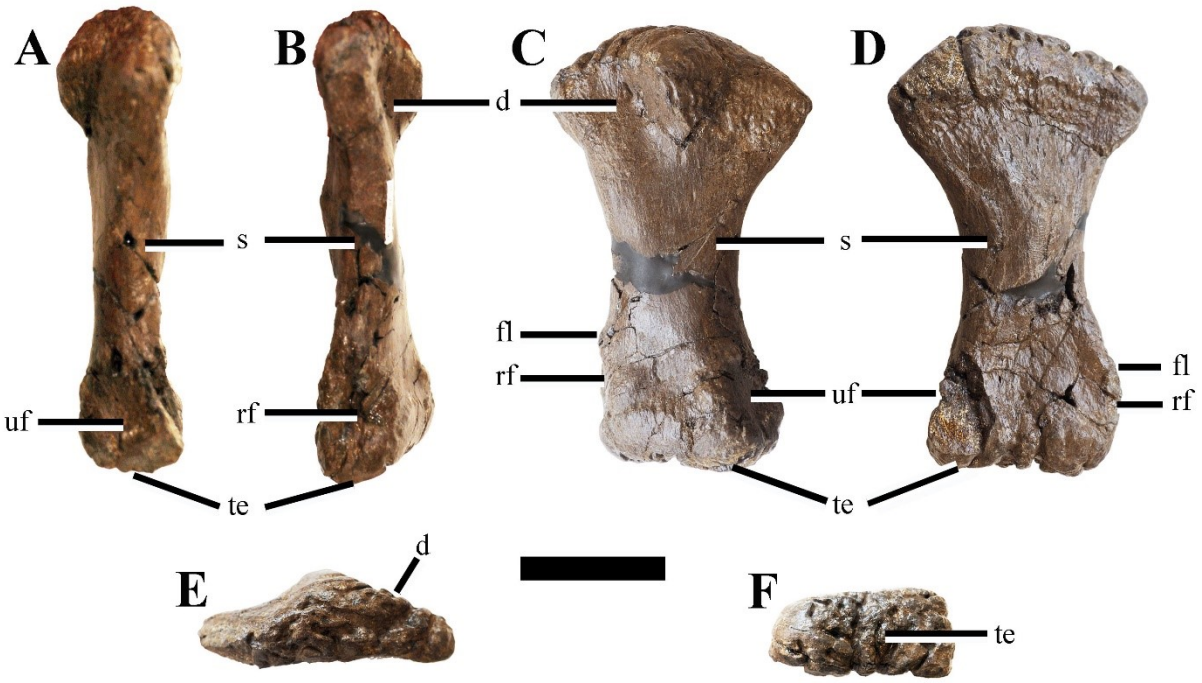

Figure 2.16. *Pachyrhinosaurus* metacarpal III or IV.
UALVP 57912, *P. lakustai* left metacarpal III or IV, in A) lateral, B) medial, C) dorsal, D) ventral, E) proximal, and F) distal. Scale is 5 cm. Hypothesized to be metacarpal IV due to being more robust than UALVP 55023, but may be metacarpal III. Abbreviations: d, depression; te, transverse expansion; f, fossa; fl, flange; s, shaft.

Metacarpal V

The only *P. lakustai* metacarpal V which could be identified in the collections examined for this study, TMP 1989.055.1369, possesses a pathological surface (described in chapter 4 of this thesis). As the pathology is less pronounced than in the pathological *P. lakustai* metacarpal I, however, TMP 1989.055.1369 is described here. The fifth metacarpal is very distinct from the other four, despite being somewhat similar to metacarpal I in its short, relatively robust general shape (Fig. 2.17). However, it is smaller than metacarpal I. TMP 1989.055.1369 is only 80 mm

long but has a circumference of 106.5 mm, making it generally more robust than metacarpal I. The proximal end of metacarpal V is mediolaterally expanded in comparison to the rest of the element, but slightly dorsoventrally compressed. The proximal end quickly tapers into a short but relatively narrow shaft. Other ceratopsian fifth metacarpals also tend to taper towards the shaft, but not quite as abruptly as seen in *P. lakustai*. For example, the tapering is more gradual in *Centrosaurus* (ROM 767, AMNH FR 5351), and *Chasmosaurus* (CMN 41357), *Triceratops* (Fujiwara, 2009). On the proximal ends of the shaft lie medial and lateral fossae as seen in most of the other fifth metacarpals in Ceratopsidae. The distal end of the element expands slightly relative to the shaft, and the distal articular surface is much more convex than in any of the other metacarpals. This round morphology is typical of all ceratopsian fifth metacarpals, but the degree of distal expansion seen in *P. lakustai* appears unique. This may be diagnostic of the species, but may also simply reflect individual variation, as only one fifth metacarpal has been identified from the Pipestone Creek Bonebed.

Overall, the fifth metacarpal of *P. lakustai* closely resembles that of centrosaurines examined for this study (e.g., *Centrosaurus,* ROM 767; and the indeterminate pachyrhinosaurin, TMP 2002.076.0001), as well as select chasmosaurines (i.e. *Chasmosaurus irvinensis*, CMN 41357, *Triceratops,* NSM PV 20379). However, other chasmosaurines tend to have long and narrow fifth metacarpals that even tend to vary in shape and proportions between the two sides of the same individual (*Anchiceratops*, CMN 8547; *Chasmosaurus belli*, ROM 843).

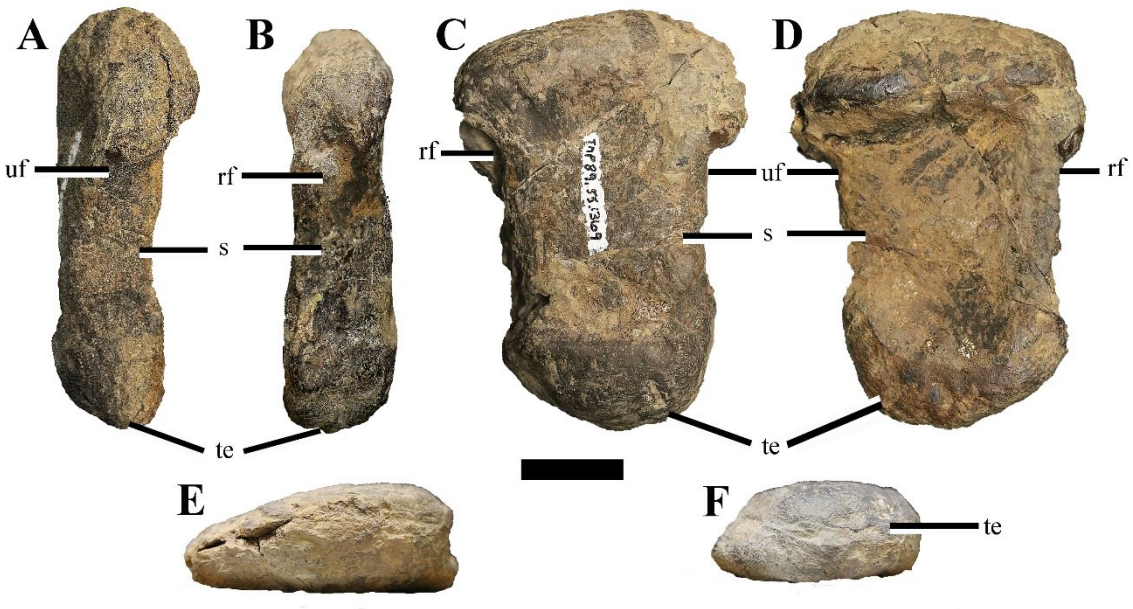

Figure 2.17. *Pachyrhinosaurus* metacarpal V.

TMP 1989.055.1369, *P. lakustai* metacarpal V, in A) lateral, B) medial, C) dorsal, D) ventral, E) proximal, and F) distal. Scale is 2 cm. Severe pathology present on medial surface, distorting normal morphology. Abbreviations: te, transverse expansion; f, fossa; fl, flange; s, shaft.

Phalanges

As with the metacarpals, it is difficult to give detailed descriptions of the phalanges of *Pachyrhinosaurus lakustai* given that all of the available specimens are disarticulated; therefore their positions within the manus cannot readily be determined. However, comparisons between phalanges from the Pipestone Creek Bonebed and those preserved in articulated manus of other ceratopsid species permit four phalanges to be assigned to specific positions, and the remainder to be separated into three distinct groups. Similar groupings were alluded to by Fujiwara (2009) but not named or described in detail. As there is little variation among ceratopsid phalanges, the system of categorization developed here should be applicable to all disarticulated ceratopsid phalangeal elements, unless otherwise specified.

Phalanx I-1

UALVP 54282 (Fig. 2.18) represents phalanx I-1 of *P. lakustai*. This phalanx is relatively similar in shape to the first metacarpal, being very robust with little tapering towards the midshaft of the element. It differs from the first metacarpal, and from the other phalanges in being as long as wide, and sub-rectangular in dorsal and ventral views. Although the proximal and distal ends of UALVP 54283 are quite weathered, this bone appears similar to the better-preserved phalanx I-1 of *Centrosaurus* ROM 767, and to the *Centrosaurus* phalanx I-1 described by Brown (1917). As in the first metacarpal, the proximal end of phalanx I-1 is relatively flat, although there is a slight depression on the proximal articular surface of the element. The bone tapers slightly to form a narrowed midshaft, but not to the extent seen in other phalanges or in any metacarpal. As in *Centrosaurus* (ROM 767) the ventral side of the phalanx is slightly concave, both proximodistally and mediolaterally, and weathered fossae are present on the medial and lateral sides of the distal end of the element. Areas of breakage occur ventral to these fossae, indicating the presence in the undamaged phalanx of medial and lateral projecting processes as seen in phalanx I-1 of *Centrosaurus* ROM 767. The distal end of the element is trapezoidal in cross-section and slightly ginglymoid.

The morphology of phalanx I-1 does appear to vary to some extent across *Ceratopsidae.* In centrosaurines the element closely resembles its counterpart in *P. lakustai,* but in chasmosaurines the proximal end is slightly more mediolaterally expanded. In the *Triceratops* specimen described by Fujiwara (2009) there appear to be no medial or lateral fossae on the distal end of phalanx I-1, but this may be due to weathering. Phalanx I-1 is the largest phalanx in the ceratopsid manus and is most readily identified by the fact that it is equally long and wide, unlike any of the other phalanges.

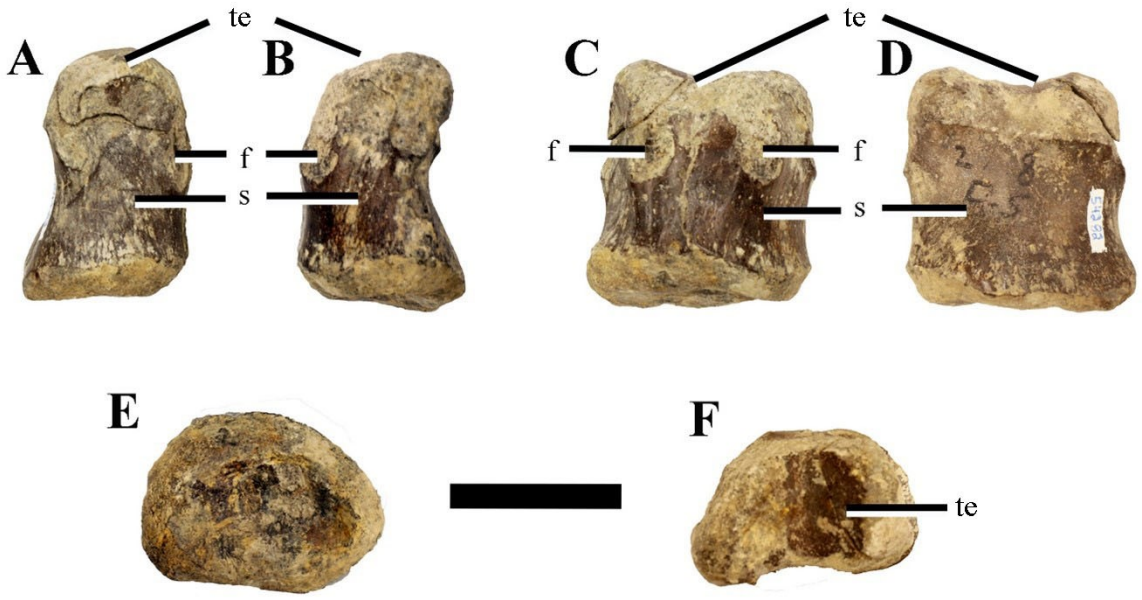

Figure 2.18. *Pachyrhinosaurus* phalanx 1-I.
UALVP 54282, *P. lakustai* phalanx 1-I , in A) medial, B) lateral, C) dorsal, D) ventral, E) proximal, and F) distal views. Scale is 5 cm. Abbreviations: te, transverse expansion; f, fossa; s, shaft.

Phalanx Group 1

The first group of phalanges includes the first phalanges of digits II (phalanx II-1), III (phalanx III-1) and IV (phalanx IV-1), and is represented by the *P. lakustai* specimens UALVP 54766, UALVP 52948 (Fig. 2.19) and UALVP 55031. Phalanges in this group are not nearly as proportionally long as phalanx I-1, as their length averages only 78% of their width. The proximal ends of the phalanges are concave, to match the convexity of the distal ends of the metacarpals, and trapezoidal in outline. They taper distally to a greater extent than phalanx I-1, but abruptly expand again mediolaterally towards the distal end. As is typical for manual elements, the ventral surface is slightly concave along its length. In other associated and

articulated ceratopsid manus (e.g., *Centrosaurus* ROM 767, *Chasmosaurus* CMN 41357), phalanx III-1 is notably longer and wider than phalanx II-1 and phalanx IV-1 of the same individual. In a bonebed sample that contains a multitude of disarticulated individuals of varying sizes, however, it becomes nigh impossible to make such distinctions.

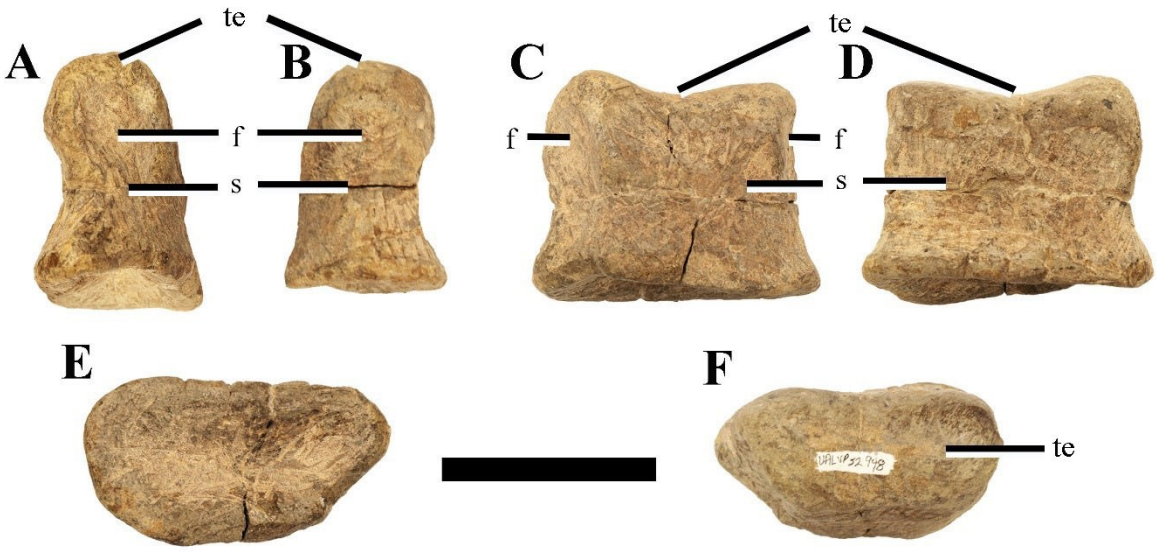

Figure 2.19. *Pachyrhinosaurus* group 1 phalanx.
UALVP 52948, *P. lakustai* phalanx in group 1, in A) lateral/medial, B) lateral/medial, C) dorsal, D) ventral, E) proximal, and F) distal views. Scale is 5 cm. Abbreviations: te, transverse expansion; f, fossa; s, shaft.

Phalanx Group 2

The second group of phalanges is the largest, and includes the second phalanges of digits II (phalanx II-2), III (phalanx III-2) and IV (phalanx IV-2) as well as the third phalanges on digits III (phalanx III-3) and IV (phalanx IV-3). This group is represented by a very large number of *P. lakustai* specimens, including UALVP 54767 (Fig. 2.20). Phalanges in this group are similar to Group 1 elements, having a concave proximal articular surface and trapezoidal

outline. Some of these phalanges have medial and lateral fossae that form distal prominences lying ventral to the fossae in some specimens. However, the development of these fossa varies greatly from one specimen to the other, and sometimes within the same specimen, as is true for all ceratopsids. Phalanges in this group are particularly squat, and the lengths of the elements range from 50-60% the transverse widths. However, their morphologies vary greatly even within the same individual, as seen in associated and articulated specimens (*Centrosaurus* ROM 767; *Chasmosaurus* CMN 41357). Generally, in associated ceratopsid manus, the concavities and fossae appear less pronounced in more distal elements. Given this, it is likely feasible to distinguish among these phalanges in a sample derived from individuals of uniform body size. However, the added complications of size variations due to ontogeny and other factors rends this impossible.

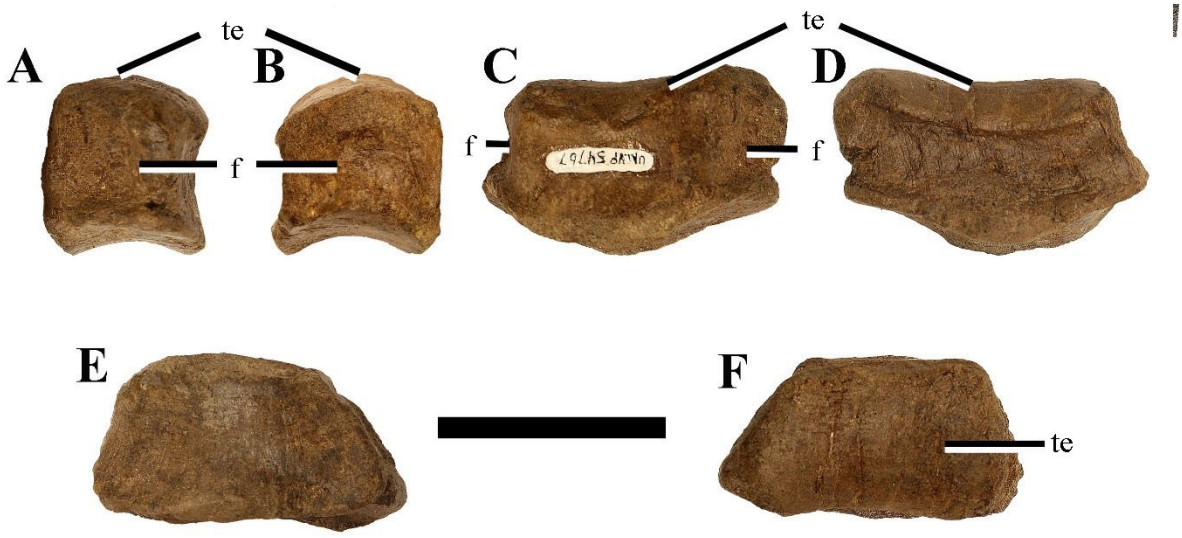

Figure 2.20. *Pachyrhinosaurus* group 2 phalanx.
UALVP 54767, *P. lakustai* phalanx from Group 2, in A) lateral/medial, B) lateral/medial, C) dorsal, D) ventral, E) proximal, and F) distal views. Scale is 5 cm. Abbreviations: te, transverse expansion; f, fossa.

Phalanx V-1

As no identifiable V-1 phalanges have been collected from Pipestone no description of this element can be given for *P. lakustai.* Based on observations from phalanx V-1 in other ceratopsids, the element is square overall with the element being approximately as long as it is mediolaterally wide. As in all other phalanges it is slightly dorsoventrally compressed and slightly concave on the ventral surface. In chasmosaurines phalanx V-1 is not rectangular, but instead the shaft of the element is more elongate and mediolaterally narrow with expansion to the proximal and distal ends.

Phalanges Group 3

The third group of phalanges consists of the manual unguals, which are consistently present on the first three digits across Ceratopsidae. As with the other phalanges, these elements are only distinguishable based on their relative sizes. Therefore, it is difficult to identify them individually within a bonebed sample containing disarticulated skeletal material representing multiple ontogenetic stages. The ungual on the first digit is more elongate than those of the second and third digits in one *Centrosaurus* specimen (ROM 767), but this is not the case in others (e.g., AMNH FR 5351). No subset of *P. lakustai* unguals were identified with this elongate morphology, however this may be a defining feature for the ungual on digit I. The overall morphologies of ceratopsid unguals vary substantially, as the thinness of the tips of these elements make them highly susceptible to breakage. In general, they are as semi-circular hoof-like structures, mounted on a relatively robust proximal end for attachment to the penultimate phalanx of the corresponding digit. This proximal end is typically quite dorsoventrally flat, and passes distally into a short shaft which then flares mediolaterally. These medial and lateral

expansions of the ungual curve back proximally, forming hook-like structures on either side of the shaft. The element narrows quite drastically dorsoventrally from proximal end to the thin distal margin. The distal margin is semi-circular in dorsal view at the tip of the toe.

Phalanx V-2

There are no identifiable examples of phalanx V-2 from the Pipestone Creek Bonebed. However, it can be inferred from articulated ceratopsian manus that *P. lakustai* possessed a second phalanx on the fifth digit, but lacked an ungual on the fourth digit, as seen in articulated ceratopsian manus. Phalanx V-2 has a generally consistent morphology across Ceratopsidae, being a small, bulbous element at the end of the fifth digit with a rounded and essentially featureless proximal end.

Discussion

The forelimb of *Pachyrhinosaurus lakustai* displays several characters that appear diagnostic of the species, or in some cases the genus. *P. canadensis* differs from *P. lakustai* in possessing a more laterally prominent and robust scapular ridge. On a generic level, *Pachyrhinosaurus* possesses a poorly defined concavity on the anterior part of the medial side of the scapula, which differs from other ceratopsids. *Pachyrhinosaurus* also has a prominent ectepicondyle on the humerus, whereas this feature is much less well-developed in other centrosaurines, such as *Wendiceratops*. The ulna of *Pachyrhinosaurus* also consistently seems to bear a posteriorly displaced anterolateral process, flanked by distinct grooves.

Based on the ceratopsids studied, the mid-blade width of the scapula tends to be relatively consistent in centrosaurines and chasmosaurines of similar size. However, measurements reveal

clear differences in the proportional widths of the anterior and posterior ends of the scapula between centrosaurines and chasmosaurines. The anterior end of the scapula is dorsoventrally wider in centrosaurines than in chasmosaurines, relative to the midpoint of the blade (ranging from 128-247% and averaging 189% in centrosaurines, and ranging from 101-120% and averaging 120% in chasmosaurines). The posterior end of the scapula, however, is dorsoventrally wider in chasmosaurines than in centrosaurines, relative to the midpoint of the blade (ranging from 97-157%, averaging 117% in centrosaurines, and ranging from 112-208%, averaging 175% in chasmosaurines). The scapular ridge is narrower and more laterally pronounced in a chasmosaurine, extending farther obliquely towards the posterior end of the blade and nearly reaching the posterior margin of the element. The two groups can also be distinguished on the basis of humeral morphologies. The humeral head is much more prominent in a chasmosaurine, protruding farther posterolaterally and dorsally than in a centrosaurine. Furthermore, each chasmosaurine possesses a distinct notch separating the medial tubercle from the main proximal surface of the humerus. Lastly, average measurements in this study indicate that the deltopectoral crests of the humeri tend to be proportionally larger in chasmosaurines, extending for about 63% of the length of the element compared to only 47% of the length of the element in centrosaurines.

In general, as the scapula of *P. lakustai* increases in length, the width proportionally decreases. This is particularly true of the maximum width, which had the lowest allometric coefficient of any scapular measurement. Conversely, the humerus tends to increase in overall robustness with age, which is expected due to its weight-bearing nature. Distal condyle width is the humeral measurement associated with the highest allometric coefficient. The radius also seems to become more robust throughout ontogeny, the width of the proximal end having the highest allometric coefficient. The ulna undergoes a more drastic increase in robustness,

allometric coefficients for width measurements are higher for this element than for the humerus and the radius. Measurements for the only available specimens of *P. canadensis* and WRB *Pachyrhinosaurus*, which were large enough to be presumed adult, tended to plot along the *P. lakustai* regression lines. This might indicate conformity to the general allometric pattern of *P. lakustai*, but measurements from less ontogenetically advanced specimens would be needed for confirmation. Despite the abundance of material from the Pipestone Creek Bonebed, the overall small sample size resulted in wide confidence intervals, all of which include 1.0 and therefore encompass isometry. The wide confidence intervals may result in part from statistical noise in the sample due to deformation of some elements and not others. The type of plastic deformation previously reported to occur at the Pipestone Creek Bonebed (Currie et al., 2008) was observed in many adult elements examined, but was much less severe in juvenile specimens. It is likely that the high incidence of deformation would have led to some inaccurate measurements, particularly with respect to lengths and circumferences. The inaccuracies may have manifested themselves as statistical noise, leading to the wide confidence intervals calculated in this study. Give the high overall R^2 values, however, it is evident that there were few outliers in the dataset.

Implications for Gait and Step-cycle

This study did not focus on modeling the step-cycle and gait of *Pachyrhinosaurus lakustai*, an endeavour that would be particularly difficult given the disarticulated state of the Pipestone specimens and the consequent near-impossibility of identifying bones that belong to the same individual. However, some inferences regarding gait can be drawn by interpreting morphological features described in this paper in the light of previous research on ceratopsian locomotion. This is a topic that has been debated for decades, dating back to Russell's (1935)

description of ceratopsid forelimb musculature. Some authors propose that ceratopsids would have had a sprawling gait with their elbow joint projecting laterally and their forelimbs in a crouched position (e.g. Johnson and Ostrom, 1995), while others have proposed an erect gait (e.g. Alexander, 1989). However, the widely-accepted hypothesis is that ceratopsids' gait was part way between sprawling and erect in what is referred to as a semi-erect gait. One such study that proposed this semi-erect gait is that by Thompson and Holmes (2007). Thompson and Holmes (2007) modeled the step-cycle of *Chasmosaurus irvinensis,* based on the nearly complete skeleton CMN 41357, using half-scale models as well as trackway data. The forelimb elements of *C. irvinensis* fall within the normal size range for *P. lakustai* specimens, ensuring that scaling effects do not complicate functional comparisons between these taxa.

Thompson and Holmes (2007) analyzed their model with reference to trackway data, and found that *Chasmosaurus* and other neoceratopsians (based on extensive similarities in overall forelimb and pectoral girdle anatomy) most likely used a semi-erect forelimb posture, somewhere between the erect stance of graviportal mammals such as elephants and the sprawling gait of typical extant lizards. In their model, the movement of the forelimb was mainly constrained by the shoulder joint. For the humeral head to remain in articulation with the glenoid fossa, without the deltopectoral crest interfering with the function of the pectoral musculature, the humerus had to be relatively horizontal. Specifically, the humerus would have been at an angle of 37° to the horizontal and 27°, when viewed anteriorly, from the parasagittal plane (Thompson and Holmes, 2007). In this position the medial tubercle of the humerus would have been directly anterior to the ninth cervical rib, and would have had 15 mm of clearance relative to the anterior portion of the rib cage. However, this clearance is most likely underestimated, given that the more anterior cervical ribs are shorter and straighter than the ninth cervical rib.

Therefore, the medial tubercle most likely did not impose a stringent kinematic constraint in *Chasmosaurus*. In centrosaurines, it would have represented even less of a constraint as the medial tubercle is typically less prominent in these taxa than in chasmosaurines. However, juvenile *P. lakustai* specimens do have proportionally large medial tubercles. Therefore, forelimb posture in this species may have changed gradually from less to more erect as the medial tubercle became proportionally smaller over the course of ontogeny. However, other characteristics of the *Pachyrhinosaurus* forelimb, and especially of the radius and ulna, nevertheless suggest a semi-erect forelimb posture. In the ulna of *P. lakustai*, for example, the olecranon process is large and the proximal articular surface for the radius lies between the anterolateral and medial processes, with the elbow flexed. These characteristics imply that the radius and ulna would probably have articulated with one another as inferred for *C. irvinensis* (Thompson and Holmes, 2007), with the olecranon process protruding posterolateral to the distal end of the humerus. If the humerus was held in a more erect orientation, there may have been less need for a tall olecranon process (Chinnery, 2004). With the limb in a semi-erect posture, however, the humerus would have been held at an oblique angle, and a strong triceps extensor moment would have been needed to prevent the elbow joint from collapsing due to the weight of the body. A large olecranon would have helped to generate such a moment, by providing the triceps musculature with both a long moment arm and a sizeable attachment area capable of accommodating a large muscle mass.

The presence of a large anterolateral process on the ulna of *P. lakustai* would have forced the radius into a somewhat anteromedial position relative to the ulna, rather than an anterior one as in basal ceratopsians (Maidment and Barrett, 2011). Shifting the radius medially would in turn have forced the forearm and manus into a pronated position (Bonnan, 2003), where the humerus would rotate anteriorly throughout the step-cycle. The type of humeral rotation described in

Thompson and Holmes (2007) would then have caused slight medial movement of the radius, leading to the manus rotating medially as well. The first and second digits of the manus would then have taken the bulk of the animal's mass as the manus pushed off the substrate and the fourth and fifth digits rotated dorsally. The inference of a pronated distal forelimb in *P. lakustai* is further supported by evidence of manual pathologies, fully described in Chapter 4, similar to those suggested to be caused by pronation in *C. irvinensis* (Rega et al., 2010).

Semi-aquatic ceratopsians

There is a particular hypothesis that continues to resurface in the literature and tends to drive home the importance of studying postcranial morphology. This is the suggestion that some ceratopsian taxa may have had adaptations for an aquatic or semi-aquatic lifestyle, a claim defended by many authors (Hatcher, 1907; Gregory and Mook, 1925; Russell, 1977) but rejected by others (Colbert 1948; Bakker, 1986; Paul and Christiansen, 2000).

Most notably, Ford and Martin (2010) argued forcefully that *Psittacosaurus* was well suited to a semi-aquatic lifestyle, and the hundreds of *Psittacosaurus* specimens that have been found in lacustrine deposits support the hypothesis of Eberth (2010) that ceratopsians preferred wetland environments. However, animals whose remains are found in sedimentary rocks laid down in a wet environment did not necessarily prefer that environment in life. Therefore, Mallon and Holmes (2010) focused on the postcranial morphology of *Anchiceratops* to test its level of adaptation for a semi-aquatic lifestyle.

Although *Psittacosaurus* may have been able to propel itself through the water by either paddling with its limbs or undulating its tail (Ford and Martin, 2010), larger ceratopsians most likely would have used a different technique given their overall large body size, making tail-

driven propulsion improbable. To test a different method that ceratopsids may have utilized, Mallon and Holmes (2010) compared *Anchiceratops* to the extant common hippo (*Hippopotamus amphibius*). Crocodylians, which might represent a more obvious extant analogue based on their status as semi-aquatic extant archosaurs, were not extensively considered in this connection given that they are generally much smaller than ceratopsids and differ from them in overall body plan. The large body size of ceratopsids makes it difficult to imagine them undulating through the water in the same manner as crocodylians. However, hippos are similarly large-bodied animals that spend nearly their entire lives in water, and only venture on to land at night to feed (Eltringham, 1993). They do not propel themselves through the water with the tail as crocodylians do, or as *Psittacosaurus* is inferred to have done (Ford and Martin, 2010), but instead simply walk on the bottom substrate, using their robust limbs to wade through mud when necessary.

Although hippos are mammals, they share characteristics with ceratopsids that may indicate a similar lifestyle. Ceratopsids were like hippos in being large herbivores that often congregated in large groups, comprising up to 100 individuals (Eltringham, 1999). *Pachyrhinosaurus lakustai* is no exception to this tendency, as the Pipestone Creek Bonebed is estimated to contain at least 600 individuals (Fanti and Currie, 2007). Mallon and Holmes (2010) identified further parallels between ceratopsids, particularly *Anchiceratops*, and hippos, many of which apply to *Pachyrhinosaurus.* For instance, *Pachyrhinosaurus* possesses a very large olecranon process relative to the length of the ulna. This feature also occurs in both *Anchiceratops* and *Hippopotamus* and may be advantageous for walking on muddy substrates (Wall and Heinbaugh, 1999). *Anchiceratops* also resembles hippos in having short limbs and an expansive ribcage. The presence of these features is difficult to assess in *Pachyrhinosaurus* due

to the disarticulated state of the available material. However, another key difference between *Hippopotamus* and ceratopsids is the expanded frill at the back of the ceratopsid skull, which would have produced intense drag if a ceratopsid attempted to move through the water. The nasal boss on *Pachyrhinosaurus*, and the proportionally large skull sizes of ceratopsids in general (VanBuren, et al., 2015), would also have weighed these animals down to a greater degree than a *Hippopotamus*.

Overall, there is no clear evidence that *P. lakustai,* or any other ceratopsid, was in fact semi-aquatic. Nevertheless, this hypothesis does highlight the importance of studying ceratopsid postcrania when attempting to resolve functional, behavioural and ecological questions that cannot be answered using cranial morphology alone.

Conclusions

All previous descriptive work on *Pachyrhinosaurus* has focused solely on crania, with postcranial elements receiving only the brief mentions to establish their presence at given localities (Langston, 1975; Fiorillo and Tykoski, 2012; Fanti et al., 2015). Although some studies with broad taxonomic sampling have included *Pachyrhinosaurus* postcrania (Chinnery, 2004), the description presented here is the first to consider *Pachyrhinosaurus* postcranial elements in detail. The scarcity of ceratopsid postcranial descriptions is a substantial gap in the ceratopsian literature. Only in recent years has there been a push to describe postcrania at all (e.g., Mallon and Holmes, 2010; Maidment and Barrett, 2011). The present description aims to expand the ceratopsid postcranial literature and encourage further research in this area.

The forelimb and pectoral girdle of *Pachyrhinosaurus lakustai* differ from those of the closely related *Pachyrhinosaurus canadensis* and WRB *Pachyrhinosaurus.* Overall, the forelimb

and pectoral girdle of *P. lakustai* is much smaller and gracile. This suggests that *P. lakustai* grew to be correspondingly smaller sizes than *P. canadensis* and WRB *Pachyrhinosaurus.* Otherwise, there are few characteristics of this part of the skeleton that seem to differ between the two species of *Pachyrhinosaurus*. They do suggest that certain characters differ between centrosaurines and chasmosaurines. Accordingly, isolated postcranial material should now be regarded as somewhat more precisely identifiable than previously appreciated, even if identification can rarely be taken to the specific or even generic level. Furthermore, this study highlights the importance of postcrania, which should encourage more palaeontologists to describe the postcrania associated with ceratopsid skulls instead of simply reporting their presence as was often done in the past. An increase in the number of thorough, well-illustrated descriptions of ceratopsid postcrania in the literature will facilitate comparisons among different taxa with respect to both morphology and life habits.

Chapter 3 - Growth and Age Distribution of *Pachyrhinosaurus lakustai* from the Pipestone Creek Bonebed in the Upper Cretaceous Wapiti Formation of Northern Alberta

Introduction

One cannot watch extinct non-avian dinosaurs grow to maturity, as is possible with extant animals. Furthermore, fossils of juvenile individuals that provide information about growth patterns are relatively rare. Therefore, many juvenile specimens that are discovered are worth a closer look. By comparing these juveniles to large, seemingly-mature, specimens, the general growth trajectory of a species can be better understood (Erickson and Druckenmiller, 2011). However, to begin studying ontogeny in dinosaurs there are prerequisites that need to be met. The first, which is rather intuitive, is that specimens from various ontogenetic stages must be available. The larger the ontogenetic range represented in a sample, the more comprehensively the growth trajectory can be investigated. The second prerequisite is that these specimens must all be of the same species. This may seem intuitive, but in dinosaur palaeontology there have been many cases in which a specimen was initially named as a new species, only later to be suggested to represent a previously undocumented stage in the ontogeny of another species. A classic example of this is the famous *Nanotyrannus* versus juvenile *Tyrannosaurus* debate. In this instance the relatively small theropod skeleton CMNH 7541 was initially named *Nanotyrannus lancensis* by Bakker and Williams (1988) but was later reinterpreted as a juvenile *Tyrannosaurus rex* by Carr (1999). This debate has continued for decades, with compelling arguments on either side (e.g., Larson, 2013; Yun, 2015). Another well-known example is the putative ceratopsid *Torosaurus latus,* which is represented by multiple specimens, the most complete skull being MOR 1122 (Scannella and Horner, 2010). Initially discovered by Marsh (1891), it was regarded as a distinct genus for over a century (Farke, 2007; Scannella and Horner, 2010). However, a recent study (Scannella and Horner, 2010) claimed that the specimens assigned to *Torosaurus latus* simply exemplify the most mature growth stage of

Triceratops horridus. As both genera come from the Hell Creek Formation of the Dakotas, Montana and Saskatchewan, and because only adult specimens of *Torosaurus* have ever been discovered, this is a very compelling argument. Once again, debate is ongoing, as claims continue to be made that *Torosaurus* is a legitimate taxon (Longrich and Field, 2012; Maiorino et al., 2013).

The debate over *Torosaurus* has arguably been made more difficult to resolve as researchers have focused solely on studying crania to attempt to differentiate the two genera and have ignored other parts of the skeleton. The tendency of researchers to concentrate on the skull has led to ceratopsid taxonomy being based entirely on cranial features, although diagnostic postcranial ones might eventually be discovered. However, a severe problem arises in that the diagnostic features of the skull may vary throughout ontogeny, as well as between the sexes and among individuals, making them much less reliable (Horner and Goodwin, 2006). The only way to truly distinguish between variation due to age and variation due to taxonomy would be to section postcrania found in association with skulls to generate a precise age estimate using lines of arrested growth (LAGs). However, most *Torosaurus* and *Triceratops* skulls lack associated postcranial elements that can be sectioned in order to provide age estimates. Whether this is due to a bias in preservation, a bias in collection, or a bias in descriptions, it poses a problem in ceratopsian palaeontology and reminds us of the importance of the postcranial skeleton.

Although there have been quite a few studies of growth in various ceratopsians, examining both the cranium (Horner and Goodwin, 2006; Ryan et al., 2001b) and the postcranium (Erickson and Druckenmiller, 2011; Erickson and Tumanova, 2000; Reizner, 2010), there are a number of ceratopsian species for which ontogenetically variable material is available but a study of growth has never been undertaken. *Pachyrhinosaurus lakustai* is one such

example. The Pipestone Creek Bonebed, the sole locality from which *P. lakustai* is definitively known, is monodominant and qualifies as one of the densest dinosaur bonebeds in the world, with nearly every bone in the skeleton represented by multiple examples ranging from juvenile to adult. The Bonebed is near the small town of Wembley, in northern Alberta and lies in the Upper Cretaceous Wapiti Formation. Although the Pipestone specimens are not articulated, it is feasible to study the ontogeny of a specific element in detail, and use that element to estimate the growth trajectory of *P. lakustai*. This approach requires that it be possible to use the element in question to estimate both age and body mass, as can be done with the femur or humerus (Campione and Evans, 2012).

Earlier attempts to reconstruct ceratopsian growth patterns focused on basal members of Ceratopsia, such as *Protoceratops* and *Psittacosaurus,* due to the large numbers of specimens available (Brown and Schlaikjer, 1940; Erickson and Tumanova, 2000). Erickson and Tumanova (2000) used a large sample of femora to acquire age estimates and body mass estimates, which they then used to plot an inferred growth trajectory for *Psittacosaurus mongoliensis*. Later attempts focused on members of Ceratopsidae, such as *Einiosaurus procurvicornis* (Reizner, 2010) and *Pachyrhinosaurus perotorum* (Erickson and Druckenmiller, 2011). However, these studies differed methodologically from one another and from the Erickson and Tumanova (2000) analysis. For *P. perotorum* a single femur from a mature individual was used to determine age based on lines of arrested growth, and to estimate the percentage of its final body length that the animal had attained at the time of deposition of each LAG (Erickson and Druckenmiller, 2011). By contrast, the growth curve for *E. procuvicornis* was based on a series of variably sized tibiae from a single bonebed, and the circumference of each element was plotted against inferred age based on LAGs (Reizner, 2010). Although these studies are informative regarding the growth of

individual species, the fact that a different variable (i.e. body mass, percent body length, or tibial circumference) was used to track growth in each case implies that the resulting growth curves cannot be readily compared, making it difficult to arrive at a broader understanding of growth within Ceratopsidae. The present study aims to use a uniform approach to generate a maximally accurate and informative growth curve for *P. lakustai*. The curve will then be available as a basis for comparing the growth pattern of *P. lakustai* to those of other ceratopsians, and indeed of other non-avian dinosaurs. However, comparisons among growth curves generated using different methods will continue to present challenges and pitfalls.

Materials and Methods

Specimen Selection and Histology

Humeri were chosen for this study due to their relative abundance and utility for estimating body mass. Campione and Evans (2012) found that most accurate body mass estimates they could generate for quadrupedal tetrapods came from combining measurements of the main weight-bearing elements, the femur and humerus, but they also generated equations for mass estimation based on each of these elements alone. As all elements incorporated in this study are disarticulated, using femoral and humeral measuremenys together would require determining which femora and humeri could be ascribed to the same individuals or at least individuals of the same size, a procedure fraught with potential inaccuracies. As this study is part of a larger investigation of the forelimb of *Pachyrhinosaurus lakustai*, humeri alone were used to generate estimates of age and mass.

Five *Pachyrhinosaurus lakustai* humeri of varying sizes (ranging from 81-242 mm in midshaft circumference) from the Pipestone Creek Bonebed were selected for sectioning (TMP

1986.055.0230, TMP 1986.055.0108, TMP 1989.055.0317, TMP 1989.055.0639, and TMP 1989.055.1571). The elements selected for sectioning all had at least one incomplete end and therefore only circumferential measurements were taken. TMP 1989.055.0317 had the largest circumference, 242 mm, of any humerus from the locality, whereas TMP 1989.055.1571 had one of the smallest circumferences, at 81 mm (33% the circumference of the largest humerus). TMP 1986.055.0108 had a circumference of 122 mm (50% of the largest humerus), TMP 1989.055.0639 had a circumference of 125 mm (52%), and TMP 1986.055.0230 a circumference of 230 mm (95%).

Before sectioning, each humerus was measured and photographed. A small section (approximately 3 cm thick) was first cut out of each specimen approximately at mid-shaft, using the table-saw attachment on an Isomet^{TM} 1000 Precision Sectioning Saw (Buehler, Lake Bluff, Illinois). The sections of bon3 were then either imbedded in EpoThin^{TM}, low-viscosity epoxy resin with the use of hardener or imbedded in Castolite AC polyester resin under a vacuum. In the cases of TMP 1986.055.0230 and TMP 1989.055.0317, the sections of bone were cut in half along the sagittal plane of the element to create smaller pieces that would fit on 50.8 mm by 76.2 mm slides. Each resin puck was then cut using an Isomet^{TM} 1000 Precision Sectioning Saw and secured to a plexiglass slide using cyanoacrylate glue to be reduced in thickness. The slides were then cut smaller and rough-ground with a Hillquist Thin Section Machine (Hillquist Inc., Denver, Colorado). Finally, the sections were ground to a desired thickness (which varied among specimens) using 600 grit SiC powder, and polished using 1000 SiC grit and a polishing cloth.

Sections were analyzed and imaged using Nikon NIS Elements Documentation software (Nikon Instruments Inc., Melville, New York) under plane-polarized and cross-polarized light. To increase the contrast and clarity of the slides, mineral oil was applied prior to viewing. Full-

section images of TMP 1986.055.0108, TMP 1989.055.0317, TMP 1989.055.0639, and TMP 1989.055.1571 were taken using a Nikon Digital Sight DS-Fi2 microscope camera head (Nikon Instruments Inc., Melville, New York) on a Nikon Multizoom AZ1000 microscope (Nikon Instruments Inc., Melville, New York). These images were taken at 4 x total magnification and 1280 x 960 resolution. To generate a full rendering of each thin section, images of different parts of the section were taken with 40% overlap and then stitched together using the NIS-Elements Basic Research software (Nikon, Inc). Full slide scans of TMP 1986.055.0230 were taken with a Nikon Super Coolscan 5000 ED.

Body Mass Calculations

To estimate the body mass of a mature individual the midshaft circumference of the largest *P. lakustai* humerus was measured and entered into Campione and Evans (2012) limb scaling equation for quadrupedal terrestrial tetrapods:

$$logBM = 2.651logC_H - 0.089$$

where 'BM' is estimated body mass and 'C_H' is midshaft humeral circumference. This produces a body mass estimate in grams for mature individuals. The caveat to this method is that, because the forelimbs of quadrupeds are often slender in proportion to the hindlimbs, using humeral circumference alone leads to underestimation of total body mass (Campione, pers. correspondence, 2019). However, mass estimates generated using this method will be proportionally comparable to each other so that the overall growth trajectory will remain an excellent point of comparison for future studies. A more serious problem is that this equation cannot be reliably used to estimate the mass of immature individuals (Erickson and Tumanova, 2000). To use the same equation on a juvenile is to assume that a juvenile is simply a scaled

down adult, which is unlikely to be entirely accurate (Calder, 1996). As a classic example, juvenile dogs have proportionally large paws, but their paws subsequently grow less quickly than the rest of the body, so that the proportional size of the paws decreases. The same is true for all tetrapods, including extinct taxa (Calder, 1996). Therefore, one cannot expect the same body mass estimate equation to give accurate estimates for both juveniles and adults.

To circumvent this problem, a new method of estimating body mass in juvenile individuals, called Developmental Mass Extrapolation (DME), was developed by Erickson and Tumanova (2000). DME estimates a juvenile's body mass by comparing a linear measurement in a juvenile to that same measurement in an individual known to be adult. In the present study Developmental Mass Extrapolation was employed, following the protocol of Erickson and Tumanova (2000) to generate one or more body mass estimates for each individual, based on the external circumference of the humerus and also on the circumferences of any internal growth lines. The extrapolation was based on the most complete adult humerus, which has a midshaft circumference of 242 mm. This yields an estimated body mass (based on Campione and Evans, 2012) of 1700 kg, which gives the equation:

$$BM_{immature} = 1700\ kg\ (C_{H,\ immature}/242\ mm)^3$$

where 'BM' is the estimated body mass and 'C_H' is the midshaft circumference of the immature humerus. Although DME was initially developed with the idea of using the lengths of elements as a basis for size comparisons between mature and immature individuals, unpublished work from the Royal Ontario Museum, led by Dr. Kentaro Chiba, strongly suggests that using the circumferences of elements yields more accurate results. Using circumferences for DME is particularly useful when estimating the body mass of an individual at various points in its life when LAGs were deposited, as LAGs are circumferential in nature.

LAGs were traced from section photographs in Adobe Illustrator to determine the circumference of the humerus at the time of deposition of each growth line. The circumferences of the LAGs were then used to estimate the body mass of the individual during the successive non-depositional periods when LAGs formed, which were assumed to have been annual. Loss of LAGs due to expansion of the medullary cavity was accounted for by superimposing the LAGs of the younger specimens on those of the mature specimen. The innermost LAG of TMP 1986.055.0108 was estimated to represent the non-depositional period during the first year of the individual's life. Each successive LAG was then assumed to mark an interruption in the following year of growth, making it possible to plot the growth trajectory of *P. lakustai.* In the case of overlapping LAGs the circumferences tended to be within 0-5 mm of one another, with the majority differing by only 1 mm.

In an effort to compare the estimated body masses of various ceratopsid taxa ten different taxa were selected based on availability of adult humeri. These included *Agujaceratops mariscalensis* UTEP P.37.7.005, *Centrosaurus apertus* ROM 767, *Centrosaurus* sp. CMN 57053, *Chasmosaurus belli* ROM 843, *Chasmosaurus irvinensis* CMN 41357, *Chasmosaurus ruselli* CMN 2280, *Paachyrhinosaurus canadensis* CMN 10640, *Pachyrhinosaurus lakustai* TMP 1989.055.0317, *Styracosaurus albertensis* CMN 344, and *Triceratops* sp. AMNH 971. Given the substantial difference in size between CMN 57053 and all other *Centrosaurus apertus* specimens observed, this is likely a different species of *Centrosaurus,* and was therefore incorporated in this study as such, although its species is unknown. For each taxon the largest humerus available was selected and the midshaft circumference measured to give a body mass estimate (Campione and Evans, 2012).

Growth Curve

Each point in the growth curve was plotted as an estimate of the body mass of the individual in question during the time of deposition of a particular LAG. In palaeontology there are two main methods employed to reconstruct a growth curve. These are commonly referred to as "Section-Stacking" and "Growth Model Fitting." Section Stacking is the process of sectioning multiple specimens of varying sizes, tracing the LAGs in each specimen, and plotting the circumferences of the LAGs against the estimated age for all specimens in a single curve (Erickson et al., 2001). This entails plotting on a single curve data from the LAGs of the youngest specimens and from those of the oldest specimens, in which LAGs from early in life may have been lost due to expansion of the medullary cavity. Growth Model Fitting requires fitting various growth models to the data from the LAGs preserved in the largest (and oldest) specimen, the assumption being that whichever model shows the best fit is most likely the actual growth trajectory (Cooper et al., 2008).

Although both methods are used frequently in the literature (e.g., Cooper et al., 2008; Erickson et al., 2001; Lee and O'Connor, 2013; Myhrvold, 2013; Prondvai, 2017), the Section Stacking approach is used in this study. This technique makes it possible to generate a growth curve using a more complete dataset based on multiple specimens, in this case taking advantage of the multitude of humeri from Pipestone. By using the Section Stacking technique it was possible to infer a relatively complete growth trajectory for *P. lakustai*.

Results

Histology and Growth

The smallest humerus, TMP 1989.055.1571 (Fig. 3.1), is markedly different from the other elements sectioned that it lacks any evidence of LAGs. Accordingly, this individual is inferred to be less than one year old. There is also no evidence of remodeling, as secondary osteons are absent and the medullary cavity does not appear to have undergone any expansion, which would have produced a zone or highly vascularized bone around the perimeter of the expanded cavity. Instead, the medullary cavity is quite small, with well-defined edges. The bone is fibrolamellar with reticular vascularization in some areas, but also displays medial canals close to the medullary cavity. The overall density and orientations of the vascular canals vary throughout the thin section, but this is likely due to preservational distortion, which is particularly noticeable anterior to the medullary cavity. This variation appears to be due to mediolateral compression of the anterior part of the humeral shaft. The most central bone on that side is so distorted and crushed that no vascular canals could be identified.

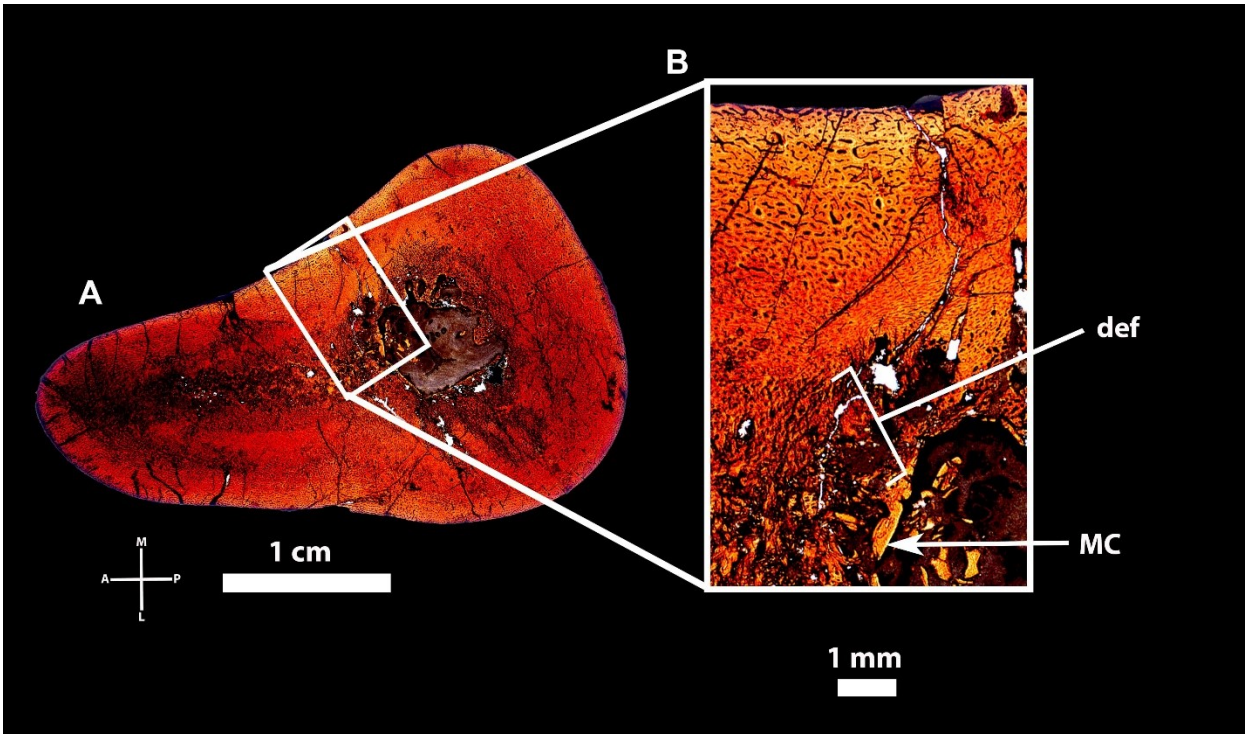

Figure 3.1. Transverse section of young *Pachyrhinosaurus lakustai* humerus. Transverse section of TMP 1989.055.1571. (A) Complete transverse section, (B) close-up view of select area from A. Lack of growth rings indicates this animal was under a year old. Note lack of secondary osteons remodeling, consistent with the inferred young age. Abbreviations: def, deformation of fibrolamellar bone due to compression on anterior side; MC, defined wall of medullary cavity showing lack of expansion due to growth.

The second humerus, TMP 1986.055.0108 (Fig. 3.2), is more deformed than any other specimen sectioned so that the section is oval with a great deal of mediolateral compression and a concave medial side. This deformation has resulted in severe crushing of the periosteum, particularly close to the medullary cavity. The anterior part of the thin section also has some major fractures, so most observations pertain to the posterior side. Given the nature of the deformation, this element was most likely much more robust in life than in its preserved state, compromising the reliability of the circumferential measurement. The severity of the

deformation makes it difficult to discern if any medullary cavity expansion has occurred, and there is no evidence of secondary osteons. The bone visible in the section is fibrolamellar, with reticular vascularization throughout the section and possible radial canals also present in its the outermost part. Four LAGs can be identified in this specimen, suggesting the animal died in its fifth year of life.

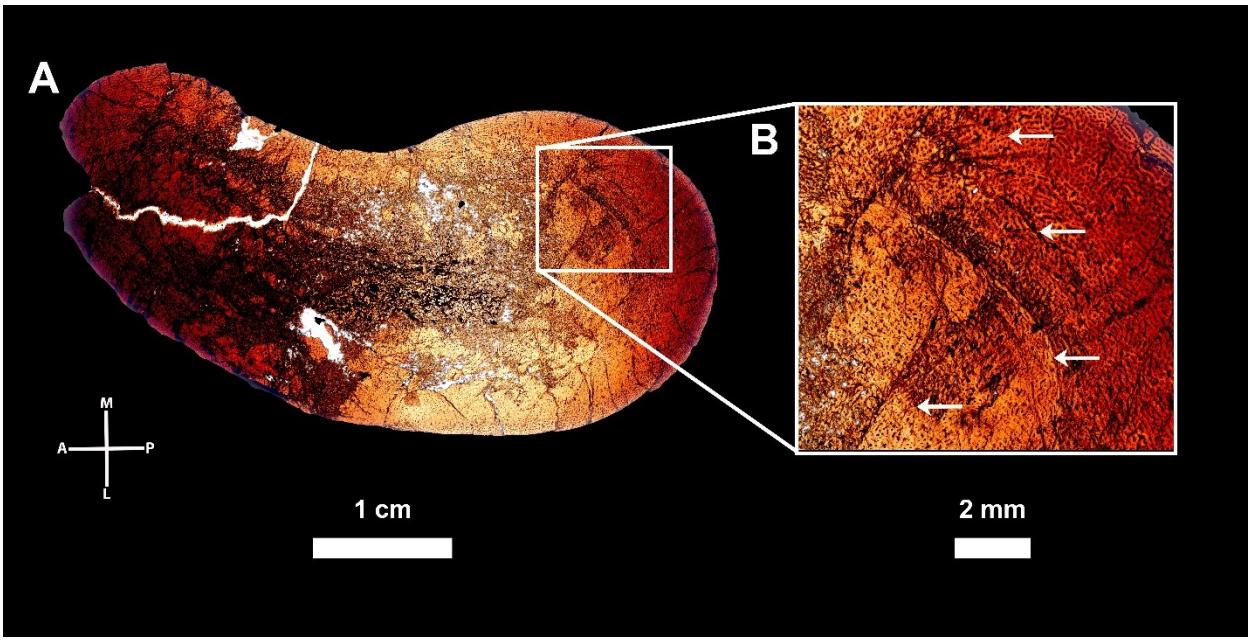

Figure 3.2. Transverse section of juvenile *Pachyrhinosaurus lakustai* humerus. Transverse section of TMP 1986.055.0108. (A) Complete transverse section, (B) Close-up view of select area from A. Growth rings are present, and medullary cavity expansion is minimal. Severe mediolateral compression has distorted shape and internal structure of section. White arrows in B indicate lines of arrested growth.

TMP 1989.055.0639 (Fig. 3.3) has a slightly larger circumference than TMP 1986.055.0108, at 125 mm (vs. 122 mm). However, this humerus does not appear to have experienced nearly as much deformation as the previous one, being subcircular in shape with no obvious signs of compression and therefore no obvious alteration of the original circumference of the element. This section has three evident LAGs, two of which are relatively close together

approximately midway between the inner-most and outer-most parts of the section, while the third resides just within margin of the section. As with the other specimens, this section mostly shows reticular canals, but also has very distinct radial canals external to each of the two inner LAGs. These radial canal zones range from 1-1.3 mm in length. The medullary cavity is proportionally larger, with increased vascularization around its edges and no defined boundary between the cavity and the region of osteon formation as seen in TMP 1989.055.1571, so some expansion of the medullary cavity had probably occurred in this specimen. However, there is no evidence of secondary osteons.

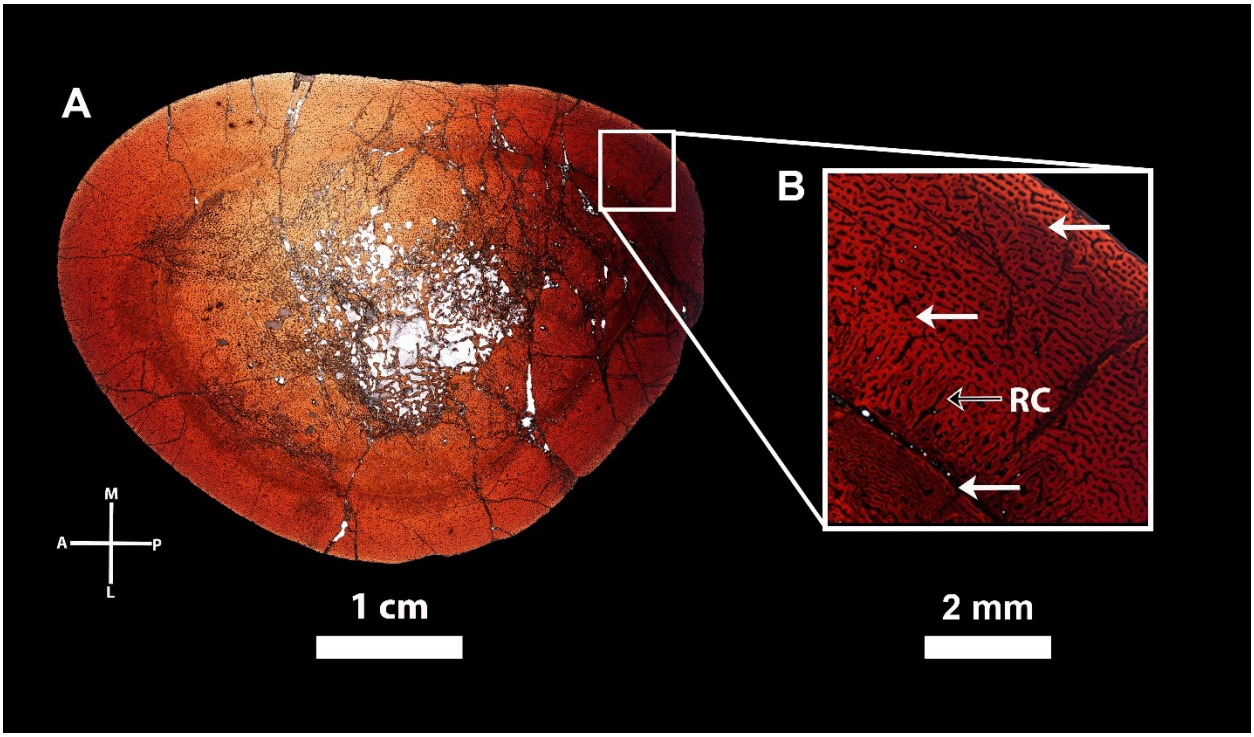

Figure 3.3. Transverse section of juvenile *Pachyrhinosaurus lakustai* humerus.
Transverse section of TMP 1989.055.0639. (A) Complete transverse section, (B) Close-up view of select area from A. Growth rings are clearly present, and medullary cavity expansion is minimal. White arrows in B indicate lines of arrested growth. Reticular canals present internal to all LAGs with a thin band containing radial canals external to each of the two inner-most LAGs. Abbreviations: RC, radial canal.

The second-largest humerus sectioned, TMP 1986.055.0230 (Fig. 3.4), shows minimal compression on the anteromedial side of the shaft, but does not appear distorted to a degree that would greatly affect the measured circumference. A total of 15 LAGs were identified in this specimen, but very few extended continuously around the entire circumference of the element, due to remodeling resulting from secondary osteons (as seen in Figure 3.4B). Despite the age of the animal and the extensive remodeling, the medullary cavity has not expanded to any great degree. The medullary cavity has a total circumference of 94 mm, which is equal to the circumference of TMP 1989.055.1571. The smallest, most internal, LAG in TMP 1986.055.0230 has a circumference of 124 mm, which is similar to the circumference of the fourth LAG in TMP 1986.055.0108 and the third LAG in TMP 1989.055.0639, suggesting this was deposited in the animal's third or fourth year of life. Assuming each LAG represents one year, this animal is estimated to have been in its nineteenth year at the time of death. The external fundamental system (EFS) is present on the outer-most region of the section as a compact cluster of four LAGs, which suggests the individual was skeletally mature at time of death.

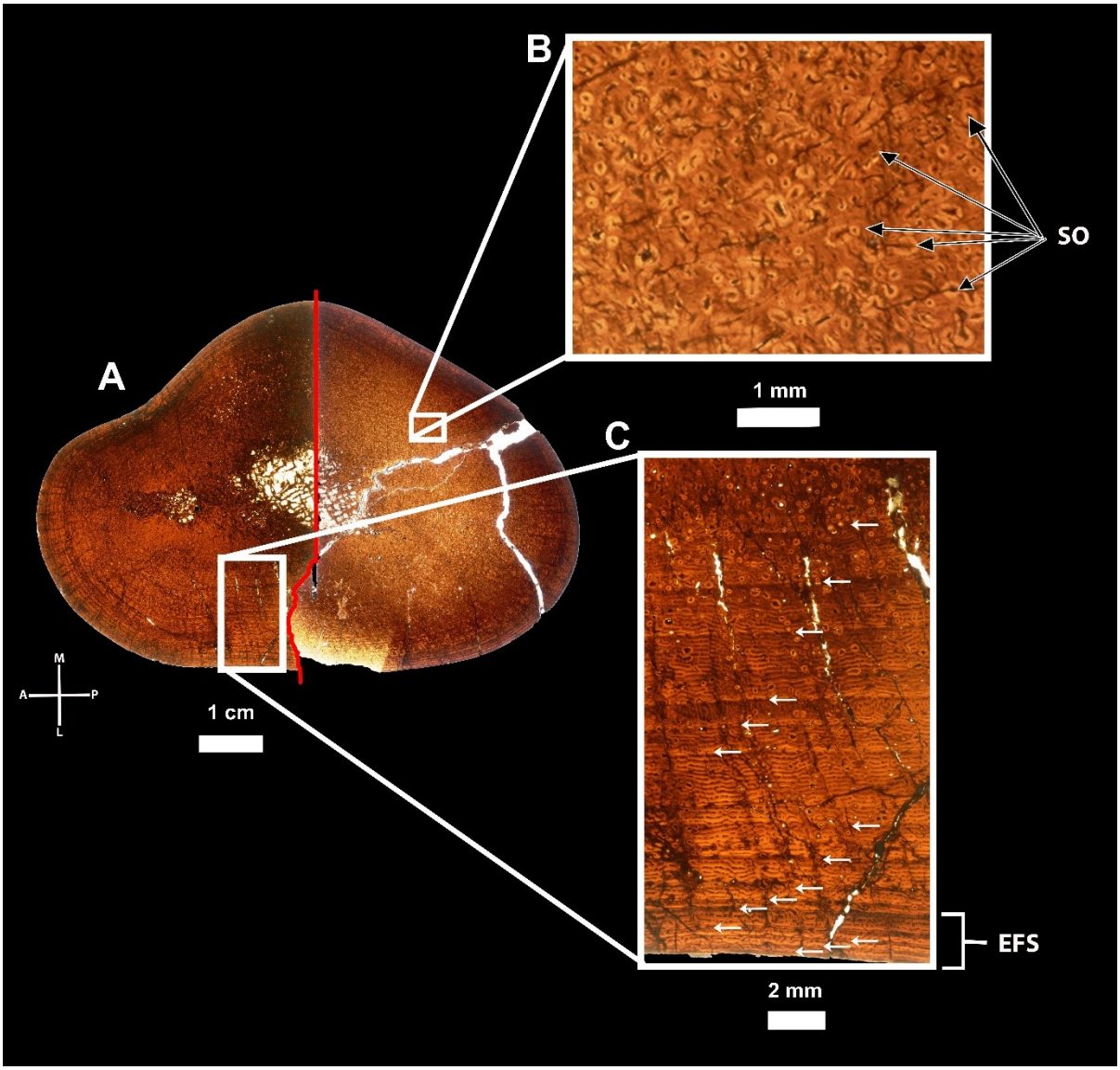

Figure 3.4. Transverse section of adult *Pachyrhinosaurus lakustai* humerus.
Transverse section of TMP 1986.055.0230. (A) Complete transverse section, (B) and (C) close-up views of select areas from A. Growth rings are clearly present, and medullary cavity expansion is minimal. Red line in A indicates plane along which element was cut during preparation of section. Wide-spread remodeling due to formation of secondary osteons is evident in B. White arrows in C indicate LAGs. EFS visible in C indicates this is a skeletally mature individual. Abbreviations: SO, secondary osteon; EFS, external fundamental system.

The final humerus sectioned, TMP 1989.055.0317 (Fig. 3.5), represents the largest, and likely most mature individual *P. lakustai* specimen in the sample. It indeed has the largest circumference (242 mm) of any humerus from the Pipestone Creek Bonebed. This section is relatively circular, indicating that there has been little to no deformation. This is further supported by the generally ordered, undistorted appearance of the tissue making up the section. Overall the bone is fibrolamellar, and the medullary cavity is greatly expanded. The medullary cavity's circumference of 160 mm exceeds the full circumferences of TMP 1986.055.0108, and TMP 1989.055.0639 and TMP 1989.055.1571, as well as the circumference of the first three LAGs in TMP 1986.055.0230. The cavity is most expanded on the posterior side. This section is also remodeled by a large number of secondary osteons throughout. The abundance of secondary osteons decreases towards the outer portion of the section, but secondary osteons are still present in this region and distort even the outermost LAGs, as seen in TMP 1986.055.0230. The multitude of closely packed LAGs towards the outer margin of the section forms the EFS, which indicates this animal was at skeletal maturity. Overall, nine LAGs were counted, plus five LAGs forming the EFS, as in TMP 1986.055.0230. Due to the heavy remodeling and expansion of the medullary cavity past the circumference of the other humeri, it can be inferred that at least twelve LAGs were lost in this individual. Therefore, this individual was probably in at least its twenty-second year.

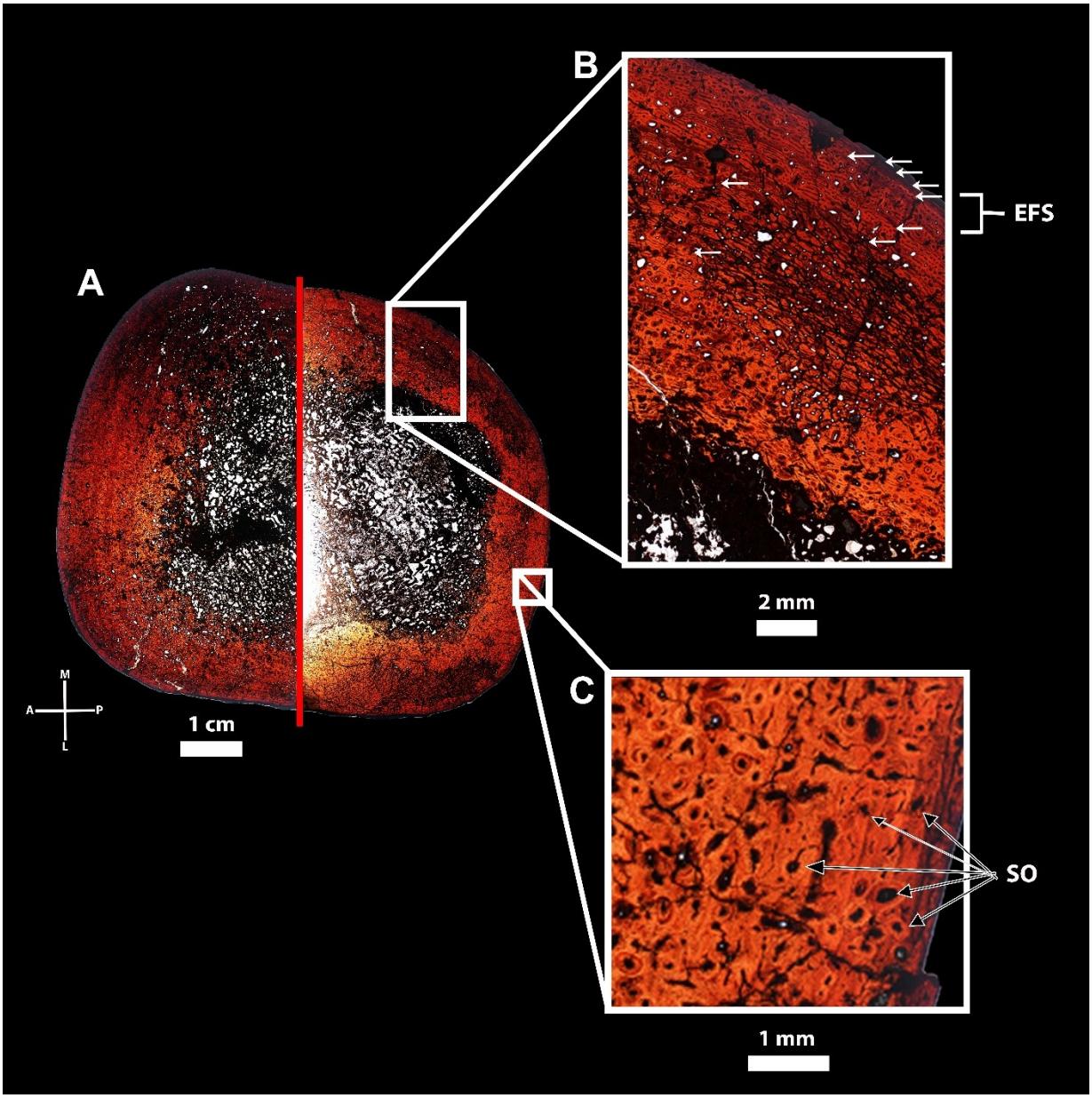

Figure 3.5. Transverse section of mature *Pachyrhinosaurus lakustai* humerus.
Transverse section of TMP 1989.055.0317. (A) Complete transverse section, (B) and (C) close-up views of select areas from A. Growth rings and signs of extensive remodeling due to medullary cavity expansion are visible in A, and widespread secondary osteons in C. White arrows in B indicate LAGs. EFS visible in B indicates this is a skeletally mature individual. Abbreviations: SO, secondary osteon; EFS, external fundamental system.

Due to the remodeling that occurred in TMP 1989.055.0317, most notably the considerable expansion of the medullary cavity, it is possible to infer that the LAGs from early in the animal's life have been lost, so that section stacking must be employed to account for the missing information. Fortunately, the LAG records of the specimens sectioned for this study seem to overlap with one another, leaving no evident gaps in the growth record (Fig. 3.6). The overall compression of TMP 1986.055.0108, however, may have altered both the circumference of the element and the circumferences of the LAGs. Therefore, it is possible that the earliest LAG in TMP 1989.055.0639 is representative of the first year of life and that the circumference of the first LAG in TMP 1986.055.0108 has been decreased due to deformation. This is further supported by the fact that the circumference of the smallest LAG is less than the overall circumference of the smallest individual, TMP 1989.055.1571, which lacks any growth rings. However, as there is only a 3 mm difference in the circumferences, this may simply represent individual variation in size. An alternative hypothesis is that the circumferences of the LAGs within TMP 1986.055.0108 are, in fact, unaltered and that the original first LAG in TMP 1989.055.0639 has been lost due to expansion of the medullary cavity. However, the medullary cavity in this specimen is only 48 mm in circumference. This is less than the circumference of the first LAG in TMP 1986.055.0108, suggesting that the medullary cavity probably did not obliterate any LAGs in 1989.055.0639. A caveat, however, is that this reasoning does not account for size variation among individuals. Within any tetrapod population it is highly unlikely that all individuals of the same age will have the same body mass, or the same humeral circumference. Although the estimates given here represent a relatively complete picture of a general growth pattern for *P. lakustai*, they cannot be assumed to hold for every individual.

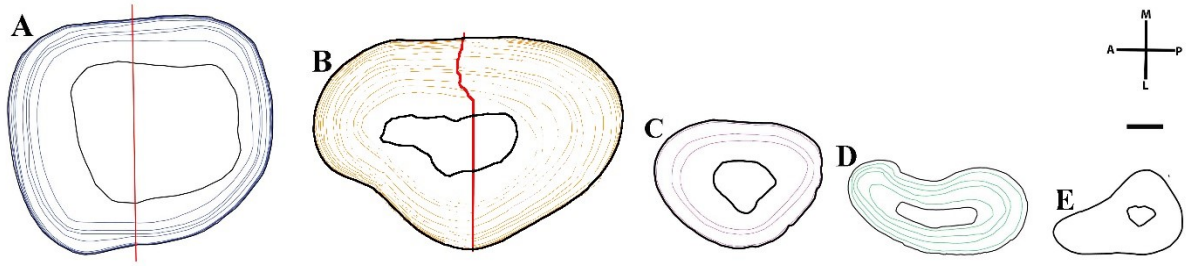

Figure 3.6. Growth rings in humeri.

Lines of arrested growth as seen in (A) TMP 1989.055.0317, (B) TMP 1986.055.0230, (C) TMP 1989.055.0639, (D) TMP 1986.055.0108 and (E) TMP 1989.055.1571. Coloured lines represent LAGs. Black lines mark the borders of the section and marrow cavity. Red line in (A) and (B) mark the planes in which the specimens were cut into portions that would fit on the available slides. Scale is 1 cm.

By plotting estimated body mass against estimated age, a tentative growth curve can be generated for *Pachyrhinosaurus lakustai* (Fig. 3.7). The smallest specimen, TMP 1989.055.1571, lacks growth rings but displays radial canals, and is probably from an animal under one year old. However, as the circumference of the element is slightly larger than that of the first growth ring in TMP 1986.055.0108, it is estimated to be approaching its first year, and assign it an age of 0.75 years for purposes of the growth curve. Based on the smallest LAG throughout the sections (measuring 78 mm in TMP 1986.055.0108), *P. lakustai* grew to approximately 58 kg in its first year of life. This most likely varied between individuals given that TMP 1989.055.1571 is estimated to have been under a year old but to have nevertheless had an estimated mass of 64 kg, based on the total circumference of the humerus. Given to this overlap between TMP 1986.055.0108 and TMP 1989.055.0639, there was clearly a degree of individual size variation in the early stages of growth, and this was likely the case throughout ontogeny. *P. lakustai* does not appear to have grown rapidly early in life, as by age four the specimens sectioned range from

an estimated 202-240 kg (TMP 1986.055.0108, TMP 1986.055.0230, and TMP 1989.055.0639). There is then an increase in rate of growth, which remains high from age five to age thirteen. This interval is represented by LAGs in TMP 1986.055.0230 and TMP 1986.055.0317, and body mass is estimated to have been 293 kg at age five compared to 1256 kg at age thirteen. In TMP 1986.055.0317 the gaps between successive LAGs gradually grow smaller towards the outer margin of the section, indicating a corresponding decrease in the rate of growth. This is apparent in the levelling off of the growth curve after an age of approximately thirteen years. The EFS in both TMP 1986.055.0230 and TMP 1986.055.0317 are represented by the flattest portion of the curve, which begins at age fifteen.

Based on this growth assessment, *Pachyrhinosaurus lakustai* grew at a rate of approximately 51 kg/year in the first four years of life. This is reflected in histological indications of rapid growth in the juvenile specimens (Fig. 3.3). After age four growth drastically accelerated to approximately 115 kg/year from age four to age twelve, only to slow to approximately 39 kg/year from age twelve onwards as the largest *P. lakustai* individuals appear to have settled into a slow, but sustained annual rate of mass increase. Mass does seem to vary among individuals of any given age, but the most variation apparently occurred towards the end of the interval of rapid growth from ages ten to thirteen.

Age Classes

As the morphology of the forelimb does not drastically change throughout ontogeny (as noted in chapter 2 of this thesis), morphological features cannot be used as the basis for defining age classes of *P. lakustai.* Kruk (2015) established size classes for the genus, but her system was based entirely on cranial material and cannot be used in the present study owing to the

disarticulated nature of the Pipestone material. Therefore, to distinguish size classes, specimens have been separated based on the various sections of the growth curve (Fig. 3.7). This only shows one, somewhat subjectively chosen, possibility for dividing the curve into age classes, and alternative approaches also might be acceptable. Juveniles are assumed to be those placed on the portion of the curve extending from zero to five years, in which mass gradually increases. Adults are assumed to have largely completed their growth, and range from 13 years onwards when their rate of growth drastically decreases. This leaves subadults positioned on the portion of the curve in which the rate of growth is maximal, from age 5 to 13.

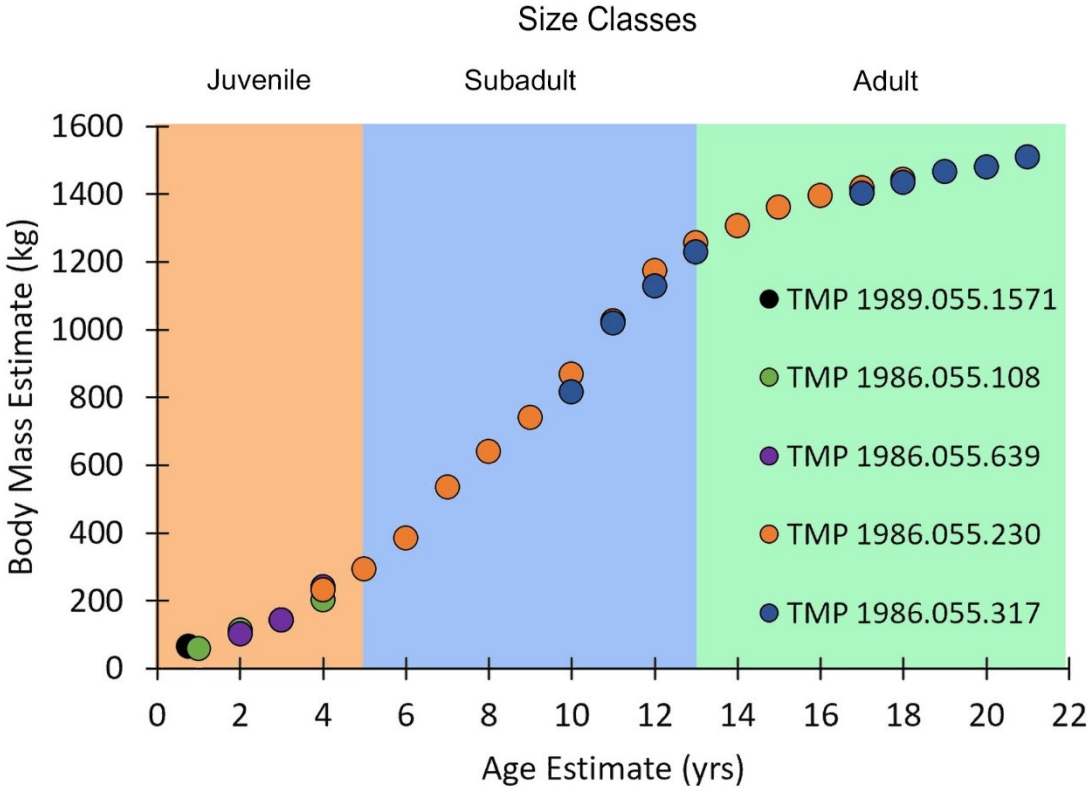

Figure 3.7. Growth curve for *Pachyrhinosaurus lakustai.*

Growth curve of *Pachyrhinosaurus lakustai* as inferred from by circumferences of LAGs within each specimen. Body mass was calculated using Developmental Mass Extrapolation with the circumference of each LAG as a proxy for the circumference of the humerus at the time of

deposition. Each LAG was assumed to represent one year of life. Curve is partitioned into age classes based on changes in the slope of the curve.

Using this framework, the circumference values corresponding to the mass values that represent boundaries between the different age classes were calculated (Tab. 3.1). This was done by solving Erickson and Tumanova's (2000) DME equation, previously described in this chapter, for midshaft circumference. These boundaries were then used to categorize the entire sample of humeri into age classes. In the case of humeri for which no circumferential measurement could be taken due to breakage or other factors, an estimated circumference was calculated using the regression of humeral circumference on humeral length from Chapter Two of this thesis, based on the near-isometric relationship between these variables. The same regression was also used to find the humeral lengths corresponding to the age class boundaries (Tab. 3.2). These calculated humeral lengths were not used to assign humeri to age classes in this study, but are available as a potential basis for classifying humeri recovered from the Pipestone Creek Bonebed in the future.

Table 3.1. Circumference ranges of *Pachyrhinosaurus lakustai* for different age classes.

Age Classes	%*	Humerus (mm)	Scapula (mm)	Ulna (mm)	Radius (mm)
Juvenile	<55	<135	<142	<113	<97mm
Subadult	55-90	135-219	142-233	113-184	97-158
Adult	>90	>219	>233	>184	>158

*Percentages calculated based on circumference of largest specimens: humerus, 242 mm; scapula, 259 mm; ulna, 205 mm; radius, 176 mm

Table 3.2. Length ranges of *Pachyrhinosaurus lakustai* for different age classes.

Age Classes	%*	Humerus (mm)	Scapula (mm)	Ulna (mm)	Radius (mm)
Juvenile	<57	<347	<413	<265	<200
Subadult	57-90	347-553	413-652	265-418	200-315
Adult	>90	>553	>652	>418	>315

*Percentages calculated based on length (or estimated length) of largest specimens: humerus, 608 mm; scapula, 725 mm; ulna, 465 mm; radius, 350 mm

Having established age classes, it was possible to roughly determine the age distribution of the assemblage by counting the number of humeri that fell within each age class (Fig. 3.8). Percentages of full adult humeral circumference (242 mm) and length (608 mm) were then calculated for each age class boundary. The circumference percentages were used to calculate age class boundary circumferences in mm for the scapula, ulna and radius (Tab. 3.1), by simply multiplying the percentage values by the circumference of the largest specimen available for each element. Boundary lengths for the various elements were also calculated (Tab. 3.2), although as in the case of humeri these were not used for age class assignments in this study.

This method depends on the assumption that the circumferences of the other elements are isometric to humerus circumference. This specific allometry was not tested in this thesis due to the disarticulated nature of the Pipestone material, which made reliable analysis of allometric rations among different skeletal elements virtually impossible. However, it is at least plausible that the circumferences of the ulna and radius should be isometric to that of the humerus, as they belong to the same limb. In *Psittacosaurus lujiatunensis* (Zhao et al., 2013), for example, the length of the tibia is nearly isometric to that of the femur. However, it is possible that this is not the case and that the ulna and radius are not isometric to the humerus, as in some other non-avian

dinosaurs (Liberona et al., 2019).

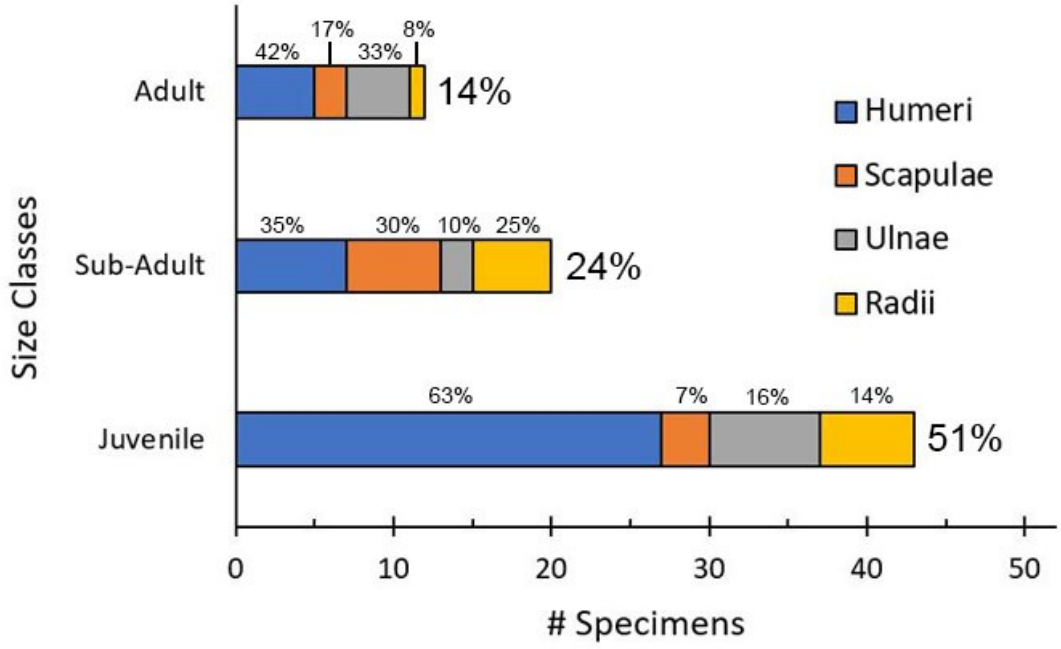

Figure 3.8. Age class distribution at the Pipestone Creek Bonebed.
Graph showing the occurrence of each age class for the *Pachyrhinosaurus lakustai* population at the Pipestone Creek Bonebed. The small percentile values represent the percentage of all elements of a given age class accounted for by each specific element type (scapulae, humeri, ulnae and radii). The large percentile values represent the percentage of all elements in the sample that belong to each age class. Isometry among the different elements with respect to circumference is assumed.

Based on the LAGs described previously, the largest individual died during its twenty-second year of life and reached adulthood by age thirteen, based on the apparent deceleration in growth at this point. As TMP 1989.055.0317 has the largest circumference of any humerus collected from the bonebed to date, and displays an EFS, the humerus comes from the largest individual of which evidence is available. This individual should be close to the maximum size *P. lakustai* would have reached, given the large sample size available at the Pipestone Creek

Bonebed. Conversely, the smallest specimens provide some indication of the size of the youngest juveniles present at the locality. TMP 1989.055.1571, lacking LAGs, confirms the presence of juveniles less than one year old. Because the circumference of the earliest LAG in TMP 1986.055.0108 is 78 mm, however, even the smallest humeri must be from individuals approaching one year of age. Only one specimen (UALVP 60004), which was not sectioned, has a circumference (75 mm) smaller than that of the earliest LAG in TMP 1986.055.0108. There were also slightly older juveniles present at Pipestone, as TMP 1989.055.0108 and TMP 1989.055.0639 are both estimated to be four years old. Although the growth of TMP 1985.055.0230 cannot be tracked through subadulthood, no humeri in this size class were available for sectioning. Of a total of 75 forelimb and shoulder girdle elements measured, 43 were identified as juvenile, 20 as subadult and 12 as adult (Fig. 3.8). Unlike most of the juvenile elements, most large elements from the locality are fragmentary, but only ones complete enough for the length and/or circumference to be reliably measured could be included in this study. Plotting the age class distribution of forelimb and pectoral girdle elements of *P. lakustai* from the Pipestone Creek Bonebed (Fig. 3.8) reveals an obvious preponderance of juvenile specimens, which is most clearly evident with respect to humeri, which are more numerous than the other elements considered in this study (most likely due to their greater robustness).

Maximum Body Mass Estimates

In this study body mass was estimated for specimens representing ten taxa based on the largest humeri available (Fig. 3.9). These specimens included both centrosaurines and chasmosaurines, including two species of Centrosaurus, three species of *Chasmosaurus,* and two species of *Pachyrhinosaurus*. Based on these estimates, *Triceratops* is irrefutably the largest

ceratopsid with an estimated maximum body mass of 6404 kg at maturity. This is almost double the mass of the second largest specimen, CMN 10640, which belongs to *Pachyrhinosaurus canadensis* and has an estimated body mass of 3287 kg. *P. canadensis* is notably larger than the remaining specimens, with those belonging to *Chasmosaurus belli* (ROM 843) and *Styracosaurus albertensis* (CMN 344) weighing in at 2756 kg and 2681 kg respectively. *Centrosaurus* sp. CMN 57053 measured only slightly smaller than *Chasmosaurus russelli* CMN 2280*,* so little difference in size exists between the two. The last four specimens are notably smaller than those previously mentioned. The largest of the four is represented by the largest *Pachyrhinosaurus lakustai* TMP 1989.055.0317 humerus and gave an estimated body mass of 1690 kg, which is just over half the estimated body mass of *P. canadensis* CMN 10640. Body mass also appears to differ substantially within *Centrosaurus*, as the estimated mass of *Centrosaurus apertus* ROM 767 is only 1477 kg. However, ROM 767 is supposedly not fully mature and may therefore be giving an inaccurate representation of the size of this species (Frederickson and Tumarkin-Deratzian, 2014).

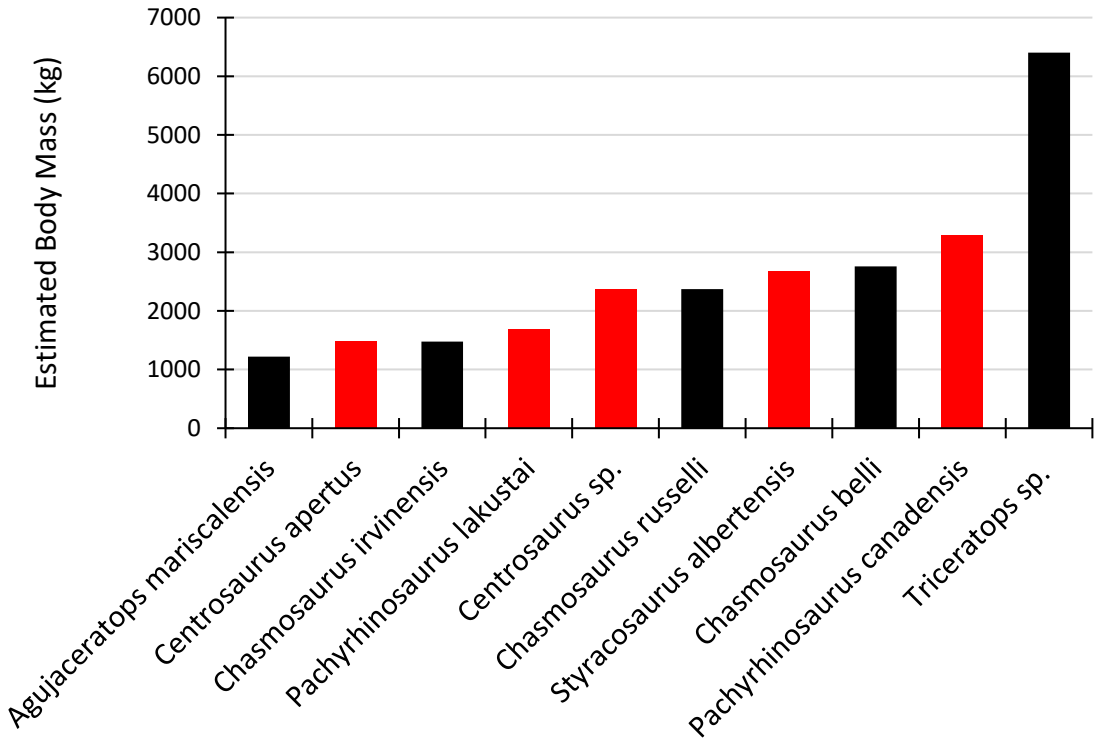

Figure 3.9. Ceratopsid body mass comparison.
Maximum adult body mass estimates based on humeral circumference for a range of Centrosaurinae (red) and Chasmosaurinae (black). Maximum size inferred based on largest humeri available. Due to utilizing humeral circumference and not femoral, these are underestimates, but they can be legitimately compared to one another.

Discussion

Longevity and LAG Count

Although not the first to examine ceratopsid growth, this study is the first to apply to this group the modern approach of plotting body mass estimates against histologically obtained age estimates. Lehman (2006) tracked the growth of *Chasmosaurus mariscalensis* by plotting body mass against the sum of humeral and femoral circumferences. Conversely, Lee (2007), Reizner (2010), and Erickson and Druckenmiller (2011) employed age estimation as a proxy for longevity, but used ulnar circumference, tibial circumference and approximate percentage of

maximum body length, respectively, as proxies for size. Body mass is a more universally applicable measure of size than the former methods as body proportions, such as ulnar or tibial robustness, and can vary among different taxa. Such proportional differences do not affect body mass, which represents the total amount of matter making up the body of the animal. Therefore, this study seeks to set the bar for future ceratopsid growth studies, which has previously been done for other non-avian dinosaur groups, such as theropods (Erickson et al., 2004).

Although the data needed to compare growth patterns among various ceratopsid taxa are currently lacking, longevity can be estimated. In the case of *Einiosaurus procurvicornis,* the oldest individuals were reported to be only in their seventh year of life (Reizner, 2010), making them evidently much younger than the twenty-one-year-old *Pachyrhinosaurus lakustai* reported in this study and the eighteen-year-old *Pachyrhinosaurus perotorum* (Erickson and Druckenmiller, 2011). However, the oldest known *E. procurvicornis* specimen still lacks an EFS, and therefore was probably skeletally immature. Although Reizner (2010) argued that the species may have undergone indeterminate growth, it is more probable that there were simply no adults in the sample. Given that *E. procurvicornis* falls phylogenetically within Pachyrhinosaurini, this species probably was similar in life span to both *Pachyrhinosaurus* species, and perhaps also to other ceratopsids. The only other growth record to have been published for a centrosaurine ceratopsid pertains to *Centrosaurus apertus* (Lee, 2007), and the largest individual in the sample was estimated to have died in its 15th year. However, Lee (2007) did not conclude if this was a mature individual and did not include any histological analysis nor indication of an EFS, preventing any straightforward comparison to *Pachyrhinosaurus*. Additionally, no comparisons can be drawn with any member of Chasmosaurinae, as the few chasmosaurines that have been histologically sampled (*Kosmoceratops, Utahceratops* by Levitt, 2013, and *Triceratops* by Rooij,

2018) did not have any identifiable LAGs. Rooij (2018) did observe two LAG-like markers on one *Triceratops* femur (referred to as Specimen #65), but these were not conclusive.

Although the ceratopsids studied by Rooij (2018) that lacked LAGs could be interpreted as under one year of age, this is highly unlikely given the large size of the individuals in question. Rooij (2018) suggested that they lived in a stable environment with limited seasonal changes. This is a reasonable assumption, as LAGs are known to form during periods when conditions are unfavourable, leading to a lack of nutrients and causing an interruption in the deposition of bone. Therefore, one would not expect to observe LAGs in animals that reside in favourable conditions year-round. Köhler et al. (2012) found this to be the case with extant ruminants, in that those residing in favourable conditions year-round lacked any evidence of LAGs, while those residing in highly seasonable environments displayed more LAGs. This concept leads to the latitudinal gradient hypothesis, which postulates that LAGs become more numerous in various taxa as latitude, and therefore seasonality, increase (Rooij, 2018). In the case of ceratopsids, the known gradient begins with *Kosmoceratops* (UMNH VP 17000 and UMNH VP 21339) and *Utahceratops* (UMNH VP 12198, UMNH VP 16800, UMNH VP 20444 and UMNH VP 20454) at a comparatively low latitude in southern Utah (Levitt, 2013). Based on the sizes of these specimens, Levitt (2013) determined they were all either subadults or adults. A total of twenty sections taken from these individuals, however, revealed no evidence of LAGs. The gradient then continues to *Triceratops* in Wyoming, in which Rooij (2018) sectioned six femora but identified only two LAG-like markers, both in one specimen (Specimen #65). North of Wyoming, in western Montana, Reizner (2010) sectioned sixteen tibiae (MOR 456 – T1-16) belonging to presumed juveniles and subadults of *Einiosaurus procurvicornis*. More LAGs were present in these specimens than in the material from farther south, with LAGs present in all but

four of the sixteen tibia sectioned, and a maximum of five LAGs present in MOR 456 – T7. In southern Alberta, Lee (2007) observed a maximum of seven LAGs in a *Centrosaurus* humerus (TMP 1979.011.0056), one of the three elements he sectioned. The Alaskan *Pachyrhinosaurus perotorum* completes Rooij's (2018) gradient, in that eighteen LAGs have been reported in a single femur (UAMES 3551) (Erickson and Druckenmiller, 2011). Northern Alberta's *Pachyrhinosaurus lakustai*, as observed in the present study, supports this latitudinal gradient hypothesis with a maximum of fifteen LAGs observed in a single humerus, just slightly fewer than the maximal count reported for *P. perotorum.* Of course, as noted by Rooij (2018), to fully test the latitudinal gradient hypothesis more northern chasmosaurines would need to be histologically sampled. Regardless, the hypothesis is very well supported in the case of centrosaurines.

Assuming that only those ceratopsids living in the harshest, and therefore most seasonal, environments reliably deposited a LAG every year, then the assumption that LAGs provide a good indication of age breaks down as proximity to the equator increases. In the most northern species, *Pachyrhinosaurus perotorum,* counting LAGs likely produces a relatively accurate representation of an individual's age. *P. lakustai,* from a slightly more southerly region that likely had correspondingly milder winters, may have failed to deposit a LAG every year, so that the LAG record would yield an underestimate of an individual's age at death. *P. lakustai* would then likely have lived to ages exceeding 21 years, the maximum age estimate obtained in this study by straightforward application of the section stacking method. The LAG record would become even less accurate in ceratopsids at lower latitudes, producing increasingly severe underestimates.

Growth

The growth trajectory of *P. lakustai* is inferred to have been sigmoidal in shape (Fig. 3.7), so that growth was relatively slow in juveniles, accelerated considerably in subadults, and then tapered off at adulthood. This overall shape is common throughout Dinosauria (Erickson, 2014), and has been documented in theropods (Erickson et al., 2004), hadrosaurs (Cooper et al., 2008) and basal ceratopsians (Erickson and Tumanova, 2000).

Despite the drastic differences in size and in phylogenetic position within Ceratopsia between *Pachyrhinosaurus lakustai* and *Psittacosaurus mongoliensis*, their overall growth patterns are quite similar based on the growth trajectory presented for the latter species by Erickson and Tumanova (2000). Both seem to have reached subadulthood near age five, if this ontogenetic transition is defined by an acceleration in growth, and reached adulthood around age twelve when growth decelerated. To attain its large adult body mass, however, *P. lakustai* grew more rapidly during the subadult stage, at a rate of approximately 122 kg/yr compared to only 4-5 kg/yr for *Psittacosaurus mongoliensis*. A similar pattern has been documented in theropods, with maximal growth rates of 767 kg/yr for *Tyrannosaurus* and 122 kg/yr for *Albertosaurus* (Erickson et al., 2004). It is probable that the tendency of larger-bodied taxa to grow more rapidly, rather than necessarily for longer periods of time, is found throughout Ceratopsia. However, plots of estimated mass as a function of estimated age will have to be generated for more ceratopsian species to confirm this hypothesis.

Body Mass

Although *Pachyrhinosaurus lakustai* is well within the size range of other centrosaurines, there is a great deal of variation within the genus. The largest specimen of *P. lakustai* weighs in

at an estimated 1690 kg, while the largest known *P. canadensis* specimen is much larger at 3287 kg. The large size of *P. canadensis* is consistent across all elements studied, with all available *P. canadensis* specimens surpassing the same elements of the largest *P. lakustai* specimens. As *P. lakustai* has been discovered at more northerly latitudes than *P. canadensis*, it is possible that this variation reflects stunted growth due to the harsh, northern climate. This hypothesis is reinforced by information from the Alaskan species *Pachyrhinosaurus perotorum*, in which the skull is comparable in size to *P. lakustai* (Fiorillo and Tykoski, 2012). *Pachyrhinosaurus perotorum* is considered to have experienced harsher conditions than almost any other dinosaur, including cold temperatures, seasonal extended periods of darkness, and limited food resources (Erickson and Druckenmiller, 2011). Although *P. lakustai* and *P. perotorum* are clearly distinct species (Currie et al., 2008), it is possible that they inhabited the same, or similar, palaeolatitudes during the time of year when resources were scarcest. That is, *P. perotorum* may have migrated south in the winter in search of more resources, much as caribou do today (Fancy et al., 1989). It has been proposed that Alaskan hadrosaurs took part in this type of migration (Parrish et al., 1986; Currie, 1989). Therefore, it is possible that *P. perotorum* migrated along the Western Interior Seaway to inhabit the same palaeolatitude as *P. lakustai,* which may explain their similarity in size. However, Fiorillo and Gangloff (2001) reassessed this migratory hadrosaur hypothesis in the light of growth, body size and inferred physiological ecology. They determined that this migration was unlikely to have occurred, as juvenile hadrosaurs would have been too small to participate in the journey, and this conclusion probably applies to *P. perotorum* as well. Furthermore, the migratory hypothesis is incompatible with the latitudinal gradient hypothesis previously discussed. If *P. lakustai* and *P. perotorum* inhabited the same palaeolatitude in the winter, they would likely have had identical maximum LAG counts, which was not observed in

the present study. Although *P. lakustai* and *P. perotorum* are unlikely to have shared the same habitat even during the winter months, both of them resided farther north than *P. canadensis* and were undoubtably smaller than that species. Therefore, it is possible that they both experienced stunted growth, relative to *P. perotorum*, due to the colder conditions.

In the modern world, the harsh conditions associated with high latitudes force the animals that reside there to adapt to extreme degrees in order to survive. This has led to the evolution in some endothermic vertebrates of thick layers of insulating fat (Castellini, 2009) or the ability to burrow in deep snow (Back et al., 1987), and in some insects of the capacity to survive by allowing freezing of the entire body (Sinclair and Chown, 2005). Similar adaptations to cold would probably have been present in some taxa that inhabited boreal parts of western North America in the Late Cretaceous, although conditions at high latitudes were likely much less severe than those seen today. Given the presumably limited food available at northern latitudes during the winter months, not many species could have survived there, so that those able to adapt to the conditions could have thrived with little competition. One line of evidence for this scenario comes from an observed increase in the size of *Troodon* teeth from northern Alaska compared to those from southern latitudes (Fiorillo, 2008). In the absence at northern latitudes of competition from large predators, smaller carnivorous species such as *Troodon* would have been able to obtain enough prey to reach larger body sizes than their southern counterparts. The opposite may have occurred in herbivores such as *Pachyrhinosaurus,* as the seasonally limited availability of food resources may have made it impossible for them to grow to the size of the southern species *P. canadensis*. Similar hypotheses have been put forward for a small sauropod species from northern Germany (Sander et al., 2006). Specifically, the small size of this taxon was suggested to be a consequence of limited resources on the palaeo-island on which it would have resided,

although the limited area of the island may have been an additional factor. To find a case of small body size among extant northern species one need not look farther than squirrels. While large-bodied grey squirrels (*Sciurus carolinensis*) are widespread in southern regions of Canada, the red squirrel (*Tamiasciurus hudsonicus*) typically resides at more northern latitudes and is, in many cases, less than half the size of a typical grey squirrel. Small body size has also been reported in the European red squirrel (*Sciurus vulgaris*) as an indicator of stress due to habitat fragmentation (Wauters et al., 1996). In both cases small size can be traced to limited resources, whether due to habitat fragmentation or a cold climate, so that a large body size would simply be unsustainable.

The Wapiti River Bonebed in the Grande Prairie area, located slightly higher (170 m, Fanti and Currie, 2007) in the Wapiti Formation than the Pipestone Creek Bonebed, has produced a *Pachyrhinosaurus* species different from *P. lakustai*. The Wapiti River Bonebed taxon is thought to be either a completely new species of *Pachyrhinosaurus* (Kruk, 2015) or conspecific with the southern species *Pachyrhinosaurus canadensis* (inferred from Fanti et al., 2015). The material from this site seems to vary in size, with most elements falling in the size range of the subadult age class for *P. lakustai.* These elements are much smaller than southern *P. canadensis* material, but some of them may simply be from younger, and therefore smaller, individuals than those found in southern Alberta. In particular, two ulnae collected from the Wapiti River Bonebed (UALVP 52044, UALVP 52592) are much smaller than the largest *P. lakustai* ulnae, but are most likely from immature individuals given their morphology (see chapter 2 of this thesis). However, other elements are similarly sized or slightly larger than *P. lakustai* specimens. Most notable is a *Pachyrhinosaurus* skull from the Wapiti River Bonebed (UALVP 53300) which measures 875 mm in length (from the rostrum to the occipital condyle)

(Kruk, 2015). This makes the Wapiti River skull slightly larger overall than the largest *P. lakustai* skull (870 mm in length) (Currie et al., 2008), much larger than the largest *P. perotorum* skull (756 mm in length), and yet much smaller than any *P. canadensis* skull so far described (Kruk, 2015). If the Wapiti River Bonebed *Pachyrhinosaurus* is referable to *P. canadensis*, it probably represents a population characterized by unusually small body size, potentially due to living in a harsh climate. Histological work will be necessary to determine whether the Wapiti River Bonebed specimens are in fact adults of a smaller species than *P. canadensis*, or whether they are simply immature.

This degree of size variation seems to be unique to *Pachyrhinosaurus.* Variation in size documented in other genera (*Centrosaurus, Chasmosaurus,* Fig 3.10) does not approach the level seen among *Pachyrhinosaurus* species. Furthermore, the latitudinal range of *Pachyrhinosaurus* is rivalled among ceratopsid genera only by *Triceratops,* which occurs from Colorado to Saskatchewan, and *Torosaurus,* which occurs from New Mexico to Saskatchewan (Diem and Archibald, 2005). Although broad, the distributions of *Triceratops* and *Torosaurus* do not extend as far north as those of *P. lakustai* and *P. perotorum.* Thus, one would not expect the size of *Triceratops* or *Torosaurus* to be limited by resources availability, even in Saskatchewan.

Age Classes and Population Ecology in Ceratopsid Bonebeds

The sample of *Pachyrhinosaurus lakustai* pectoral girdle and forelimb bones from the Pipestone Creek Bonebed includes a particularly large number of juvenile elements. A few more subadult individuals are present than adults (Fig. 3.7). However, there may be a distinct sampling bias in these numbers as fragmentary elements were not used in this study, and based on personal observation, large adult specimens seem to be more likely to fracture than small juvenile

specimens. This bias may have skewed the proportions of the age classes from the assemblage, but juveniles are nevertheless so much more abundant than subadults and adults that the discrepancy cannot be ignored. This leads to the hypothesis that the assemblage at the Pipestone Creek Bonebed represents the weakest individuals within a herd of *Pachyrhinosaurus lakustai*. This hypothesis is consistent with the long-standing interpretation that the Pipestone Creek Bonebed is the result of a flooding event in which a large herd perished while attempting to cross what may have normally been shallow or slow moving waterway (Currie et al., 2008). In this case the smallest individuals (juveniles) and the weakest individuals (oldest and presumably largest adults) would be expected to be overrepresented in the sample, which is the case at Pipestone Creek. A contrasting example is provided by a large *Centrosaurus* bonebed in southern Alberta, Bonebed 43 (Ryan et al., 2001b), at which the cause of death is also thought to have been a flooding event. From this site Ryan et al. (2001b) reported a strong preponderance in the sample of adults (88.6%), and a much lower percentage of juveniles than that seen at Pipestone Creek (4.4%, vs. 51% at Pipestone). However, this discrepancy may be due to a strong postmortem filter in Bonebed 43 that removed many of the juvenile elements (Ryan et al., 2001b).

Lehman (2006) noticed a size distribution broadly resembling that at Pipestone in a *Chasmosaurus mariscalensis* bonebed in which only one out of nineteen individuals was a fully-grown adult, with the majority of the other individuals estimated to be under five years of age. Lehman (2006) interpreted this pattern as evidence of age segregation in which the youngest individuals lived apart from the adult population until they reached sexual maturity. Similar hypotheses have been put forward with respect to other non-avian dinosaurs as well. Myers and Fiorillo (2009) highlighted two separate sauropod bonebeds that contained only juvenile

individuals, as well as multiple other sites that contained only adult remains. They argued this was evidence of minimal, or absent, parental investment. Although adult material is present at both Pipestone and the *C. mariscalensis* bonebed, or Bonebed 43 Mathews et al. (2009) described a *Triceratops* bonebed, the "Homer Site", that contained only juvenile individuals, again potentially indicating a lack of parental investment. Another *Triceratops* bonebed yielded a juvenile, a subadult, and a young adult (Keenan and Scannella, 2014). Due to taphonomic differences, as well as lithological differences in the surrounding matrix, Keenan and Scannella (2014) determined the juvenile was buried prior to the older individuals, which represented an isolated pair. Age segregation yet again characterizes the *Triceratops* bonebed described by Rooij (2018), in which only subadults and adults were found.

In the absence of a consistent pattern across ceratopsid bonebed assemblages, the population structures of a ceratopsid herd was evidently variable and could change depending on the resources available, as well as the time of year. In modern ungulates a herd tends to segregate by age when this will increase the overall fitness of its members (Ruckstuhl and Neuhaus, 2000). With intraspecific body size differences come intraspecific differences in movement rates and individual activity budgets. Therefore, segregation based on body size can lead to an increase in fitness as the animals more readily synchronize their behaviours. In times of limited resources ceratopsid populations may likewise have segregated based on age, and therefore body size, in order to better take advantage of the available resources and improve their overall fitness. In extant elk (*Cervus elaphus*) populations, the extent of this type of segregation varies not only seasonally, but also seemingly at random throughout the year (Bender and Haufler, 1999). Although some ceratopsid bonebeds may represent populations that segregated according to age

on a seasonal basis, segregation patterns were seemingly highly inconsistent, as in modern ungulates.

Conclusion

The Pipestone Creek Bonebed contains individuals ranging from under one year old to twenty-one years old. Histological sampling of the largest individual resulted in the identification of an External Fundamental System, indicating this individual was fully grown at death. Based on humeral circumference this individual had a body mass of approximately 1690 kg. Although this size is likely an underestimate, *P. lakustai* is smaller than its southern relative, *P. canadensis*. This small body size may be due to limited resources in a colder climate. As is typical for dinosaurs, the growth curve of *P. lakustai* is sigmoidal in shape with the highest rate of growth occurring in subadulthood. Comparing this study to other histological analyses of centrosaurines shows a clear latitudinal gradient in which increasing in latitude, and therefore seasonality, seems to increase the amount of LAGs likely to be present in a specimen. However, histological sampling of more northern chasmosaurines is necessary to determine if this gradient holds true throughout Ceratopsidae. There seems to be a large number of juveniles within the Pipestone Creek Bonebed assemblage, which may indicate age segregation in the population. However, the seemingly random occurrence of age segregation in extant herd animals weighs against the idea of consistent age segregation throughout Ceratopsidae, or even within any single ceratopsid species. The abundance of juveniles is more likely a taphonomic bias in which juveniles were less likely to survive a flooding event at Pipestone Creek.

Overall, ontogenetic analysis of *P. lakustai* has yielded a great deal of information as to the overall growth of these animals, providing a basis for comparisons with other ceratopsids.

Further analysis of other ceratopsid bonebeds will enable comparable conclusions to be drawn for other species and potentially shed light on the population structure of ceratopsids as a whole.

Chapter 4 - Manual Pathology in *Pachyrhinosaurus lakustai* and its Implications for the Gait and Step Cycle of Centrosaurine Ceratopsians

Introduction

Palaeopathologies are relatively common in the fossil record. They have been documented in most parts of the skeleton in nearly every group of non-avian dinosaurs from hadrosaurs (Straight et al., 2009) to theropods (Hanna, 2002), and from large sauropods such as camarasaurids (Tschopp et al., 2014) to relatively small ornithopods such as *Dysalotosaurus* (Witzmann et al., 2008). Not only have these abnormalities been observed in body fossils, but theropod trackways and footprints also show signs of pathologies (McCrea et al., 2015). Ceratopsians are no exception to the prevalence of pathological features, which have been described in taxa ranging from basal ceratopsians such as *Psittacosaurus* (Lü et al., 2007) to larger ceratopsids such as *Chasmosaurus* (Rega et al., 2010).

Although pathologies are often observed in ceratopsians, they are not commonly described, particularly in detail. The palaeontological purpose of diagnosing a pathology is quite different from that which a medical doctor would have in diagnosing a patient. As Rega et al. (2010) described, the objective is not to cure the disease, but rather to use the evidence of it to gain a better understanding of how the animal lived. In short, how did the disease affect the animal's life? Answering this question may be relatively simple with regards to pathologies caused by injuries. For instance, it is easy to observe a *Triceratops* pelvis with multiple bite marks and hypothesize that the flesh surrounding the bone made a meal for a *Tyrannosaurus rex* (Erickson and Olson, 1996). However, there are many more possibilities with regard to pathologies caused by diseases, which can be more difficult to diagnose and to understand in terms of their impact on the individual organism.

Most ceratopsian pathology studies have focused on injuries to the skull. Like a number of other authors, Farke et al. (2009) used pathologies in skulls of *Triceratops* to test if these

animals did indeed use their cranial horns for intraspecific combat. A notable exception, however, is provided by speculations that centrosaurines such as *Pachyrhinosaurus* took part in flanking behaviour (Tanke and Rothschild, 2010). This behaviour involves head-butting conspecifics in the flank, causing posterior ribs to fracture; these ribs then retain visible pathologies upon healing. However, not all ceratopsian postcranial pathologies are combat-related. An excellent example is the humerus of *Spiclypeus shipporum* (CMN 57081), in which Mallon et al. (2016) described bone remodeling and an abscess cavity to be indicative of a chronic infection. They speculated that the cause of the infection may have been a fungus or even tuberculosis, but neither hypothesis could be confirmed, exemplifying the difficulty of arriving at concrete diagnoses for potentially complex pathologies in fossil vertebrates.

Despite the prevalence of uncertainty in palaeopathological studies, hypotheses are sometimes advanced with a level of solid evidence and justification that takes them out of the realm of speculation. One such case involves pathologies of the manus in two chasmosaurine specimens (Rega et al., 2010). This type of pathology was described first by McGowan (1991) in *Chasmosaurus belli* ROM 843, and was later followed by Thompson and Holmes (2007) in *Chasmosaurus irvinensis* CMN 41357. The observed pathological features were very similar between the two specimens and included overall rugose texture, as well as indications of bone reabsorption and remodeling in certain manual elements (Rega and Holmes, 2006). The pathological features were described in the first digit (the thumb) of the right manus of CMN 41357, affecting MC (metacarpal) I and Ph I-1 (phalanx) as well as Ph I-2, and to a lesser extent in MC V. In ROM all elements of the first digit on both the left and right manus presented pathologies, as well MC V on both the left and right manus, and MC IV on the right manus.

As well as noting pathologies in CMN 41357, Thompson and Holmes (2007) utilized half-scale models and trackway data to reconstruct the probable step cycle of *Chasmosaurus.* In doing so they remarked that the forces experienced by the manus during propulsion would cause repetitive stress to the manual elements, potentially explaining the observed pathologies. Rega et al. (2010) extended this hypothesis to ROM 843 and determined that the pathology was due to repeated stress on the first digit of the manus, caused by the medial rolling of the manus during the propulsive phase of the step cycle proposed by Thompson and Holmes (2007). Rega et al. (2010) noted this was most likely exacerbated by a pathogen.

The present study describes the first known centrosaurine manual elements with pathologies that may be comparable to those seen in CMN 41357 and ROM 843. These elements include MC I, MC V and Ph I-1 (see Chapter 2 of this thesis for ceratopsid manual element identification), belonging to *Pachyrhinosaurus lakustai* from the Upper Campanian Pipestone Creek Bonebed in the Wapiti Formation near Wembley, Alberta. Unlike the chasmosaurine specimens, these elements do not belong to a skeleton found in association, but instead are among the hundreds of disarticulated *P. lakustai* bones that have been recovered from Pipestone Creek, one of the densest non-avian dinosaur bonebeds in the world (Currie et al., 2008). The Pipestone material includes a wide range of manual elements of varying ontogenetic stages. Pipestone has previously produced other pathological elements, including a suspected pathological nasal boss (TMP 1989.055.0899) and 15 other cranial elements and 18 postcranial elements exhibiting various deformities (Tanke and Rothschild, 2010). However, the only manual element among the Pipestone specimens with a pathology was a single phalanx with a partially healed stress fracture (TMP 1985.112.0070). In any case there has been no account of manual pathologies due to bone degradation by disease in the Pipestone assemblage.

Due to the rarity of pathological manual elements, the ones described in this paper could not be sectioned for histological analysis. However, in more recent years computed tomography (CT) scanning has been increasingly utilized as a non-destructive method of examining the internal structure of fossils. The main objective of these CT studies has been to map the distribution of pathological tissues in three dimensions. As fossils are usually much denser than unpermineralized bone scanned in medical-grade CT scanners, palaeontologists rely on micro-CT technology to generate a high-resolution scan that may capture pertinent information. However, even if a specimen has been fully prepared the matrix in which the specimen was preserved will fill the internal spaces within a bone. The lithology, and particularly density, of this matrix directly effects the informativeness of micro-CT scans. It was likely this factor that prevented Rega et al. (2010) from discerning any internal morphology in their scans of the terminal phalanges of CMN 41357. In the present study micro-CT scanning was used to investigate the internal morphology of the only known pathological first metacarpal of *P. lakustai* (UALVP 57914) in an attempt to determine the extent of the structural alteration caused by the pathology. A pathological MC V and Ph I-1 were also examined and assessed from a palaeopathological perspective, although they could not be CT scanned.

Materials and Methods

Specimen Selection

Pachyrhinosaurus lakustai manus material was surveyed in the University of Alberta Laboratory for Vertebrate Palaeontology (UALVP) collections, including those housed at the Philip J. Currie Dinosaur Museum (PJCDM). *Pachyrhinosaurus lakustai* manus material was also surveyed at the Royal Tyrrell Museum of Palaeontology (TMP) to identify any specimens

with potential pathological features similar to those seen in CMN 41357 and ROM 843. This resulted in identification of the pathological phalanx I-1 UALVP 57662, the pathological fifth metacarpal TMP 1989.055.1369, and the pathological first metacarpal UALVP 57914. All three specimens were photographed and described, and UALVP 57914 was selected for CT-scanning because the specimen appeared more severely affected by the pathology than the others, and because pathological first metacarpals had been previously discussed by Rega et al. (2010).

Micro CT-scanning and analysis

UALVP 57914 was scanned using a SkyScan 1076 X-ray computed tomography scanner in the Faculty of Pharmacy and Pharmaceutical Sciences at the University of Alberta (Edmonton, AB). The scan was performed at 100 kV and 100 μA. This produced a stack of 2677 images each measuring 1968 px by 1968 px, and aligned approximately transverse to the long axis of the metacarpal. Frame averaging was set to 2, and the rotation step was 0.700 degrees with a pixel size of 34.4000 μm. The scan data was imported into SkyScan DataViewer and SkyScan CTvox (Bruker Corporation) as a series of stacked TIF images for easy visualization and rendering.

Results

Metacarpal I (UALVP 57914)

The overall shape of UALVP 57914 (Fig. 4.1) is standard for a ceratopsid first metacarpal, consistent with the fact that little variation in first metacarpal morphology is seen throughout Ceratopsidae (as described in Chapter 2 of this thesis). The distal end is typical in being trapezoidal, but the proximal end is more triangular than those of other first metacarpals, which tend to be subcircular. This is particularly true of the *Pachyrhinosaurus* specimen UALVP

57434 from the Wapiti River Bonebed near Grande Prairie, Alberta. The proximal surface bears distinct, irregularly distributed round pits. The metacarpal appears somewhat sinuous in dorsal and ventral view. The dorsal and ventral surfaces are relatively smooth, unlike in CMN 41357 and ROM 843, but a small area on the proximomedial corner of the dorsal surface is an exception. Here the surface of the bone is quite distorted, bearing elevated irregular nodules. This surficial irregularity also extends down the entire length of the medial side of the element. The fossa on the medial side of the element remains oval in shape, as is typical for ceratopsids, but is more elongate than in the non-pathological first metacarpal UALVP 57434. The bone dorsal to the fossa represents the only smooth area on the medial side of the element, whereas the bone ventral to the fossa displays the abnormal nodules present all over the medial side. Interspersed with the nodules are multiple depressions, which are possibly indicative of bone resorption. Directly proximal to the medial fossa lies a subcircular medial prominence 10 mm in diameter, and there is a nearly identical prominence on the lateral side. A protrusion of the same type is present on the distal end of CMN 41357 (Rega et al., 2010). The lateral surface of the element is unfortunately mostly broken away. However, there is a small section of intact but abnormal bone surface, proximal to where the fossa would have been, that bears nodules identical to those found on the medial side. The proximal and distal ends of the element are relatively smooth and are comparable to those of other ceratopsid metacarpals. However, a few 1 mm long abrasions run parallel to, and close to, the dorsolateral side of the proximal end. A small circular depression lies on the proximal end of the dorsal surface of the element, and the ventral side of the element bears a similar depression. These may be indicative of bone resorption, but may also represent some other kind of pathology or damage.

Figure 4.1. Pathological *Pachyrhinosaurus lakustai* first metacarpal.

UALVP 57914, left first metacarpal, in A) lateral, B) medial, D) dorsal, E) ventral, F) proximal and G) distal views. C) Close-up of irregular surface on medial side of metacarpal. Scale is 2 cm for A, B, and D-G, and 1 cm for C. Abbreviations: f, fossa; lp, lateral prominence; mp, medial prominence; p, pits.

Phalanx I-1 (UALVP 57662)

This phalanx (Fig. 4.2) is most similar in overall shape to UALVP 54282, identified as an example of Ph I-1 in Chapter 2 of this thesis. However, the proximal end is more expanded in UALVP 57662 and does not exhibit the flatness seen in the non-pathological phalanx I-1. Instead, the proximal end (Fig. 4.2F) is relatively convex, and bears an elongate mediolaterally aligned and centrally positioned trough. This feature probably formed as a result of bone resorption. Beyond the proximal end, the element tapers sharply to form a narrow shaft, resembling that of a non-pathological phalanx I-1. The distal end has one clear collateral ligament fossa, located on the ventral portion of the medial side of the element. The part of the ventral surface adjacent to the fossa bears clear grooves not seen in other phalanges. Similar lineations are present on the dorsal side of the distal end. Dorsal to the medial fossa is a clear protrusion. In other elements from Pipestone similar protrusions seem to be a product of crushing of the element, but that does not appear to be the case here. This knob extends as far medially as does the flared proximal end of the phalanx. The distal end of the element is more mediolaterally compressed than the proximal end, the discrepancy being much greater than is seen in other phalanges and overall is relatively rounded. The distal end also bears a series of grooves as is typical in ceratopsid manual elements. Although retaining a generally trapezoidal shape, the distal end protrudes farther medially than those of other phalanges.

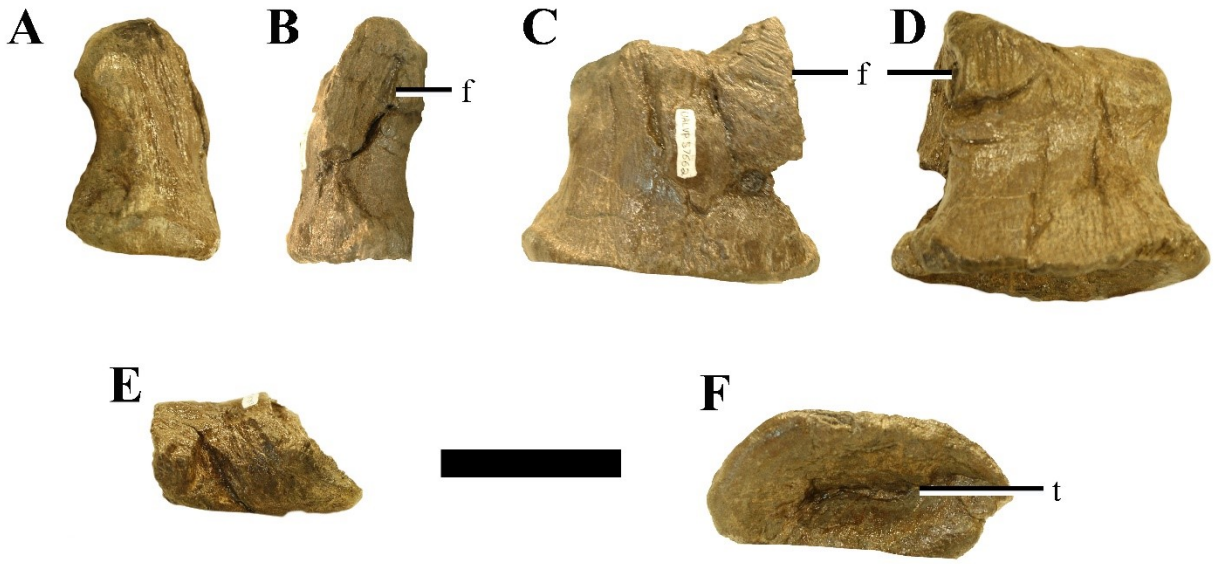

Figure 4.2. Distorted *Pachyrhinosaurus lakustai* phalanx I-1.
UALVP 57662, manual phalanx I-1, in A) lateral/medial, B) lateral/medial, C) dorsal, D) ventral, E) distal and F) proximal views. Scale is 5 cm. Abbreviations: f, fossa; t, trough.

Metacarpal V (TMP 1989.055.1369)

TMP 1989.055.1369 is typical of ceratopsid fifth metacarpals in general shape (Fig. 4.3), having a mediolaterally expanded proximal end and a narrower distal end as described in Chapter 2 of this thesis. The indications of pathology on this element are mostly limited to the medial side, unlike in UALVP 57914 (Fig. 4.3C). This surface of the element bears a clearly discernible medial fossa at the proximal end. It also has the same abnormal surface texture of irregular elevated nodules and pits described in UALVP 57914 along the ventral side of the fossa and extending along the entire medial surface. Ventral to the fossa there is also a subcircular medial protrusion, but this feature is much smaller than the similar one on UALVP 57914. There are small patches of the irregular surface texture on the distal end of the element, and on the lateral side along the shaft as well as just distal to the level of the proximal end. This element

shows is no clear evidence of resorption.

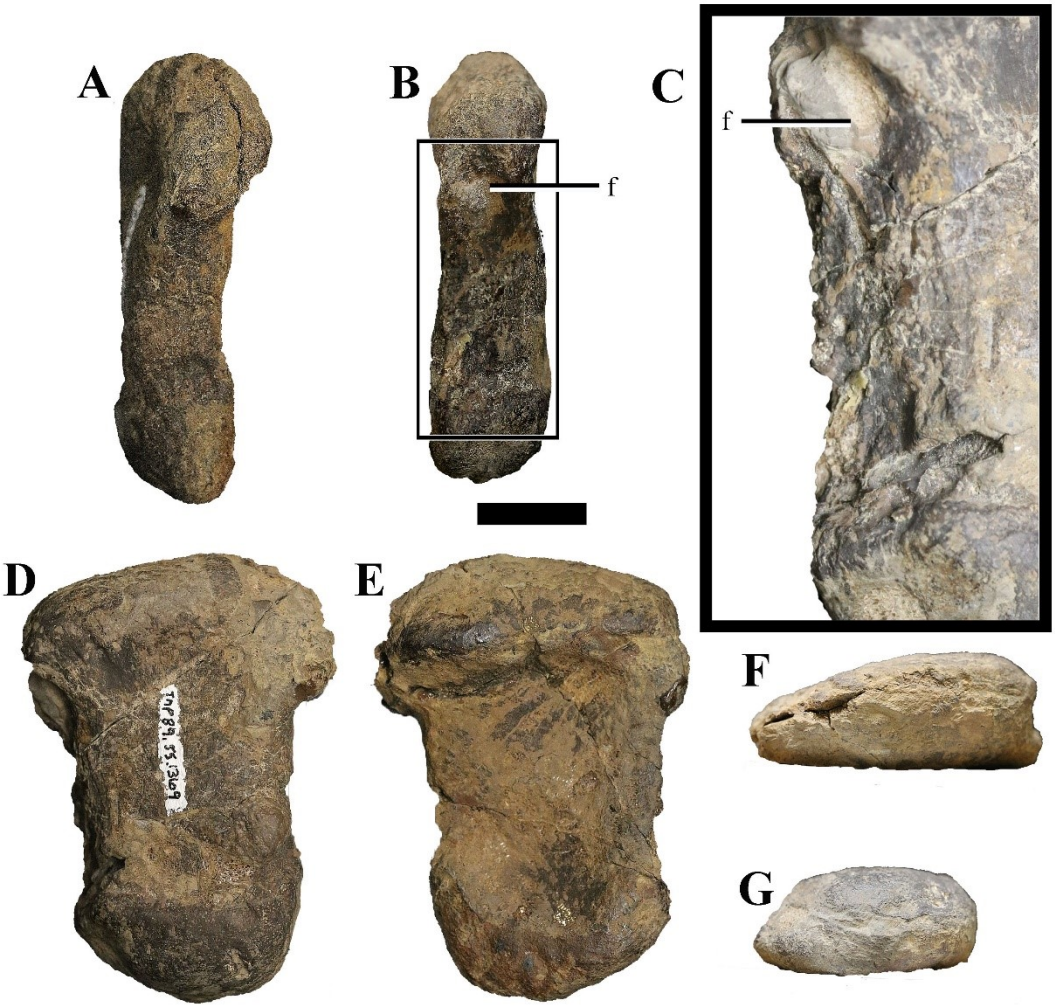

Figure 4.3. Pathological *Pachyrhinosaurus lakustai* fifth metacarpal.

TMP 1989.055.1369, left fifth metacarpal, in A) lateral, B) medial, D) dorsal, E) ventral, F) proximal and G) distal views. C) Close-up of apparent pathological feature on medial side of metacarpal, shown in a somewhat oblique view for greater clarity. Scale is 2 cm for A, B, and D-G and 1 cm for C. Abbreviations: f, fossa.

Micro-CT Analysis

UALVP 57917 proved to be extremely dense, and micro-CT scanning therefore yielded limited information with regard to its internal morphology, particularly close to the exterior of the element. The irregular surface texture was evident in the volume rendering of the scan (Fig. 4.4), but details were unclear.

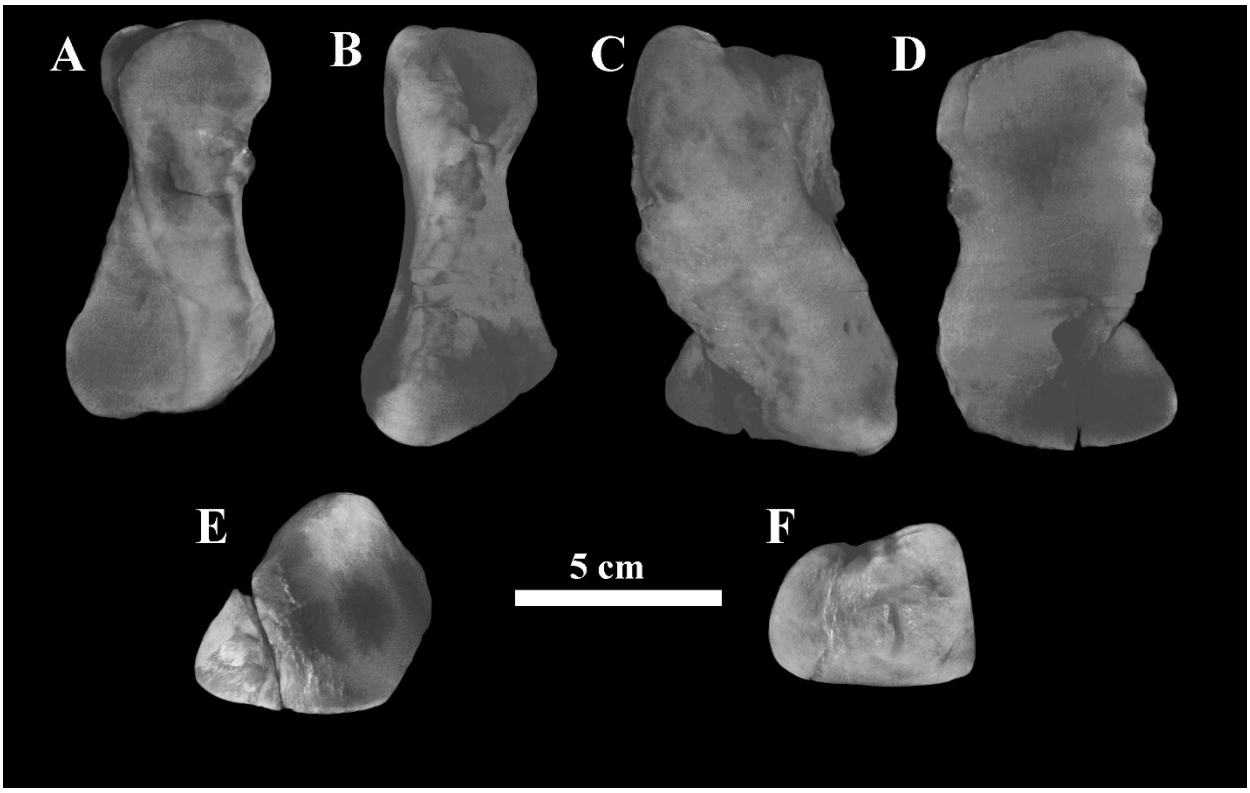

Figure 4.4. 3D model of pathological *Pachyrhinosaurus lakustai* first metacarpal.
3D model of left first metacarpal UALVP 57914, generated from micro-CT data in A) lateral, B) medial, C) dorsal, D) ventral, E) proximal and F) distal views. Scale is 5 cm.

The individual CT slices revealed a distinct porous texture in isolated areas of the element. The porous areas contain multiple small irregularly-shaped cavities, separated by thin walls of bone, and are no larger than about 5 mm by 8 mm in the cross-sectional plane, with a maximum depth of 3 mm. These porous areas are associated with the large nodules of irregular

bone on the medial and lateral surfaces of the element. On the medial side the porous texture is restricted to the largest nodule (Fig 4.5) and seems to dissipate into the regular texture of the element towards the centre of the element (Fig 4.5D). As seen in the dorsoventral plane the porous texture fills the entirety of the nodule and is not limited to the surface (Fig 4.5A)

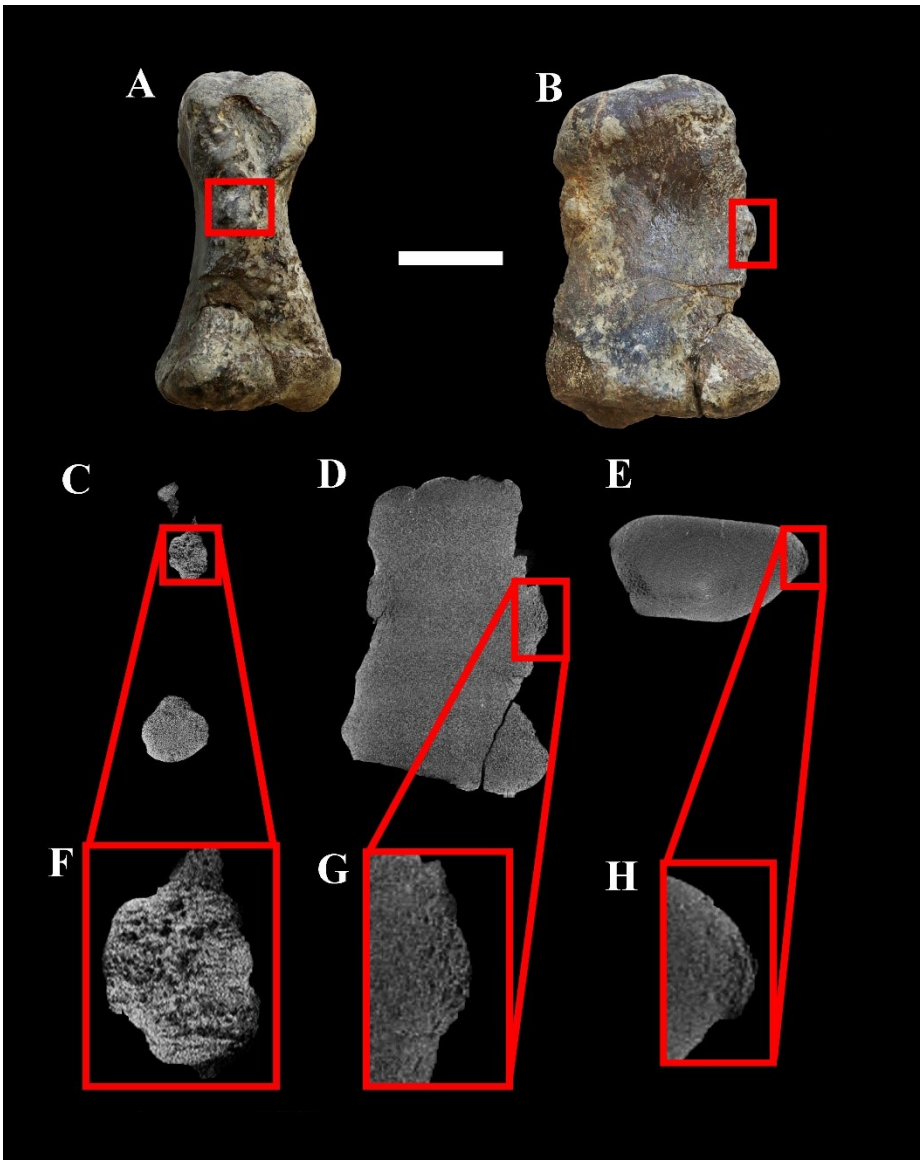

Figure 4.5. Micro-CT scans of region of pathological bone on medial side of *Pachyrhinosaurus lakustai* first metacarpal.

UALVP 57914 in A) medial and B) ventral views, with scans in the C) parasagittal plane, D) coronal plane and E) transverse plane with respective closeups F, G and H. Red rectangles frame

proposed pathological feature causing porous texture in CT scans. Scale is 3 cm for A-E and 1 cm for F-H.

On the lateral side of the bone, the porous texture extends 5 mm internally (Fig. 4.6) and appears to be associated with the irregular lateral prominence visible on the surface of the element (Fig. 4.6C and F). The porous texture only extends 1.5 mm internally on the medial side, but again is associated with the prominence on the adjacent part of the surface of the element (Fig. 4.5C and F). Furthermore, the proximodistal extent of the porous texture within the element is also much greater on the lateral side than on the medial side (Fig. 4.6 AB and DE). Unlike in the case of the medial side, however, the porous texture on the lateral side is associated with a fracture in the element. There is also a region of dense texture partially surrounding the porous texture, as seen in the parasagittal CT image (Fig. 4.6A and B). This dense region lacks the small internal cavities previously described in the porous area, and instead appears as a solid mass of bone that extends the whole interior of the bone, apart from the region of porous texture previously described.

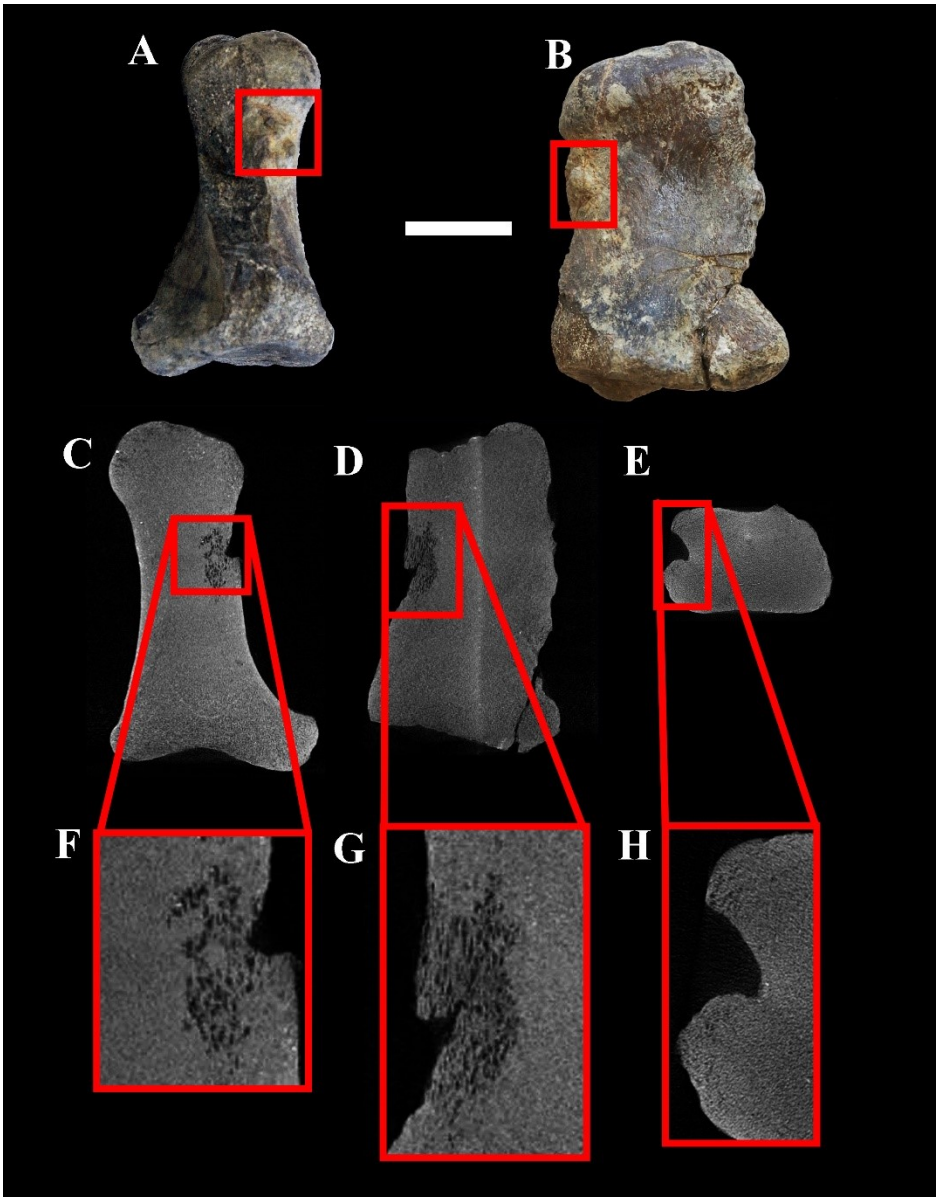

Figure 4.6. Micro-CT scans of region of pathological bone on lateral side of *Pachyrhinosaurus lakustai* metacarpal I.

UALVP 57914 in A) lateral and B) ventral views, with CT scans in the C) parasagittal plane, D) coronal plane and E) transverse plane with respective closeups F, G and H. Red rectangles frame proposed pathological feature causing porous texture in CT scans. Scale is 3 cm for A-E and 1 cm for F-H.

Discussion

Ceratopsid palaeopathologies are relatively common. However, instances of similar pathologies in multiple taxa are relatively rare. Thompson and Holmes (2007) noted the possibility that repeated stress on the first manual digit had caused the pathology in CMN 41357. Rega et al. (2010) observed the similarities between *Chasmosaurus irvinensis* CMN 41357 and *Chasmosaurus belli* ROM 843, allowing for the extension of this hypothesis to a second species of *Chasmosaurus*. These similarities led Rega et al. (2010) to hypothesize that the repeated stress due to similar locomotory patterns may have caused the manual pathology in two different *Chasmosaurus* specimens, and one reason the pathologies described here are of interest.

The elements described here are highly rugose in places, showing an irregular external texture not evident in any other manual elements excavated from the Pipestone Creek Bonebed. Both metacarpals (TMP 1989.055.1369, UALVP 57914) display irregular surface patterns featuring areas of resorption as well as large nodules, just as in both previously described *Chasmosaurus* specimens with pathological manual first digits (Rega et al., 2010). The deformed Ph I-1, however, does not share the irregular surface texture of the metacarpals. Instead, the elongate cavity on the proximal end of the element (Fig. 4.2F) is similar to those previously reported on the distal end of the humerus of *Spiclypeus* CMN 57081, between the radial condyles (Mallon et al., 2016). Based on a CT analysis of *Spiclypeus*, Mallon et al. (2016) concluded that the pathology was due to chronic osteomyelitis, or in other words a severe and long-lasting infection of the bone. Similar cavities were observed by García et al (2016) on the posterior articular surfaces of a series of twelve vertebrae of an adult titanosaur sauropod from the Upper Cretaceous of Argentina, and were also determined to be caused by an osteomyeletic infection. Although the cavity appears less pronounced in UALVP 57662 than in CMN 57081, it is similar

in appearance to those described by García et al. (2016), and its presence suggests the possibility of osteomyelitis in UALVP 57662. However, micro-CT or histological analysis will be necessary to draw firm conclusions regarding the pathological features of this phalanx.

Similar distortion of bones has been described in extant Nile crocodiles, in which a number of juvenile and adult humeri were found to exhibit some areas in which the bone had collapsed inward to form cavities (Huchzermeyer et al., 2013). The cavities were determined to likely have been caused by a form of osteodystrophy, the development of defective bone, or osteochondrosis, a pattern of bone resorption followed shortly by bone growth (probably brought on by stress). As the specimens in question represent animals raised in captivity, there was little accompanying information collected that might shed light on any geographical or epidemiological patterns, making a precise diagnosis difficult. However, the pathological crocodile humeri provide an important point of comparison to dinosaur specimens that show evidence of bone disease, as very few other studies have attempted to connect pathologies observed in extant reptiles to those in extinct reptiles. Instead, studies of disease in extant reptiles tend to focus on soft tissue pathologies rather than osteological ones.

Both *P. lakustai* metacarpals lack distinct cavities like the one described in UALVP 57662. The irregular surface textures of these bones are comparable to those seen in some manual elements in the *Chasmosaurus* specimens CMN 41357 and ROM 843 described by Rega et al. (2010), but the elements show much less overall distortion and the irregular texture is restricted to more limited areas. Although Rega et al. (2010) focused on the first digit of the *Chasmosaurus* manus, deformation has also severely affected the fifth digit of CMN 41357 and the fourth and to some extent the fifth digits of the right manus of ROM 843. It is probable that the observed pathology on the *P. lakustai* fifth metacarpal has the same root cause as the

pathology on the first metacarpal given that pathologies of these same elements co-occur in the *Chasmosaurus* specimens.

The surficial morphologies of the pathological *Pachyrhinosaurus lakustai* metacarpals are similar to those described by Rega et al. (2010). The *P. lakustai* metacarpals exhibit the same type of irregular nodules described in the *Chasmosaurus* specimens, and also share with them the presence of isolated, 8-10 mm, subcircular nodules that protrude more than the other nodules on the same surfaces. As previously noted, however, the irregular surface texture is not as widespread on the individual *P. lakustai* elements as on the *Chasmosaurus* ones. While the pathological manual elements of CMN 41357 and ROM 843 are entirely covered in the irregular, rugose texture, this texture is limited to the medial and lateral sides of both TMP 1989.055.1369 and UALVP 57914, and is evident primarily on the medial sides. Personal observations of CMN 41357 and ROM 843 revealed that the irregular textures on these manual elements are best developed on the medial surface as well. Rega et al. (2010) even noted that the medial part of the proximal joint surface of the first digit of CMN 41357 bore various pits, similar to the ones described on the proximal surface of UALVP 57914, and was the region that differed most strikingly in shape from its counterpart in non-pathological specimens. Keeping these similarities in mind, it is possible that the pathology seen in *P. lakustai* had the same origin as that previously documented in *Chasmosaurus,* but was less developed in that it had not affected the entirety of the element as in both *Chasmosaurus* specimens.

Rega et al. (2010) hypothesized that the pathology observed in the *Chasmosaurus* material was due to stress on the digits caused by the habitual movements of the manus during locomotion, coupled with a chronic infection or disease. The kinematic pattern of the manus was reconstructed using Thompson and Holmes' (2007) step-cycle analysis of CMN 41357 coupled

with ceratopsid trackway data, which acted as restraint for the articulation and pattern of movement of the forelimb. Their analysis described a semi-erect posture in which anterior rotation of the long-axis of the humerus during the step-cycle, which caused medial movement of the radius and therefore caused the manus to rotate medially as it left the substrate throughout the propulsive phase with the bulk of the animal's weight on the most medial digits. This rolling action would have placed considerable stress on the medial digits, and particularly on the first digit (Rega et al., 2010). The reconstruction of the *Chasmosaurus* step cycle proposed by Thompson and Holmes (2007) also applies to *P. lakustai* given the overall similar morphology of the forelimb, as described in the first chapter of this thesis. Furthermore, the amount of stress experienced by the manus would have been similar in *P. lakustai* and in the two *Chasmosaurus* species due to their similar body masses, as described in Chapter 3 of this thesis. Therefore, it is likely that the pathology seen in TMP 1989.055.1369 and UALVP 57914 was caused by the mechanism described by Rega et al. (2010).

As noted by Rega et al. (2010), the deformation was most likely due to habitual stress on the element combined with chronic osteomyelitic infection or another underlying disease, which would have increased the susceptibility of the digits to deformation. The exact nature of the osteomyeletic infection or disease is uncertain. Rega et al. (2010) speculated that the deformation in ROM 843 might be due to dyschondroplasia, a developmental defect causing cartilaginous degeneration that is known to occur in modern chickens (Edwards and Veltmann, 1983). However, a developmental disorder would likely affect the animal throughout its life, and therefore should be evident in specimens from various ontogenetic stages. In *Pachyrhinosaurus* and *Chasmosaurus*, however, manual pathologies have so far been documented only in specimens that appear to represent skeletally mature individuals. In addition to the irregular

surface textures, the first digits of CMN 41357 and ROM 843 notably deviated from the alignment typically seen in ceratopsians (Rega et al., 2010). The authors compared this morphology to hallux valgus; a condition causing bunions in humans (Tamer and Simpson, 2017). Hallux valgus is known to occur in adult humans and is typically found in the first digit of the foot, but has also been observed in the fifth digit (Tamer and Simpson, 2017). UALVP 57914 shows slight evidence of lateral deviation and torsion of the element that may also be indicative of hallux valgus. However, as this element is not part of an articulated manus, it cannot be confirmed if it would in fact have deviated from the general orientation of the digits. Furthermore, as this is the only identifiable first metacarpal from the locality, the morphology cannot be compared to that of a non-pathological element. TMP 1989.055.1369 does not show any evidence of deviation or torsion.

Another possible diagnosis is a form of metabolic bone disease (MBD), an osteopathy resulting in overall degradation and weakening of bones, such as osteoporosis. This common disease was described as the leading cause of nutritional pathologies in extant lizards by the Ontario Veterinary College Teaching Hospital (McWilliams and Leeson, 2001), followed by hemosiderosis and obesity, and has also been observed in caimans (Becker et al., 2018). As the name suggests, MBD is closely tied to the animal's nutrition and can arise due to a lack of essential nutrients in the environment (McWilliams and Leeson, 2001). For this reason MBD is typically associated with animals in captivity, but there have been reports of it occurring in a few wild animals, such as collared doves (Cousquer et al., 2007). Therefore, it is plausible that this condition may also have afflicted ceratopsids. Furthermore, MBD has been found in metacarpals of modern Komodo dragons (*Varanus komodoensis*) as large calcium deposits on and around the joint surfaces (Rothschild et al., 2012). As *P. lakustai* likely lived in less favourable conditions

for part of the year, due to the likely seasonality of what is now northern Alberta in the Late Cretaceous, this species might have been susceptible to the kind of nutrient deprivation that could cause MDB. As described in Chapter 3 of this thesis, the seasonal decline in productivity of the ecosystem may have caused populations to segregate by age in order to efficiently utilize the limited resources accessible to them. This may have resulted in particularly large, old, individuals not obtaining enough nutrients and suffering from MBD as a result. However, this age segregation may have alternatively benefitted the large and old individuals therefore negating this hypothesis.

Regardless of the precise diagnosis, Rega et al. (2010) commented that the manual pathology resulted in part from the size and age of the individuals. The *Chasmosaurus* specimens in which the pathological features occurred were most likely skeletally mature adults. If they were particularly old individuals, they would have been especially susceptible to diseases and infections, which would have caused degradation of the bone. This holds true for *P. lakustai* as well, although due to the disarticulated nature of the material from the Pipestone Creek Bonebed the ages of the individuals to which the metacarpals belong cannot definitively be assessed. Based, however, on the sample of metacarpals analysed at the Philip J. Currie Dinosaur Museum, the Royal Tyrrell Museum of Palaeontology, and the University of Alberta Laboratory for Vertebrate Palaeontology, TMP 1989.055.1369 and UALVP 57914 are the largest first and fifth metacarpals collected from the site and are proportional in size to the largest second, third and fourth metacarpals from the site. Therefore, these elements most likely belong to some of the largest, and therefore oldest, individuals in the Pipestone sample. With this assumption in mind these elements most likely belonged to individuals that had a body mass of about 1690 kg. This would make them slightly larger than CMN 41357, which most likely had a minimum body mass

of 1478 kg, and slightly smaller than ROM 843, with a minimum mass of 2756 kg. No juvenile, or seemingly subadult, manual elements collected from Pipestone show any deformation. Due, however, to the disarticulated nature of the elements from this site it is difficult to discern the overall size, and therefore age class, of an individual based on manual elements alone, except in the case of the smallest specimens.

Micro-CT Analysis

Unfortunately, the CT data were by no means maximally informative, due to the density of UALVP 57914. However, there were distinct areas of porous texture associated with large nodules (Fig. 4.5 and 4.6) on pathological areas of the element's surface. The material making up these areas would have been less dense than the rest of the element. Such porous texture has also been described in an *Edmontosaurus annectens* metacarpal (BHI 6191) (Anné et al., 2015). In the case of BHI 6191, however, there is a great deal of mediolateral swelling of the bone, forming a large, rough callus that clearly surrounds a healed fracture. Due to the poor resolution of the scans, it cannot be guaranteed that UALVP 57914 is free of fractures. However, this specimen lacks any distinct large calluses of the type seen in BHI 6191, and therefore its pathological features are likely not due to an undetected fracture.

The porosity is unlikely to be explained by osteoarthritis, involving degeneration of the cartilage and the underlying ossified joint surfaces, as porosity is not indicative of osteoarthritis (Woods, 1995). Instead osteoarthritis tends to occur in non-contact and non-weight bearing areas. Therefore, the porosity may be instead be a result of osteoporosis, a disease in which bones become weak and porous to the point where their overall density is substantially reduced (Rothschild and Martin, 2006). However, one of the key indicators of osteoporosis is the loss of

trabecular bone, which is not evident in the CT scans of UALVP 57914. Instead the interior of the element is entirely made up of densely texture bone with no discernible marrow cavity.

Pathologies at Pipestone

Despite the diagnosis of the deformation described here, it is unlikely that this type of pathology would have been limited to one part of on the skeleton. As described by Rega et al. (2010), the degradation of the bone was most likely due to an underlying health condition that was exacerbated by stress associated with weight-bearing. This seems to be the case with both *Chasmosaurus* specimens, as ROM 843 bears additional deformations on some of the ribs, as well as on the horn cores and the left squamosal (Tanke and Farke, 2007). CMN 41357 also displays a number of deformations of the skeleton (Rega et al., 2010). The numerous pathologies described in the *Chasmosaurus* specimens are thought to be due to a number of different conditions, and not just a single underlying disease. However, in both specimens the manual pathologies are thought to be linked to at least one other pathology elsewhere in the skeleton. Therefore, the manual pathology in *P. lakustai* may have also been linked to another pathology in the skeleton, although this is impossible to determine from bonebed material.

However, Tanke and Rothschild (2010) compiled a list of all pathological or abnormal elements collected from Pipestone Creek, and few known pathological specimens have been collected since then. Although some observed pathologies are evidently due to fractures or similar traumas, there are a few that Tanke and Rothschild (2010) described as resulting from pseudoarthrosis, the formation of a false joint caused by fibrous tissue forming at a fracture within a bone. The elements affected by pseudoarthrosis include multiple ribs (TMP 1985.112.0039, TMP 1985.112.0086), reminiscent of the pathological ribs in the *Chasmosaurus*

specimens. This may indicate that the condition causing the characteristic pattern of manual pathology in ceratopsids also tends to manifest itself in the ribs. However, there is no way of determining if these pathological ribs are from the same individual as the pathological metacarpals.

Given Tanke and Rothschild's (2010) study, as well as my own observations, the number of pathological elements collected from Pipestone is small in proportion to the size of the sample from the locality. While hundreds of specimens have been collected from the site, and over 99% of those specimens are ceratopsid, only thirty-seven deformed elements have been identified, including those described in the present study. As stated in Chapter 3 of this thesis, it is likely that the Pipestone Creek Bonebed is the result of a flooding event that drowned a large herd of *P. lakustai*. Under this scenario, the sample is likely to comprise mainly of the remains of weak individuals, including the young, the very old, and the ill. As illustrated in Chapter 3, the sample is dominated by juvenile specimens and contains fewer adults and subadults. Therefore, one might expect the majority of the larger specimens to be ill, and accordingly to show signs of disease or other ailments; but this does not seem to be the case. However, it is important to note that 85.3% of the pathologies reported by Tanke and Rothschild (2010) were in adult specimens, highlighting the importance of age in the occurrence of such deformations. Additionally, this limited number of pathological specimens is quite standard for centrosaurine bonebeds (Tanke and Rothschild, 2010). For instance, only 9 pathological elements have been collected from *Centrosaurus* Bonebed 43 in Dinosaur Provincial Park.

The limited number of pathological elements at Pipestone, paired with the lesser degree of deformation of the metacarpals compared to the *Chasmosaurus* specimens examined by Rega et al (2010), may indicate that *P. lakustai* was unusually resistant to osteopathies. However, this

may not be the case given the pathological features in the *Pachyrhinosaurus*-like ceratopsid (TMP 2002.076.0001) described by Ryan et al. (2010). This specimen is otherwise known as the "Iddesleigh ceratopsid", given where it was discovered in Dinosaur Provincial Park. Although clearly a member of the clade Pachyrostra, the specimen cannot be identified to the generic level due to the absence of the diagnostic posterior part of the parietal. However, this specimen is highly pathological, showing deformation of the anterior parietal bar and of the phalanges. Ryan et al. (2010) took these pathologies to indicate that the specimen represented an elderly individual, but did not speculate regarding the cause of the pathologies beyond citing age.

Conclusion

The *Pachyrhinosaurus lakustai* metacarpals TMP 1989.055.1369 and UALVP 57914 bear close similarities to previously described pathological manual elements in *Chasmosaurus belli* ROM 843 and *Chasmosaurus irvinensis* CMN 41357. Based on the overall morphology of the metacarpals it is probable that the pathologies have the same root cause as in the *Chasmosaurus* specimens. Given the advanced ontogenetic stage represented by the specimens, as inferred from their size, it is likely that the deformation was caused by an underlying disease or infection, coupled with repeated weight-bearing stress due to the rolling action of the thumb as proposed by Thompson and Holmes (2007).

Due to the overall density of UALVP 57914, the Computed Tomography analyses were limited in their informativeness. However, a major increase in the porosity of the bone, within the irregular nodules visible on the surface, clearly implies alteration to and degradation of the element. This may indicate osteoporosis, but the exact nature of the pathology cannot be conclusively determined without higher-resolution scans of the internal structure of the element

or histological sectioning. Regardless of the underlying cause, this is the first report of this type of manual pathology in any centrosaurine. As the pathological features are most pronounced on the medial first digit (UALVP 57914) they are likely a result of the same medially-concentrated stress described by Rega et al. (2010). It can therefore be inferred that *P. lakustai* walked in a similar manner to *Chasmosaurus,* placing considerable stress on digit I of large adult individuals. Although this type of pathology has not at present been documented in any other centrosaurine, its occurrence in *P. lakustai* may indicate that centrosaurines tended to utilize the same type of step cycle that was proposed by Thompson and Holmes (2007) for *Chasmosaurus.* Identification of this pathology in other centrosaurines would be required to strengthen this conclusion.

Chapter 5 – General Conclusions

The forelimb and pectoral girdle of *Pachyrhinosaurus lakustai* are relatively informative both as a source of diagnostic features and with regard to the life history of the species. Although few postcranial characteristics differentiate species of *Pachyrhinosaurus* from one another, there are certainly postcranial characteristics that are unique to the genus *Pachyrhinosaurus.* These include a prominent epicondyle on the humerus, and a posteriorly displaced anterolateral process on the ulna. Furthermore, there are evident differences between centrosaurine and chasmosaurine scapulae and humeri. In centrosaurines the anterior end of the scapula is proportionally dorsoventrally wide in comparison to chasmosaurines. However, the posterior end of the scapula is dorsoventrally narrower than in chasmosaurines. The scapular ridge is also more pronounced in chasmosaurines, and extends farther obliquely towards the posterior end of the element. Chasmosaurine humeri possess a distinct notch separating the medial tubercle from the main proximal surface of the humerus. Chasmosaurines also have more prominent humeral heads and proportionally longer deltopectoral crest than centrosaurines.

By analyzing the forelimb and pectoral girdle, hypotheses regarding the behaviour of these animals, such as the semi-aquatic ceratopsian hypothesis, can be tested. Although most likely false, this hypothesis underlines the importance of postcranial features for studying some palaeobiological questions. Histological analysis of *P. lakustai* humeri provides insights into the growth trajectory of this taxon. Based on this analysis, *P. lakustai* lived to be at least 21 years of age, although the youngest individuals recognized at Pipestone Creek Bonebed were determined to be less than a year old. Furthermore, studying the size and abundance of postcranial elements at the locality makes it possible to understand the population structure of the herd. Based on humeral measurements, the largest individual had a minimum mass of 1690 kg, which confirms that *P. lakustai* is relatively small in comparison to its close relative *P. canadensis.* The

Pipestone Creek assemblage has an abundance of juvenile elements, which is likely due to juveniles inability to cope with a fording a river in the event of a flood, which is hypothesized to be the case at the locality.

Lastly, identification and analysis of unique postcranial elements from the bonebed made it possible to identify an informative manual pathology in *P. lakustai* MC I and V. This pathology seems to indicate that *P. lakustai* used a step cycle pattern previously only described in chasmosaurines. Not only does this analysis shine light on the habitual behaviours of *P. lakustai*, but it also provides the first evidence that these behaviours occurred in at least some centrosaurines and were therefore widespread across Ceratopsidae. Based on the overall morphology and location of the pathology, the most likely cause is stress imposed by the medial rolling of the manus during normal locomotion, resulting in added stress on the first digit of the manus.

Overall, this thesis has expanded our knowledge of *P. lakustai* and the Pipestone Creek Bonebed, and of ceratopsids as a whole. It has opened the door to informative comparisons among ceratopsid postcrania as well as behavioural inferences based on postcrania alone. However, more work remains to be done. Further comparative studies are needed to identify diagnostic characters in the axial skeleton, pelvic girdle and hindlimb. As taxonomically informative characteristics have been identified in the pectoral girdle and forelimb in the source of this research, it stands to reason that similar features should exist in the pelvic girdle and hindlimb. Such studies will allow for easier identification of ceratopsid specimens in the future. Furthermore, by studying the postcrania of various ceratopsids, their life histories can be compared and their growth, lifestyle and locomotory patterns can be understood. There is still so

much to be gained from studying the different parts of these animals. Although the cranium will forever be iconic in ceratopsians, the postcranium will expand that iconic picture for the future.

References

Alexander, R. M. (1989). *Dynamics of dinosaurs and other extinct giants*. Columbia University Press.

Andrews, S. M., and Westoll, T. S. (1970). IX.—The postcranial skeleton of *Eusthenopteron foordi* Whiteaves. *Earth and Environmental Science Transactions of The Royal Society of Edinburgh*, *68*(9), 207–329.

Anné, J., Garwood, R. J., Lowe, T., Withers, P. J., and Manning, P. L. (2015). Interpreting pathologies in extant and extinct archosaurs using micro-CT. *PeerJ*, *3*, e1130.

Back, G. N., Barrington, M. R., and McAdoo, J. K. (1987). Sage grouse use of snow burrows in Northeastern Nevada. *The Wilson Bulletin*, *99*(3), 488–490.

Bakker, R. T., and Williams, M. (1988). *Nanotyrannus*, a new genus of pygmy tyrannosaur, from the Latest Cretaceous of Montana. *Hunteria, 1*(5), 1.

Becker, M., Souza, M. A., Moraes, L. G., Silva, G. S., Antoniassi, N. A. B., Souza, R. L., Colodel, E. M., Becker, M., Souza, M. A., Moraes, L. G., Silva, G. S., Antoniassi, N. A. B., Souza, R. L., and Colodel, E. M. (2018). Bone quality evaluation of experimental osteometabolic disease in Pantanal alligators (*Caiman yacare*) by High Resolution Computerized Microtomography (μCT). *Pesquisa Veterinária Brasileira*, *38*(5), 981–990.

Bender, L. C., and Haufler, J. B. (1999). Social group patterns and associations of nonmigratory elk (*Cervus elaphus)* in Michigan. *The American Midland Naturalist*, *142*(1), 87–95.

Bonnan, M. F. (2003). The evolution of manus shape in sauropod dinosaurs: Implications for functional morphology, forelimb orientation, and phylogeny. *Journal of Vertebrate Paleontology*, *23*(3), 595–613.

Brown, B. (1917). A complete skeleton of the horned dinosaur *Monoclonius*, and description of a second skeleton showing skin impressions. *Bulletin of the AMNH , 37,* article 10.

Brown, B., and Schlaikjer, E. M. (1940). *The origin of ceratopsian horn-cores.* American Museum of Natural History.

Calder, W. A. (1996). *Size, function, and life history*. Mineola, NY. Dover Publications, Inc.

Campione, N. E., and Evans, D. C. (2012). A universal scaling relationship between body mass and proximal limb bone dimensions in quadrupedal terrestrial tetrapods. *BMC Biology*, *10*(1), 60.

Carr, T. D. (1999). Craniofacial ontogeny in tyrannosauridae (Dinosauria, Coelurosauria). *Journal of Vertebrate Paleontology*, *19*(3), 497–520.

Castellini, M. (2009). Thermoregulation. In Perrin, W. F., Thewissen, J. G. M., Wursig, B (Ed.). *Encyclopedia of Marine Mammals* (2nd ed., pp. 16-117). USA. Academic Press.

Chinnery, B. (2004). Morphometric analysis of evolutionary trends in the ceratopsian postcranial skeleton. *Journal of Vertebrate Paleontology*, *24*(3), 591–609.

Cooper, L. N., Lee, A. H., Taper, M. L., and Horner, J. R. (2008). Relative growth rates of predator and prey dinosaurs reflect effects of predation. *Proceedings of the Royal Society B: Biological Sciences*, *275*(1651), 2609–2615.

Cousquer, G. O., Dankoski, E. J., and Patterson-Kane, J. C. (2007). Metabolic bone disease in wild collared doves (*Streptopelia decaocto*). *Veterinary Record*, *160*(3), 78–84.

Currie, P. J., Langston, Jr., W., and Tanke, D. (2008). A new species of *Pachyrhinosaurus* (Dinosauria, Ceratopsidae) from the Upper Cretaceous of Alberta, Canada. In Currie, P. J., Langston, W., Tanke, D. H. (Ed.). *A New Horned Dinosaur from an Upper Cretaceous Bone Bed in Alberta* (pp. 1–108). Ottawa, ON. NRC Research Press.

Diem, S., and Archibald, D. (2005). Range extension of southern chasmosaurine ceratopsian dinosaurs into northwestern Colorado. *Journal of Paleontology, 79*(2), 251-258.

Edwards, H. M., and Veltmann, J. R. (1983). The role of calcium and phosphorus in the etiology of tibial dyschondroplasia in young chicks. *The Journal of Nutrition*, *113*(8), 1568–1575.

Eltringham, S. K. (1993). The common hippopotamus *(Hippopotamus amphibius*). In *Pigs, Peccaries, and Hippos: Status Survey and Conservation Action Plan* (pp. 43–55). IUCN.

Erickson, G. M. (2014). On dinosaur growth. *Annual Review of Earth and Planetary Sciences*, *42*(1), 675–697.

Erickson, G. M., and Druckenmiller, P. S. (2011). Longevity and growth rate estimates for a polar dinosaur: A *Pachyrhinosaurus* (Dinosauria: Neoceratopsia) specimen from the North Slope of Alaska showing a complete developmental record. *Historical Biology*, *23*(4), 327–334.

Erickson, G. M., Makovicky, P. J., Currie, P. J., Norell, M. A., Yerby, S. A., and Brochu, C. A. (2004). Gigantism and comparative life-history parameters of tyrannosaurid dinosaurs. *Nature*, *430*(7001), 772–775.

Erickson, G. M., and Olson, K. H. (1996). Bite marks attributable to *Tyrannosaurus rex*: Preliminary description and implications. *Journal of Vertebrate Paleontology*, *16*(1), 175–178.

Erickson, G. M., Rogers, K. C., and Yerby, S. A. (2001). Dinosaurian growth patterns and rapid avian growth rates. *Nature*, *412*(6845), 429.

Erickson, G. M., and Tumanova, T. A. (2000). Growth curve of *Psittacosaurus mongoliensis* Osborn (Ceratopsia: Psittacosauridae) inferred from long bone histology. *Zoological Journal of the Linnean Society*, *130*(4), 551–566.

Fancy, S. G., Pank, L. F., Whitten, K. R., and Regelin, W. L. (1989). Seasonal movements of caribou in arctic Alaska as determined by satellite. *Canadian Journal of Zoology*, *67*(3), 644–650.

Fanti, F., and Currie, P. (2007). A new *Pachyrhinosaurus* bonebed from the Late Cretaceous Wapiti Formation. In Braman, D., Therrien, F., Koppelhus, I., and Taylor, W. (Ed.) *Dinosaur Park Symposium - Short Papers, Abstracts, and Programs* (pp. 39–43). Special Publication of the Royal Tyrrell Museum.

Fanti, F., Currie, P. J., and Burns, M. E. (2015). Taphonomy, age, and paleoecological implication of a new *Pachyrhinosaurus* (Dinosauria: Ceratopsidae) bonebed from the Upper Cretaceous (Campanian) Wapiti Formation of Alberta, Canada. *Canadian Journal of Earth Sciences*, *52*(4), 250–260.

Farke, A. (2007). Cranial osteology and phylogenetic relationships of the chasmosaurine ceratopsid *Torosaurus latus*. In Carpenter, K. (Ed.) *Horns and Beaks: Ceratopsian and ornithopod Dinosaurs* (pp. 235–257). Bloomington and Indianapolis, IN. Indiana University Press.

Farke, A. A., Wolff, E. D. S., and Tanke, D. H. (2009). Evidence of Combat in Triceratops. *PLOS ONE*, *4*(1), e4252.

Fiorillo, A. R. (2008). On the occurrence of exceptionally large teeth of *Troodon* (Dinosauria: Saurischia) from the Late Cretaceous of Northern Alaska. *PALAIOS*, *23*(5), 322–328.

Fiorillo, A. R., and Gangloff, R. A. (2001). The caribou migration model for Arctic hadrosaurs (Dinosauria: Ornithischia): A reassessment. *Historical Biology*, *15*(4), 323–334.

Fiorillo, A. R., and Tykoski, R. S. (2012). A new Maastrichtian species of the centrosaurine ceratopsid *Pachyrhinosaurus* from the North Slope of Alaska. *Acta Palaeontologica Polonica*, *57*(3), 561–573.

Frederickson, J. A., and Tumarkin-Deratzian, A. R. (2014). Craniofacial ontogeny in *Centrosaurus apertus*. *PeerJ*, *2*, e252 10.7717/peerj.252

Fujiwara, S.I. (2009). A reevaluation of the manus structure in *Triceratops* (Ceratopsia: Ceratopsidae). *Journal of Vertebrate Paleontology*, *29*(4), 1136–1147.

Galton, P. M. (1981). *Dryosaurus*, a hypsilophodontid dinosaur from the Upper Jurassic of North America and Africa postcranial skeleton. *Paläontologische Zeitschrift*, *55*(3–4), 271–312. https://doi.org/10.1007/BF02988144

García, R. A., Cerda, I. A., Heller, M., Rothschild, B. M., and Zurriaguz, V. (2017). The first evidence of osteomyelitis in a sauropod dinosaur. *Lethaia*, *50*(2), 227–236.

Gilmore, C. W. (1917). Brachyceratop*s: A ceratopsian dinosaur from the Two Medicine Formation of Montana, with notes on associated fossil reptiles*. U.S. Government Printing Office.

Hanna, R. R. (2002). Multiple injury and infection in a sub-adult theropod dinosaur *Allosaurus fragilis* with comparisons to allosaur pathology in the Cleveland-Lloyd Dinosaur Quarry Collection. *Journal of Vertebrate Paleontology*, *22*(1), 76–90.

Hatcher, J. B., Marsh, O. C. and Lull, R. S. (1907). The ceratopsia*. U. S. Geological Survey Monograph,* 49, 1-300.

Holmes, R. B. (2014). The postcranial skeleton of *Vagaceratops irvinensis* (Dinosauria, Ceratopsidae). *Vertebrate Anatomy Morphology Palaeontology*, *1*, 1–21.

Holmes, R. B., and Ryan, M. J. (2013). The postcranial skeleton of *Styracosaurus albertensis*. *Kirtlandia*, *58*, 5–37.

Holmes, R. B., Ryan, M. J., and Murray, A. M. (2006). Photographic atlas of the postcranial skeleton of the type specimen of *Styracosaurus albertensis* with additional isolated cranial elements from Alberta. *Syllogeus*, *75*, 1–75.

Horner, J. R., and Goodwin, M. B. (2006). Major cranial changes during *Triceratops* ontogeny. *Proceedings of the Royal Society B: Biological Sciences*, *273*(1602), 2757–2761.

Huchzermeyer, F. W., Groenewald, H. B., Myburgh, J. G., Steyl, J. C. A., and Crole, M. R. (2013). Osteoarthropathy of unknown aetiology in the long bones of farmed and wild Nile crocodiles (Crocodylus niloticus). *Journal of the South African Veterinary Association*, *84*(1), 1–5.

Johnson, R. E., & Ostrom, J. H. (1995). The forelimb of *Torosaurus* and an analysis of the posture and gait of ceratopsian dinosaurs. In *Functional morphology in vertebrate palaeontology* (pp. 205–218). Cambridge University Press.

Keenan, S. W., and Scannella, J. (2014). Paleobiological implications of a *Triceratops* bonebed from the Hell Creek Formation, Garfield County, northeastern Montana. In Wilson, G. P., Clemens, W. A., Horner, J. R., and Hartman, J. H. *Through the End of the Cretaceous in the Type Locality of the Hell Creek Formation in Montana and Adjacent Areas* (pp. 349–364). Boulder, CO. Geological Society of America.

Kruk, E. (2015). *A new species of* Pachyrhinosaurus *from the Wapiti Formation (Late Campanian) of Alberta* (Unpublished Master's thesis, University of Alberta, Edmonton, Canada)

Langston Jr., W. (1967). The thick-headed ceratopsian dinosaur *Pachyrhinosaurus* (Reptilia: Ornithischia), from the Edmonton Formation near Drumheller, Canada. *Canadian Journal of Earth Sciences*, *4*(1), 171–186.

Larson, P. (2013). The case for *Nanotyrannus*. In Parrish, J. M., Molnar, R. E., Currie, P. J. and Koppelhus, E. B. (Eds.) *Tyrannosaurid paleobiology* (pp. 15–53). Bloomington, IN. Indiana University Press.

Lee, A. H., and O'Connor, P. M. (2013). Bone histology confirms determinate growth and small body size in the noasaurid theropod *Masiakasaurus knopfleri*. *Journal of Vertebrate Paleontology*, *33*(4), 865–876.

Lee, A. H. (2007). *Interplay between growth and mechanics in the evolution of bone microstructure in dinosaurs* (Doctoral Dissertation) Available through ProQuest Dissertations and Theses Global: Science and Technology. Berkeley, CA. University of California.

Lehman, T. (2006). Growth and population age structure in the horned dinosaur *Chasmosaurus*. In Carpenter, K. (Ed.) *Horns and Beaks: Ceratopsian and Ornithopod Dinosaurs* (p. 259). Bloomington and Indianapolis, IN. Indiana University Press.

Levitt, C. G. (2013). *Bone histology and growth of chasmosaurine ceratopsid dinosaurs from the late Campanian Kaiparowitis Formation, Southern Utah.*(Master's Thesis, University of Utah, Salt Lake City, USA)

Liberona, J. A. P., Soto-Acuña, S., Mendez, M. A., and Vargas, A. O. (2019). Assesment and interpretation of negative forelimb allometry in the evolution of non-avian Theropoda. *Frontiers in Zoology*, *16*(1), 1–13.

Longrich, N. R., and Field, D. J. (2012). *Torosaurus* is not *Triceratops*: ontogeny in chasmosaurine ceratopsids as a case study in dinosaur taxonomy. *PLOS ONE*, *7*(2), e32623.

Lü, J., Kobayashi, Y., Lee, Y.-N., and Ji, Q. (2007). A new *Psittacosaurus* (dinosauria: ceratopsia) specimen from the Yixian Formation of western Liaoning, China: the first pathological psittacosaurid. *Cretaceous Research*, *28*(2), 272–276.

Maidment, S., and Barrett, P. (2011). A new specimen of *Chasmosaurus belli* (Ornithischia: Ceratopsidae), a revision of the genus, and the utility of postcrania in the taxonomy and systematics of ceratopsid dinosaurs. *Zootaxa* 2963:1-47

Maiorino, L., Farke, A. A., Kotsakis, T., and Piras, P. (2013). Is *Torosaurus Triceratops*? Geometric morphometric evidence of Late Maastrichtian ceratopsid dinosaurs. *PLOS ONE*, *8*(11), e81608.

Mallon, J. C., and Holmes, R. B. (2006). A reevaluation of sexual dimorphism in the postcranium of the chasmosaurine ceratopsid *Chasmosaurus belli* (Dinosauria: Ornithischia). *The Canadian Field-Naturalist*, *120*(4), 403–412.

Mallon, J. C., Ott, C. J., Larson, P. L., Iuliano, E. M., and Evans, D. C. (2016). *Spiclypeus shipporum* gen. et sp. nov., a boldly audacious new chasmosaurine ceratopsid (Dinosauria: Ornoithischia) from the Judith River Formation (Upper Cretaceous: Campanian) of Montana, USA. *PLOS ONE*, *11*(5), e0154218.

Mallon, J., and Holmes, R. (2010). Description of a complete and fully articulated chasmosaurine postcranium previously assigned to *Anchiceratops*. In Eberth, D. A., Ryan, M. J., Chinnery-Allgeier, B. J. (Ed.) *New Perspectives on Horned Dinosaurs* (pp. 189-202).Bloomington, IN. Indiana University Press.

Mathews, J. C., Brusatte, S. L., Williams, S. A., and Henderson, M. D. (2009). The first *Triceratops* bonebed and its implications for gregarious behavior. *Journal of Vertebrate Paleontology*, *29*(1), 286–290.

McCrea, R. T., Tanke, D. H., Buckley, L. G., Lockley, M. G., Farlow, J. O., Xing, L., Matthews, N. A., Helm, C. W., Pemberton, S. G., and Breithaupt, B. H. (2015). Vertebrate ichnopathology: Pathologies inferred from dinosaur tracks and trackways from the Mesozoic. *Ichnos*, *22*(3–4), 235–260.

McWilliams, D. A., and Leeson, S. (2001). Metabolic bone disease in lizards: Prevalence and potential for monitoring bone health. *AZA-NAG*, 5.

Myers, T., and Fiorillo, A. R. (2009). Evidence for gregarious behavior and age segregation in sauropod dinosaurs. *Palaeogeography, Palaeoclimatology, Palaeoecology*, *274*(1–2), 96–104.

Myhrvold, N. (2013). Revisiting the estimation of dinosaur growth rates. *PLOS ONE*, *8*(12), e81917.

Prondvai, E. (2017). Medullary bone in fossils: Function, evolution and significance in growth curve reconstructions of extinct vertebrates. *Journal of Evolutionary Biology*, *30*(3), 440–460.

Ralrick, P., and Tanke, D. (2008). Comments on the quarry map and preliminary taphonomic observations of *Pachyrhinosaurus* (Dinosauria: Ceratopsidae) bone bed at Pipestone Creek, Alberta, Canada. In Currie, P. J., Langston, W., Tanke, D. H. (Ed.). *A New Horned Dinosaur from an Upper Cretaceous Bone Bed in Alberta* (pp. 109–116). Ottawa, ON. NRC Research Press.

Rega, E, Holmes, R., and Tirabasso, A. (2010). Habitual locomotor behavior inferred from manual pathology in two Late Cretaceous chasmosaurine ceratopsid dinosaurs, *Chasmosaurus irvinensis* (CMN 41357) and *Chasmosaurus belli* (ROM 843). In Eberth, D. A., Ryan, M. J., Chinnery-Allgeier, B. J. (Ed.) *New Perspectives on Horned Dinosaurs* (pp. 340-354).Bloomington, IN. Indiana University Press.

Rega, Elizabeth, and Holmes, R. (2006). Manual pathology indicative of locomotor behavior in two chasmosaurine ceratopsid dinosaurs. *Journal of Vertebrate Paleontology*, *26, supplement to number 3*(114A).

Reizner, J. A. (2010). *An ontogenetic series and population histology of the ceratopsid dinosaur* Einiosaurus procurvicornis. (Master's Thesis, Montana State University, Bozeman, Montana).

Rooij, J. de. (2018). *Discovery of a* Triceratops *bonebed:* Triceratops *long bone histology and implications on social behaviour* (Master's thesis, Utrecht University, Utrecht, Netherlands).

Rothschild, B. M., and Martin, L. D. (2006). *Skeletal impact of disease, 33*. New Mexico Museum of Natural History and Science. Bulletin.

Rothschild, B. M., Schultze, H.-P., and Pellegrini, R. (2012). *Herpetological osteopathology: Annotated bibliography of amphibians and reptiles*. Springer Science and Business Media.

Ruckstuhl, K., and Neuhaus, P. (2000). Sexual segregation in ungulates: a new spproach. *Behaviour*, *137*(3), 361–377.

Russell, L. S. (1935). Musculature and functions in the Ceratopsia. *National Museum of Canada Bulletin (Geology)*, *77*, 39–48.

Ryan, M., Eberth, D., Brinkman, D., Currie, P., and Tanke, D. (2010). A new *Pachyrhinosaurus*-Like ceratopsid from the Upper Dinosaur Park Formation (Late Campanian) of Southern Alberta, Canada. In Eberth, D. A., Ryan, M. J., Chinnery-Allgeier, B. J. (Ed.) *New Perspectives on Horned Dinosaurs* (pp. 141-155).Bloomington, IN. Indiana University Press.

Ryan, M. J., Russell, A. P., Eberth, D. A., and Currie, P. J. (2001a). The taphonomy of a *Centrosaurus* (Ornithischia: Certopsidae) bone bed from the Dinosaur Park Formation (Upper Campanian), Alberta, Canada, with Comments on Cranial Ontogeny. *PALAIOS*, *16*(5), 482–506.

Sander, P. M., Mateus, O., Laven, T., and Knotschke, N. (2006). Bone histology indicates insular dwarfism in a new Late Jurassic sauropod dinosaur. *Nature*, *441*(7094), 739–741.

Scannella, J., and Honrer, J. (2010). *Torosaurus* Marsh, 1891, is *Triceratops* Marsh, 1889 (Ceratopsidae: Chasmosaurinae): Synonymy through ontogeny. *Journal of Vertebrate Paleontology*, *30*(4), 1157–1168.

Sinclair, B. J., and Chown, S. L. (2005). Climatic variability and hemispheric differences in insect cold tolerance: Support from southern Africa. *Functional Ecology*, *19*(2), 214–221.

Stokely, P. S. (1947). The post-cranial Skeleton of *Aprasia repens*. *Copeia*, *1947*(1), 22–28. JSTOR.

Straight, W. H., Davis, G. L., Skinner, H. C. W., Haims, A., McClennan, B. L., and Tanke, D. H. (2009). Bone lesions in hadrosaurs: Computed tomographic imaging as a guide for paleohistologic and stable-isotopic analysis. *Journal of Vertebrate Paleontology*, *29*(2), 315–325.

Tamer, P., and Simpson, S. (2017). Evolutionary medicine: Why do humans get bunions? *Evolution, Medicine, and Public Health*, *2017*(1), 48–49.

Tanke, D., and Farke, A. (2007). Bone resoption, bone lesions, and extracranial fenestrae in ceratopsid dinosaurs: A preliminary assessment. In Carpenter, K. (Ed.) *Horns and Beaks: Ceratopsian and Ornithopod Dinosaurs* (pp. 319-347). Bloomington and Indianapolis, IN. Indiana University Press.

Tanke, D. H. (2006). Read all about it! The interpretive value of newspapers from old unidentified dinosaur quarries and paleontological fieldcamps in Alberta, Canada. *Paludicola*, *6*, 22–30.

Tanke, D. H., and Rothschild, B. M. (2010). Paleopathologies in Albertan ceratopsids and their behavioral significance. In Ryan, M. J., Chinnery-Allegeier, B. J., Eberth, D. A. (Ed.) *New Perspectives on Horned Dinosaurs* (pp. 355-384). Bloomington, IN. Indiana University Press.

Thompson, S., and Holmes, R. (2007). Forelimb stance and step cycle in *Chasmosaurus Irvinenesis* (dinosauria: Neoceratopsia). *Palaeontologia Electronica* 10(1), 5A, 1-17.

Tschopp, E., Wings, O., Frauenfelder, T., and Rothschild, B. M. (2014). Pathological Phalanges in a Camarasaurid Sauropod Dinosaur and Implications on Behaviour. *Acta Palaeontologica Polonica*, *61*(1), 125–134.

Wauters, L. A., Dhondt, A. A., Knothe, H., and Parkin, D. T. (1996). Fluctuating asymmetry and body size as indicators of stress in red squirrel populations in woodland fragments. *Journal of Applied Ecology*, *33*(4), 735–740.

Witmer, L. M., and Ridgely, R. C. (2008). Structure of the brain cavity and inner ear of the centrosaurine ceratopsid *Pachyrhinosaurus* based on CT scanning and 3D visualization.

In Currie, P. J., Langston, W., Tanke, D. H. (Ed.). *A New Horned Dinosaur from an Upper Cretaceous Bone Bed in Alberta* (pp. 1117-144). Ottawa, ON. NRC Research Press.

Witzmann, F., Asbach, P., Remes, K., Hampe, O., Hilger, A., and Paulke, A. (2008). Vertebral pathology in an ornithopod dinosaur: A hemivertebra in *Dysalotosaurus lettowvorbecki* from the Jurassic of Tanzania. *The Anatomical Record*, *291*(9), 1149–1155.

Yun, C. (2015). Evidence points out that "*Nanotyrannus*" is a juvenile *Tyrannosaurus rex*. *PeerJ PrePrints 3* (e852v1).